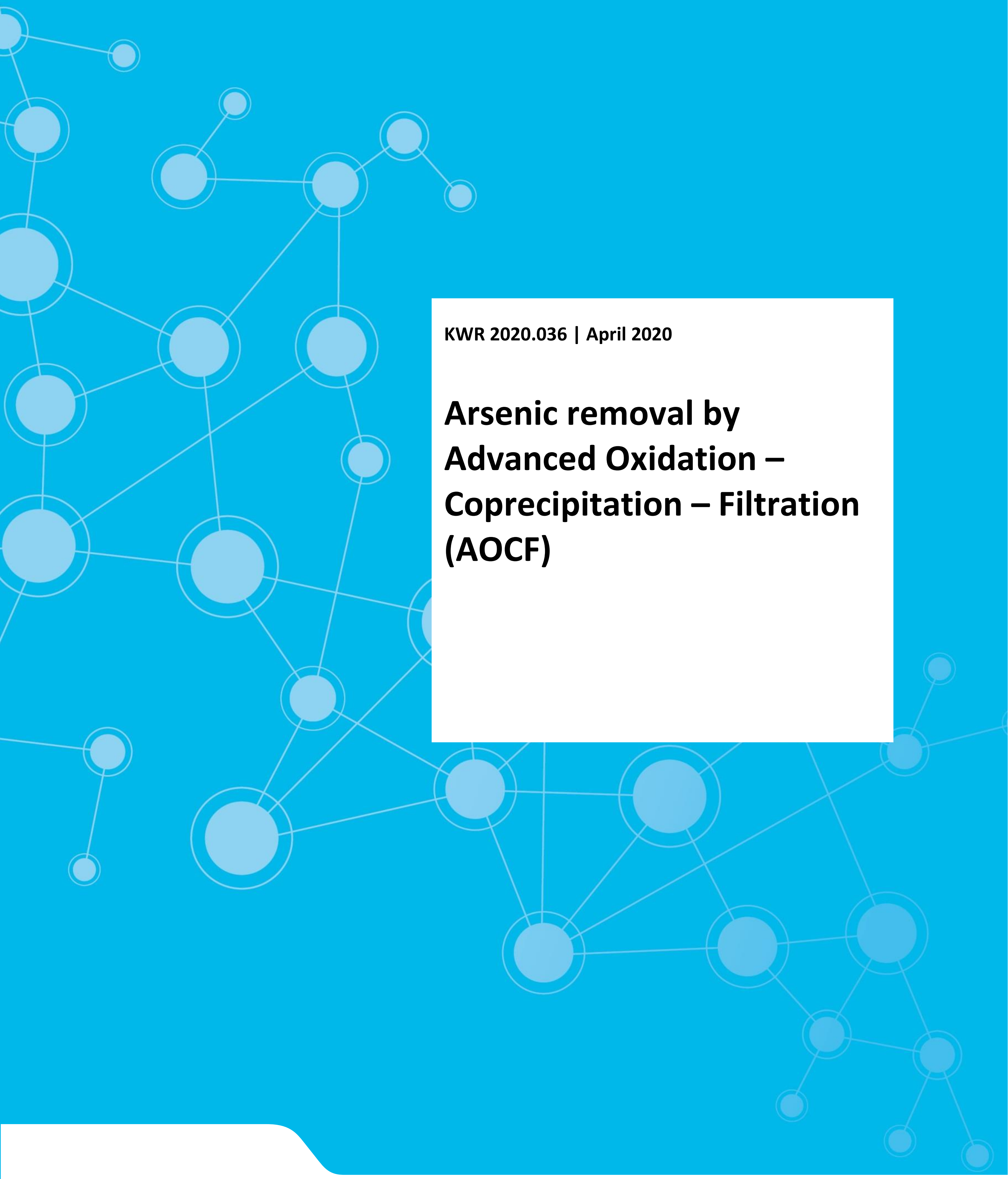

KWR 2020.036 | April 2020

Arsenic removal by Advanced Oxidation – Coprecipitation – Filtration (AOCF)

Bridging Science to Practice

Arsenic removal by Advanced Oxidation – Coprecipitation – Filtration (AOCF)

KWR 2020.036 | April 2020

Project number

401721

Project manager

Erwin Beerendonk (KWR)

Client

Aquaminerals B.V., Brabant Water N.V., Carus Europe, Dunea Duin & Water, Evides Waterbedrijf N.V.

Author(s)

Arslan Ahmad, Luuk de Waal, Martin Korevaar (KWR)

Brent Pieterse, Wim Oorthuizen (Dunea)

David de Ridder, Shahnaaz Abdoel Gafoer, Anthonie Hogendoorn (Evides)

Quality Assurance

Emile Cornelissen (KWR)

Sent to

Aquaminerals B.V., Brabant Water N.V., Carus Europe, Dunea Duin & Water, Evides Waterbedrijf N.V.

Keywords

Arsenic, groundwater treatment, coprecipitation, filtration, oxidation, drinking water

Year of publishing
2020

More information
Arslan Ahmad
T +31 (0) 646 95 02 31
E Arslan.Ahmad@kwrwater.nl

PO Box 1072
3430 BB Nieuwegein
The Netherlands

T +31 (0)30 60 69 511
F +31 (0)30 60 61 165
E info@kwrwater.nl
I www.kwrwater.nl

April 2020 ©

All rights reserved. No part of this publication may be reproduced, stored in an automatic database, or transmitted, in any form or by any means, be it electronic, mechanical, by photocopying, recording, or in any other manner, without the prior written permission of the publisher.

Summary

Arsenic (As) contamination of drinking water is a global issue, affecting health of millions of people in many countries. Drinking water companies in the Netherlands have recently established 1 µg/L as the guideline for As in drinking water based on dose-effect modelling of low-level As in Dutch drinking water which has shown that 10 µg/L is not sufficiently protective for the health of Dutch population. In the Netherlands some of the water treatment plants (WTPs) produce drinking water with higher than 1 µg/L As and currently Dutch drinking water companies are investigating options to reduce As to <1 µg/L at these WTPs.

Arsenic removal by Advanced Oxidation – Coprecipitation – Filtration (AOCF) is a promising As removal method. It involves dosing a strong oxidant (e.g. $NaMnO_4$) and an iron (Fe) based coagulant (e.g. $FeCl_3$) in water to remove As from water. The permanganate (MnO_4) rapidly oxidizes As(III) to As(V) and $FeCl_3$ produces Fe(III)(oxyhydr)oxides in water that adsorb As(V) from water. The As bearing Fe(III)(oxyhydr)oxides are removed typically in a rapid sand filter. The overall objective of this study was to investigate As reduction to <1 µg/L by Advanced Oxidation – Coprecipitation – Filtration (AOCF) under different ion compositions and filtration conditions, as well as to gain mechanistic understanding of the process to determine the key guiding principles for full scale implementation.

In an extensive laboratory study, we combined macroscopic measurements of precipitate aggregation and chemical composition with X-ray absorption spectroscopy to investigate the solids formed by co-oxidation of Fe(II) and Mn(II) with O_2, $KMnO_4$, and NaOCl in the presence of groundwater ions at near-neutral pH. We found that in the absence of phosphate (P), silicate (Si) and calcium (Ca), O_2 and HOCl produced suspensions that aggregated rapidly, whereas co-oxidation of Fe(II) and Mn(II) by MnO_4 generated colloidal stable suspensions. The aggregation tendency of all the suspensions decreased in P and Si bearing solutions, but the presence of Ca counteracted these oxyanion effects, i.e. improved aggregation of the precipitates. The speciation of oxidized Fe and Mn in the absence of P and Si also depended on the type of oxidant, with O_2 producing Mn(III)-incorporated lepidocrocite, HOCl producing Mn(III)-incorporated hydrous ferric oxide (HFO) and MnO_4 producing poorly-ordered MnO_2 and HFO as separate phases. In general, the presence of P and Si in solution decreased the crystallinity of the Fe(III) phase and increased the Mn/Fe solids ratio, which was found by Mn K-edge XAS analysis to be due to an increase in surface-bound Mn(II). In contrast, Ca decreased the Mn/Fe solids ratio and decreased the fraction of Mn(II) associated with the solids, suggesting that Ca and Mn(II) compete for adsorption sites. Based on these results, we conclude that the composition of water and the identity of the oxidant strongly determines the macroscopic and molecular-scale characteristics of Fe and Mn bearing precipitates generated by Fe(II) and Mn(II) co-oxidation. Future work on molecular scale structural analysis of Fe and Mn precipitates should also include other strong oxidants such as H_2O_2 and O_3, as well aa the influence of a broad spectrum of ions in water including bicarbonate, sulphate, nitrate etc.

A laboratory study was performed to gain more understanding of the independent and combined effects of Si, P, natural organic matter (NOM) and Ca on As(V) co-precipitation efficiency and the size of Fe(III) precipitates formed by the hydrolysis of $FeCl_3$ at near-neutral pH. We found that, in complex solutions, containing multiple solutes and high levels of Ca, Si and P presence in typical groundwater concentrations reduce As(V) removal slightly, mainly due to a decreased adsorption of As(V) onto Fe(III) precipitates. On the other hand, NOM concentrations reduced As(V) removal to a much greater extent, due to possible formation of mobile Fe(III)–NOM complexes that were difficult to remove by 0.45 µm disc filtration.

These findings indicate that at WTPs the effectiveness of As removal not only depends on As adsorption to Fe(III)(oxyhydr)oxide precipitates, but also on the separation of As bearing Fe(III) precipitates from water. Calcium effectively counteracts the negative effect of oxyanions and promotes the growth of Fe(III) precipitates, which can be easily separated from water by gravitation settling and rapid sand filtration. Thus, hardness of water should be

carefully considered in designing As removal processes that rely on the co-precipitation of As and Fe. Obviously, effective separation of the colloidal particles can also be achieved by employing low-pressure membrane filtration (MF/UF) instead of the conventional rapid sand filtration for effective separation of the colloidal particles. Nevertheless, also in this case, the charge and size distribution of Fe(III) precipitates will remain crucial in determining the membrane fouling mechanisms.

Pilot investigations to assess the feasibility of AOCF concept were carried out at WTPs Dorst (Brabant Water), Katwijk (Dunea) and Ouddorp (Evides). During the investigations, experiments were carried out to study the impact of individual and combined dosing of treatment chemicals ($NaMnO_4$, $FeCl_3$, $FeSO_4$) on As removal, as well the removal of Fe, Mn and NH_4^+ in rapid sand filters. Moreover, process parameters such as filter run time and settling characteristics of backwash water were also studied. Following major conclusions can be drawn based on the pilot investigations.

- MnO_4–Fe(III) dosing in the influent of rapid sand filters is an effective technique to improve As removal in rapid sand filters. The optimum dosages of MnO_4 and Fe(III) were found to be dependent on the concentration of As(III) in water and ionic composition of the water matrix. In general, raw water with a higher concentration of reduced Fe(II), Mn(II) and As(III) required a higher dose of MnO_4. The raw water with a higher concentration of oxyanions and NOM required a higher dose of Fe(III).

- MnO_4–Fe(III) dosing in rapid sand filters did not show any negative effect on NH_4^+ and Mn removal in rapid sand filters

- The dosing of MnO_4—Fe(III) improved the settling rate of backwash solids. Thus, the implementation of MnO_4–Fe(III) dosing at WTPs is expected to have benefits for backwash water treatment, i.e. reduction in settling time in sedimentation basins.

- General filtration performance can be enhanced with MnO_4–Fe(III) dosing in pilot column. At WTP Katwijk we observed that the turbidity of the filter effluent was reduced from 0.3 FTU to about 0.03 FTU.

- The runtime of the pilot filters was decreased significantly due to the MnO_4–Fe(III) dosing. This means that an adjustment in the design of rapid sand filters, e.g. by replacing filter media with another size fraction will be required for a sustainable operation of full-scale rapid sand filter

- Although achieving and maintaining accurate dosing of chemicals (MnO_4, Fe(II), Fe(III)) during pilot experiments remained an issue in this pilot study at WTP Ouddorp, it can be concluded that dosing a combination of MnO_4 and Fe(III) in the influent of rapid sand filters can be an effective method to reduce As concentration to <1 µg/L, however further research is proposed using virgin filter media because we observed a release of As in the filter bed from the filter media (obtained from a full scale filter of WTP Ouddorp) which hindered consistent As reduction to <1 µg/L in the filter effluent. Thus, further research at WTP Ouddorp is recommended with virgin filter media to investigate the feasibility of MnO_4-Fe(III) dosing for WTP Ouddorp.

We have demonstrated a model suited to investigate the influence of changes in the water composition on arsenic and phosphate loading. For accurate predictions however, the order of magnitudes are too far off. It should be viewed as a model to *investigate* the system, not one to predict with (yet). Moreover, iron filterability could not be predicted by this model. To apply this model to determine arsenic removal, it is vital that not only arsenic loading is predicted correctly, but also the filterability of the precipitates. One key aspect to achieve that, is to get better estimates (and validation) of their surface charge.

Contents

1 Introduction

Arsenic (As) contamination of drinking water is a global issue. Most of the exposed population lives in South Asia, particularly in Bangladesh, India, Pakistan and Nepal (Mukherjee et al. 2006). Major reports of groundwater As contamination have also been emerged from other countries such as Argentina, Bolivia, China, Mexico, Turkey and USA (Herath et al. 2016). Arsenic is highly toxic and its chronic ingestion is associated with several types of cancer and other detrimental effects on human health (Smith et al. 1992). In spite of a substantial database on the association between many chronic diseases and the consumption of As, there remains a considerable uncertainty about the health risks due to chronic intake of low As concentrations, especially close to the current WHO guideline for As in drinking water, i.e.10 μg/L (Ahmad and Bhattacharya 2019, Kozisek 2017, Saint-Jacques et al. 2018, Schmidt 2014). In the Netherlands, drinking water is of high quality and As concentrations in drinking water are much lower than 10 μg/L (Ahmad et al. 2015). Drinking water companies in the Netherlands have recently established 1 μg/L as the guideline for As in drinking water based on dose-effect modelling of low-level As in Dutch drinking water which has shown that 10 μg/L is not sufficiently protective for the health of Dutch population (Ahmad et al. 2019b). In the Netherlands some of the water treatment plants (WTPs) produce drinking water with higher than 1 μg/L As and currently Dutch drinking water companies are investigating options to reduce As to <1 μg/L at these WTPs.

The overall objective of this study was to investigate As reduction to <1 μg/L by Advanced Oxidation – Coprecipitation – Filtration (AOCF) under different ion compositions and filtration conditions, as well as to gain mechanistic understanding of the process to determine the key guiding principles for full scale implementation.

AOCF is a promising As removal method. It involves dosing a strong oxidant (e.g. $NaMnO_4$) and an iron (Fe) based coagulant (e.g. $FeCl_3$) in water to remove As from water. The permanganate (MnO_4) rapidly oxidizes As(III) to As(V) and FeCl3 produces Fe(III)(oxyhydr)oxides in water that adsorb As(V) from water. The As bearing Fe(III)(oxyhydr)oxides are removed typically in a rapid sand filter. The As adsorption efficiency can be affected by the ionic composition of water. The most abundant oxyanions that may impact As(V) adsorption to Fe(III)(oxyhydr)oxides are silicate and phosphate (Meng et al. 2000, van Genuchten et al. 2012b, Van Genuchten et al. 2014b). Moreover, natural organic matter, especially the humic substances, can adversely affect As(V) adsorption to Fe(III)(oxyhydr)oxides (Davis and Edwards 2017, Sharma et al. 2010, Weng et al. 2009). These inorganic and organic solutes can modify the structure, composition and identity of the Fe(III)(oxyhydr)oxide precipitates, thereby affecting their size and As(V) uptake behaviour (Sposito 2008, Van Genuchten et al. 2014b). Moreover, these solutes compete with As(V) for adsorption sites on Fe(III)(oxyhydr)oxide precipitates (Chen et al. 2014, Dixit and Hering 2003, Hering et al. 1996, Meng et al. 2000, Su and Puls 2001, Weng et al. 2009, Wilkie and Hering 1996, Youngran et al. 2007). Calcium and magnesium ions in water, on the other hand, can increase As(V) removal during Fe(III) based co-precipitation. It has been shown that Ca increases the size of Fe(III)(oxyhydr)oxide precipitates (Ahmad et al. 2019a) and also results in an increased uptake of As(V) by Fe(III) precipitates. Most of the available studies of As removal by Fe based coprecipitation/adsorption have focused on the interactions between As(V) and Fe(III)(oxyhydr)oxide precipitates in simple solutions (Laky and Licskó 2011, Weng et al. 2008, Weng et al. 2009), whereas systematic studies providing understanding of the As(V)–Fe(III) interactions in complex multi-solute solutions are currently lacking. In this study, we aim to develop this understanding.

At a typical groundwater treatment plant that relies on atmospheric O2 (and microorganisms) for redox reactions, the dissolved Fe(II) in raw water oxidizes homogeneously, heterogeneously or biologically, or by a combination of these processes (Jessen et al. 2005, Van Beek et al. 2012, Vries et al. 2017). Oxidation of Mn(II) by dissolved O2 alone in a treatment plant is generally negligible because of the slow oxidation kinetics in the pH range of most groundwater streams (Diem and Stumm 1984, Lytle et al. 2005) and bacteria and surface catalysts on the filter media grains are known to transform Mn(II) to insoluble Mn(IV)-precipitates (Bruins et al. 2015, Katsoyiannis et al. 2008).

Permanganate is highly reactive and also a proven oxidant for Fe(II) and Mn(II) (Knocke et al. 1991). So when MnO4 dosing would be adopted at an existing treatment plant for As(III) oxidation ($3H_3AsO_3 + 2MnO_4^- \rightarrow 3H_2AsO_4^- + 2MnO_{2(s)} + H_2O + H^+$), it may also react with Fe(II) ($3Fe^{2+} + MnO_4^- + 7H_2O \rightarrow 3Fe(OH)_{3(s)} + MnO_{2(s)} + 5H^+$), Mn(II) ($3Mn^{2+} + 2MnO_4^- + 2H_2O \rightarrow 5MnO_{2(s)} + 4H^+$) and ammonium ($NH_4^+$) and change their established removal mechanisms in rapid sand filters. This can in turn have a profound impact on the operation of the rapid sand filters. MnO_4 dosing may not only have implications on the natural removal mechanisms of Fe(II), Mn(II), NH_4^+ and operation of the filter, but also the backwash water quality and treatment, as reported by some drinking water companies which have explored dosing MnO_4 for As removal at WTPs. The existing literature does not describe the potential implications of dosing MnO_4 at existing aeration-rapid sand filtration type treatment plants. In this study, we aim to address this lack of knowledge.

This project report is divided into 8 chapters, with each chapter reporting the details of a sub-study with the TKI-AOCF project. Following is an overview of the chapters and the scope of each chapter.

- Chapter 1: Introduction
- Chapter 2: Laboratory study on the characteristics of Fe and Mn bearing precipitates generated by Fe(II) and Mn(II) co-oxidation with O_2, MnO_4 and HOCl in the presence of groundwater ions
- Chapter 3: Laboratory study on assessing the impact of phosphate, silicate and natural organic matter on the size of Fe(III) precipitates and arsenate co-precipitation efficiency
- Chapter 4: Pilot study at WTP Dorst (Brabant Water) to investigate arsenic removal by permanganate—ferric treatment
- Chapter 5: Pilot study at WTP Katwijk (Dunea) to investigate arsenic removal by permanganate—ferric treatment
- Chapter 6: Pilot study at WTP Ouddorp (Evides) to investigate arsenic removal by permanganate—ferric treatment
- Chapter 7: This chapter describes a model for arsenic removal by coprecipitation with Fe(III)(oxyhydr)oxides
- Chapter 8: Conclusions and future work

References

Ahmad, A. and Bhattacharya, P. (2019) Arsenic in Drinking Water: Is 10 μg/L a Safe Limit? Current Pollution Reports.

Ahmad, A., Kools, S., Schriks, M., Stuyfzand, P. and Hofs, B. (2015) Arsenic and chromium concentrations and their speciation in groundwater resources and drinking water supply in the Netherlands p. 78, KWR Water Cycle Research Institute, Nieuwegein, The Netherlands.

Ahmad, A., van der Wal, B., Bhattacharya, P. and van Genuchten, C.M. (2019a) Characteristics of Fe and Mn bearing precipitates generated by Fe(II) and Mn(II) co-oxidation with O2, MnO4 and HOCl in the presence of groundwater ions. Water Research.

Ahmad, A., Van der Wens, P., Baken, K., De Waal, L., Bhattacharya, P. and Stuyfzand, P. (2019b) Arsenic reduction to <1 ug/L in Dutch drinking water. Environ Int.

Bruins, J.H., Petrusevski, B., Slokar, Y.M., Kruithof, J.C. and Kennedy, M.D. (2015) Manganese removal from groundwater: Characterization of filter media coating. Desalination and Water Treatment 55(7), 1851-1863.

Chen, C., Dynes, J.J., Wang, J., Karunakaran, C. and Sparks, D.L. (2014) Soft X-ray Spectromicroscopy Study of Mineral-Organic Matter Associations in Pasture Soil Clay Fractions. Environmental Science & Technology 48(12), 6678-6686.

Davis, C.C. and Edwards, M. (2017) Role of Calcium in the Coagulation of NOM with Ferric Chloride. Environmental Science & Technology 51(20), 11652-11659.

Diem, D. and Stumm, W. (1984) Is dissolved Mn^{+2} being oxidized by O_2 in absence of Mn-bacteria and surface catalysts? Geochimica et Cosmochimica Acta 48, 1571-1573.

Dixit, S. and Hering, J.G. (2003) Comparison of arsenic(V) and arsenic(III) sorption onto iron oxide minerals: Implications for arsenic mobility. Environmental Science and Technology 37(18), 4182-4189.

Herath, I., Vithanage, M., Bundschuh, J., Maity, J.P. and Bhattacharya, P. (2016) Natural Arsenic in Global Groundwaters: Distribution and Geochemical Triggers for Mobilization. Current Pollution Reports 2(1), 68-89.

Hering, J.G., Chen, P.-Y., Wilkie, J.A., Elimelech, M. and Liang, S. (1996) Arsenic removal by ferric chloride. American Water Works Association 88(4), 155-167.

Jessen, S., Larsen, F., Koch, C.B. and Arvin, E. (2005) Sorption and Desorption of Arsenic to Ferrihydrite in a Sand Filter. Environmental Science & Technology 39(20), 8045-8051.

Katsoyiannis, I.A., Zikoudi, A. and Hug, S.J. (2008) Arsenic removal from groundwaters containing iron, ammonium, manganese and phosphate: A case study from a treatment unit in northern Greece. Desalination 224(1-3), 330-339.

Knocke, W.R., Van Benschoten, J.E., Kearney, M.J., Soborski, A.W. and Reckhow, D.A. (1991) Kinetics of Manganese and Iron Oxidation by Potassium Permanganate and Chlorine Dioxide. AWWA 83(6), 80-87.

Kozisek, F. (2017) Best Practice Guide on the Control of Arsenic in Drinking Water. . Bhattacharya, P., Polya, D.A. and Jovanovic, D. (eds), IWA Publishing, London, UK.

Laky, D. and Licskó, I. (2011) Arsenic removal by ferric-chloride coagulation – effect of phosphate, bicarbonate and silicate. Water Science and Technology 64(5), 1046-1055.

Lytle, D.A., Sorg, T.J. and Snoeyink, V.L. (2005) Optimizing arsenic removal during iron removal: Theoretical and practical considerations. Journal of Water Supply: Research and Technology - AQUA 54(8), 545-560.

Meng, X., Bang, S. and Korfiatis, G.P. (2000) Effects of silicate, sulfate, and carbonate on arsenic removal by ferric chloride. Water Research 34(4), 1255-1261.

Mukherjee, A., Sengupta, M.K., Hossain, M.A., Ahamed, S., Das, B., Nayak, B., Lodh, D., Rahman, M.M. and Chakraborti, D. (2006) Arsenic contamination in groundwater: A global perspective with emphasis on the Asian scenario. Journal of Health, Population and Nutrition 24(2), 142-163.

Saint-Jacques, N., Brown, P., Nauta, L., Boxall, J., Parker, L. and Dummer, T.J.B. (2018) Estimating the risk of bladder and kidney cancer from exposure to low-levels of arsenic in drinking water, Nova Scotia, Canada. Environ Int 110, 95-104.

Schmidt, C.W. (2014) Low-Dose Arsenic: In Search of a Risk Threshold. Environ Health Perspect 122(5), A131-134.

Sharma, P., Ofner, J. and Kappler, A. (2010) Formation of Binary and Ternary Colloids and Dissolved Complexes of Organic Matter, Fe and As. Environmental Science & Technology 44(12), 4479-4485.

Smith, A.H., Hopenhayn-Rich, C., Bates, M.N., Goeden, H.M., Hertz-Picciotto, I., Duggan, H.M., Wood, R., Kosnett, M.J. and Smith, M.T. (1992) Cancer risks from arsenic in drinking water. Environ Health Perspect 97, 259-267.

Sposito, G. (2008) The Chemistry of Soils, Oxford University Press, New York.

Su, C. and Puls, R.W. (2001) Arsenate and Arsenite Removal by Zerovalent Iron: Effects of Phosphate, Silicate, Carbonate, Borate, Sulfate, Chromate, Molybdate, and Nitrate, Relative to Chloride. Environ. Sci. Technol. 35(22), 4562-4568.

Van Beek, C.G.E.M., Hiemstra, T., Hofs, B., Bederlof, M.M., van Paassen, J.A.M. and Reijnen, G.K. (2012) Homogeneous, heterogeneous and biological oxidation of iron(II) in rapid sand filtration. Journal of Water Supply: Research and Technology—AQUA 61(1), 1-2012.

van Genuchten, C.M., Addy, S.E.A., Peña, J. and Gadgil, A.J. (2012) Removing Arsenic from Synthetic Groundwater with Iron Electrocoagulation: An Fe and As K-Edge EXAFS Study. Environmental Science & Technology 46(2), 986-994.

Van Genuchten, C.M., Pena, J., Amrose S, E. and Gadgil, A.J. (2014) Structure of Fe(III) precipitates genberated by the electrolytric dissolution of Fe(0) in the presence of groundwater ions. Geochimica et Cosmochimica Acta 127, 285-304.

Vries, D., Bertelkamp, C., Schoonenberg Kegel, F., Hofs, B., Dusseldorp, J., Bruins, J.H., de Vet, W. and van den Akker, B. (2017) Iron and manganese removal: Recent advances in modelling treatment efficiency by rapid sand filtration. Water Research 109, 35-45.

Weng, L., Van Riemsdijk, W.H. and Hiemstra, T. (2008) Humic nanoparticles at the oxide-water interface: Interactions with phosphate ion adsorption. Environmental Science and Technology 42(23), 8747-8752.

Weng, L., Van Riemsdijk, W.H. and Hiemstra, T. (2009) Effects of Fulvic and Humic Acids on Arsenate Adsorption to Goethite: Experiments and Modeling. Environmental Science & Technology 43(19), 7198-7204.

Wilkie, J.A. and Hering, J.G. (1996) Adsorption of arsenic onto hydrous ferric oxide: effects of adsorbate/adsorbent ratios and co-occurring solutes. Colloids and Surfaces A: Physicochemical and Engineering Aspects 107, 97-110.

Youngran, J., Fan, M., Van Leeuwen, J. and Belczyk, J.F. (2007) Effect of competing solutes on arsenic(V) adsorption using iron and aluminum oxides. Journal of Environmental Sciences 19(8), 910-919.

2 Characteristics of Fe and Mn bearing precipitates generated by Fe(II) and Mn(II) co-oxidation with O_2, MnO_4 and HOCl in the presence of groundwater ions

This chapter has been published as:

Ahmad, A., van der Wal, B., Bhattacharya, P., & van Genuchten, C. M. (2019). Characteristics of Fe and Mn bearing precipitates generated by Fe(II) and Mn(II) co-oxidation with O2, MnO4 and HOCl in the presence of groundwater ions. Water Research. 161, 505-516

2.1 Introduction

Groundwater is treated by aeration followed by rapid sand filtration to remove dissolved iron (Fe(II)) and manganese (Mn(II)) to avoid sedimentation in distribution pipelines and discoloration issues (Vries et al. 2017). Aeration saturates the groundwater with dissolved oxygen (O_2), which facilitates oxidation and precipitation of Fe and Mn solids. The Fe and Mn bearing precipitates accumulate in filters until backwashing is applied to dislodge the solids from the filtration media. While O_2 is often capable of oxidizing Fe(II) on the time scale of typical groundwater treatment, O_2 alone is ineffective at oxidizing Mn(II) to Mn(III,IV) and As(III) to As(V), the more easily removed arsenic species (Diem and Stumm 1984, Gude et al. 2016, Van Beek et al. 2012). To rapidly oxidize Mn(II) and As(III) at water treatment plants, stronger chemical oxidants, such NaOCl or $KMnO_4$, can be used (Ahmad et al. 2018, Sorlini and Gialdini 2010).

Although chemical oxidants (i.e. NaOCl and $KMnO_4$) can improve co-oxidative removal of Fe(II), Mn(II) and As(III), little is known about how different oxidants impact key properties of the solid end-products, including the structure, composition and crystallinity. These differences are important because poorly-ordered Fe(III) (oxyhydr)oxides have a higher specific surface area than crystalline solids, which would increase sorption of ions (e.g. As) per mass of Fe. Similarly, poorly-ordered Mn(IV) oxides are favoured when microorganisms oxidize Mn(II) rapidly, whereas Mn(III) oxides can form from slow, surface-catalyzed Mn(II) oxidation by O_2 (Lan et al. 2017, Tebo et al. 2005).

In addition to the type of chemical oxidant, the structure of Fe and Mn bearing solids can also be altered by the presence of common groundwater ions, such as silicate (Si), phosphate (P), As, and calcium (Ca). By binding strongly to precipitate surfaces, P and Si oxyanions can inhibit crystal growth, leading to poorly-ordered solids (Kaegi et al. 2010, Senn et al. 2017). Moreover, Si and P oxyanions can decrease the particle surface charge, which strongly influences particle aggregation and sedimentation efficiency (Sposito 2008), whereas Ca can counteract the effects of P and Si.

We combined macroscopic measurements of aggregation and sedimentation (i.e. turbidity and filterability) with Fe and Mn K-edge X-ray absorption spectroscopy to investigate the solids formed by Fe(II) and Mn(II) co-oxidation with O_2, MnO_4, and HOCl. We performed batch Fe(II) and Mn(II) co-oxidation experiments in solutions with systematically varied concentrations of As, P, Si, and Ca. The knowledge generated in this study is critical to select the most effective oxidant in groundwater treatment, considering the co-removal of Fe(II), Mn(II) and As(III) and the aggregation properties of the end-products.

2.2 Materials and methods

2.2.1 Chemicals

All chemicals were reagent grade. The stock solutions for Fe(II), Mn(II) and HOCl were prepared by dissolving 24.9 g/L $FeSO_4{\cdot}7H_2O$ (Boom BV®), 1.8 g/L $MnCl_2$ (Merck®) and 4.66 g/L NaOCl (Acors Organics®) in 100 mL oxygen-free ultrapure water (18.2 MΩ cm, Purelab® Chorus: Veolia Water). The stock solutions for Si, HCO_3, NaCl and MnO_4 were prepared by dissolving 75.7 g/L $Na_2SiO_3{\cdot}5H_2O$ (Aldrich®), 0.87 g/L $NaHCO_3$ (J.T. Baker®), 0.26 g/L NaCl (J.T. Baker®) and 6.3 g/L $KMnO_4$ (J.T. Baker®) in ultrapure water. The stock solutions for P and Ca were obtained by dissolving 1.11 g/L $NaH_2PO_4{\cdot}H_2O$ (J.T. Baker®) and 138.5 g/L $CaCl_2$ (J.T. Baker®) in 0.1 M HCl. For As(III) addition, a certified solution (1000 mg As(III)/L, Inorganic ventures®) set in HCl matrix was used without any dilution. The concentration of the As(III) stock was 1000 mg/L. For pH control during the experiments, 0.1 M NaOH and 0.1 M HCl solutions were used.

2.2.2 Experiments

Experiments were performed with a 5 L glass reactor connected to a controller (ez-Control, Applikon® Biotechnology) for adjusting, maintaining and logging (BioXpertV2 software) reaction parameters, including the pH, temperature, oxidant supply and stirring speed (Figure 1). The experiments were carried out at pH 7.5 and 20ºC, with stirring set to 100 rpm. Fe(II), Mn(II) and As(III) oxidation was initiated by dosing O_2, $KMnO_4$ or NaOCl to anaerobic solutions that initially contained Fe(II), Mn(II), As(III), Si, P and Ca in different concentrations (Table 1). The range of ionic compositions studied in this work was derived from an analysis of groundwater quality in the Netherlands (Ahmad et al. 2015). For each oxidant, the initial solutions in the reference experiments (herein referred to as Ref) contained 90 µM Fe(II) (5.0 mg/L), 9.0 µM Mn(II) (0.5 mg/L) and 0.7 µM As(III) (0.05 mg/L) without Si, P and Ca. In Mn18 experiments, the initial solution contained 18 µM Mn instead of 9 µM Mn. The rest of the experiments are identified by the ions added in µM to the Ref solution (i.e. Si150 consists of 150 µM Si, 90 µM Fe(II), 9.0 µM Mn(II) and 0.7 µM As(III)). All solutions also contained 2.5 mM $NaHCO_3$ and 0.6 mM NaCl to provide alkalinity and ionic strength.

For the O_2 experiments, the initial solutions were bubbled with air to reach saturation (≈9 mg O_2/L). For MnO_4 and HOCl systems, the doses of the $KMnO_4$ and NaOCl stocks were based on the combined stoichiometric demand of Fe(II), Mn(II) and As(III) oxidation to produce Fe(III), Mn(IV) and As(V), respectively (Ghurye and Clifford 2001).

The experimental procedure included: (i) preparation of the initial solutions in the reaction vessel under anaerobic conditions, (ii) dosing the oxidant (O_2, MnO_4 or HOCl) and allowing for oxidation and precipitation while stirring at 100 rpm and (iii) collection of suspension samples 30 min after oxidant addition, which were filtered over 0.45 µm filters and stored for subsequent analysis. A 30 min reaction interval was selected based on PHREEQC simulations showing complete Fe(II) oxidation in the O_2 system in 30 min. Samples for aqueous and total Fe and Mn were collected in 100 mL plastic bottles that contained 0.5 mL of 65% HNO_3 and were stored at 4 ºC until analysis by Inductively Coupled Plasma Mass Spectrometry (ICP-MS) (Thermo Scientific XSERIES 2 ICP-MS, Thermo Fisher Scientific, Breda, The Netherlands) at Aqualab Zuid B.V. in The Netherlands. The removal of Mn and Fe and the Mn/Fe solid ratios (mol/mol) were determined from the difference between the Fe and Mn concentrations of the initial and final filtered solutions. Solids generated in each experiment were also collected and reserved for XAS analysis.

The aggregation and settling characteristics of the particles were studied by measuring the turbidity of the suspensions as a function of time using a 2100Q Portable Turbidimeter, Hach® USA. Following the addition of oxidant and 30 min of mixing, the turbidity of the suspension was measured by removing an aliquot 5 cm below the water surface during mixing. After the initial turbidity measurement, the stirring was stopped and the suspension was allowed to settle by gravity. A second turbidity measurement was made after 1 h of settling by removing another aliquot 5 cm below the water surface. The turbidity measurement vessel was rinsed twice with ultrapure water and oxalic acid (pH 1-3) between measurements.

2.2.3 X-ray absorption spectroscopy

2.2.3.1 Data collection

X-ray absorption spectra at the Fe and Mn K-edges were collected at room temperature at beamline 4-1 of the Stanford Synchrotron Radiation Lightsource (SSRL) and the DUBBLE beamline (BM-26a) of the European Synchrotron Radiation Facility (ESRF). The design of the DUBBLE beamline is described by Borsboom et al., (1998) and Nikitenko et al., (2008). Fe K-edge XAS data were recorded in transmission mode out to *k* of 13 Å^{-1}. Mn K-edge XAS data were collected in transmission and fluorescence modes out to *k* of 12 Å^{-1}, with spectra of superior data quality selected for subsequent analysis. Fe(0) or Mn(0) foils were used to calibrate the beam at 7112 eV or 6539 eV, respectively. Spectra were aligned, averaged and background-subtracted using SixPack software (Webb 2005) following standard methods described previously (van Genuchten et al. 2012a). The k^3-weighted EXAFS spectra ($\chi(k)k^3$) were Fourier-transformed using a Kaiser-Bessel window with dk of 3 Å^{-1} typically over the *k*-range 2 – 12 Å^{-1} for the Fe spectra and 2 – 10.5 Å^{-1} for the Mn spectra.

2.2.3.2 Data Analysis

The Fe K-edge EXAFS spectra were analyzed by principal component analysis (PCA) and linear combination fits (LCFs). For the PCA, the ITFA program suite (Rossberg et al. 2003, Scheinost et al. 2006) was used to determine the number of independent components that reproduced the major variance of the data set based on minimizing the indicator (IND) function. The LCFs were performed with the SixPack software (Webb 2005) using the EXAFS spectra of Fe(III)-bearing standard minerals. Details on the synthesis of these standards (e.g. lepidocrocite, 2-line ferrihydrite, oxyanion-rich hydrous ferric oxide) are reported elsewhere (van Genuchten et al. 2018, Van Genuchten et al. 2014b) The fit-derived fractions of the standards in each sample were normalized to one.

The Mn K-edge XANES spectra were analyzed by LCFs to determine the fraction of solid-associated Mn(II), Mn(III), and Mn(IV). SixPack software was used to perform the LCFs on the normalized XANES spectra, with a fit range of 6530 to 6590 eV. The Mn K-edge EXAFS spectra of representative samples were analyzed by shell-by-shell fits. Since the presence of multiple Mn oxidation states in a single sample complicates the interpretation of shell-by-shell fits, we applied this approach on samples that were determined by XANES LCFs to consist of primarily a single oxidation state (i.e. Mn(II), Mn(III), or Mn(IV)). Theoretical curve fits were performed in $R+\Delta R$-space (Å) using the SixPack software with algorithms based on the IFEFFIT library (Newville 2001). Single scattering paths (Mn-O, Mn-Mn) were derived from the structure of birnessite (MnO_2) (Lanson et al. 2002), with theoretical phase and amplitude functions calculated using FEFF6 (Rehr et al. 1992). Because Mn and Fe have similar atomic numbers, these backscattering atoms cannot be distinguished in shell-by-shell fits. Consequently, the second shell fitting results for the Mn data are reported as $CN_{Mn\text{-}Mn/Fe}$ and $R_{Mn\text{-}Mn/Fe}$. The goodness-of-fit was assessed based on the R-factor, which is the mean square difference between the fit and the data on a point-by-point basis: $R = \sum_i (data_i - fit_i)^2 / \sum_i (data_i)^2$. A reasonable fit is considered to yield an R-factor less than 0.05 (Kelly et al. 2008). A similar shell-by-shell fitting approach was followed for select Fe spectra.

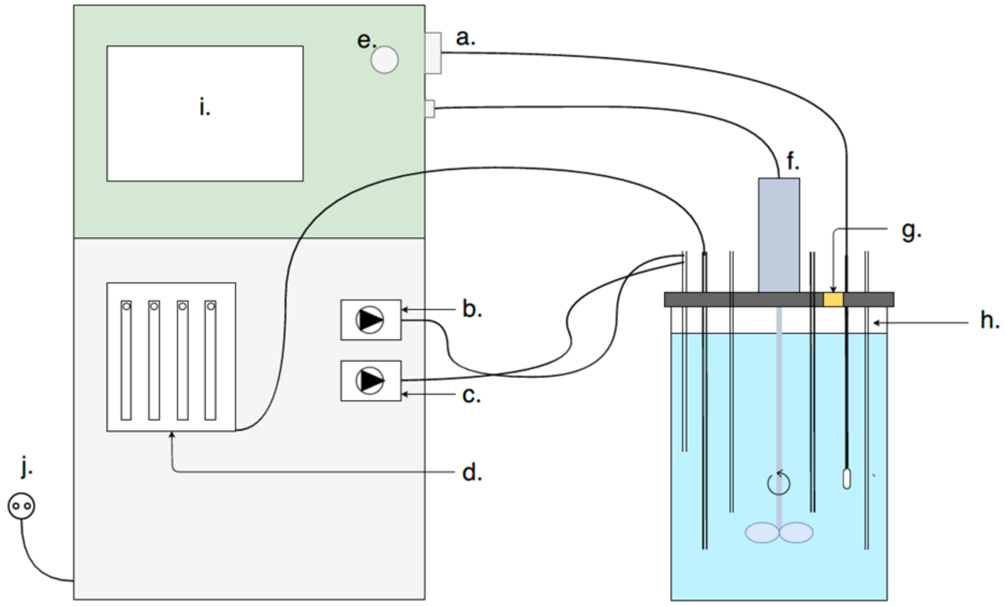

Figure 1. A schematic overview of the assembly used in precipitation and settling experiments. a. data logger (pH. temperature. dissolved oxygen); b. acid pump; c. alkali pump; d. nitrogen and air supply; e. on/off; f. stirrer; g. chemical injection port; h. sampling port; i. controller display; j. power supply.

Table 1: Nomenclature, initial composition, Fe and Mn removed by 0.45 µm filtration and solids ratio in O_2, MnO_4 and HOCl experiments.

Experiment code	Initial solution composition										Fe and Mn removed by 0.45 µm filter						Solids ratio		
											O_2		MnO_4		HOCl		O_2	MnO_4	HOCl
	Fe	Mn	As	Si	P	Ca	Mn/Fe	As/Fe	Si/Fe	P/Fe	Ca/Fe	Fe	Mn	Fe	Mn	Fe	Mn	Mn/Fe	Mn/Fe	Mn/Fe
	(µmol/L)						(molar ratio)					(%)		(%)		(%)		(molar ratio)		
Ref	90	9	0.7	–	–	–	0.1	0.008	–	–	–	99.9	18.6	54.5	44.8	99.1	79.6	0.01	0.50	0.08
Mn18	90	18	0.7	–	–	–	0.2	0.008	–	–	–	99.9	8.2	6.1	55.6	98.3	83.2	0.02	x	0.18
Si150	90	9	0.7	150	–	–	0.1	0.008	1.7	–	–	67.4	16.0	27.0	23.0	80.7	57.4	0.03	0.53	0.08
Si350	90	9	0.7	350	–	–	0.1	0.008	3.9	–	–	2.2	5.8	*	*	35.4	28.6	x	*	0.08
Si750	90	9	0.7	750	–	–	0.1	0.008	8.3	–	–	0.0	1.9	4.8	16.6	12.0	12.0	x	x	x
Si350 + Ca500	90	9	0.7	350	–	500	0.1	0.008	3.9	–	6	96.8	26.0	99.8	93.2	97.7	47.2	0.03	0.53	0.05
Si750 + Ca1000	90	9	0.7	750	–	1000	0.1	0.008	8.3	–	11	95.7	16.8	99.8	92.4	95.8	45.9	0.02	0.56	0.05
Si750 + Ca2500	90	9	0.7	750	–	2500	0.1	0.008	8.3	–	28	92.1	13.0	99.9	93.0	97.7	50.5	0.01	0.56	0.06
P4	90	9	0.7	–	4	–	0.1	0.008	–	0.04	–	98.9	30.0	34.7	24.1	98.4	75.1	0.03	0.52	0.08
P10	90	9	0.7	–	10	–	0.1	0.008	–	0.11	–	96.8	36.7	9.3	9.8	96.5	68.0	0.04	x	0.08
P16	90	9	0.7	–	16	–	0.1	0.008	–	0.18	–	89.0	39.0	0.0	4.4	75.1	51.4	0.05	x	0.08
P16 + Ca1000	90	9	0.7	–	16	1000	0.1	0.008	–	0.18	11	99.9	14.8	99.9	87.2	99.9	50.0	0.02	0.54	0.05

* Data not available

x Not determined because of low precipitate retention

The (range of) concentration of Fe, Mn, As, Si, P and Ca in the initial solution in mg/L was 5.0, 0.5, 0.05, 0.5—1.0, 5.0—20, 0.1—0.5 and 20—100 , respectively.

2.3 Results

2.3.1 Macroscopic precipitate properties

2.3.1.1 Settling and filterability

In the O_2 system, the Ref and Mn18 experiments had an initial turbidity of ≈8 NTU (Figure 2) and a similarly low final turbidity of <3 NTU (≈70% turbidity decrease), which indicates rapid flocculation and sedimentation. These particles were highly filterable (>99%) by 0.45 µm filters (pore size used to approximate filterable particles in rapid sand filters). The addition of 150 to 750 µM Si decreased the initial turbidity from 6 to 2 NTU, resulting in translucent light yellow suspensions that were colloidally stable (i.e. no difference in initial and final turbidity, Figure 2A, and low filterability, Table 1). The addition of Ca to the 350 and 750 µM Si solutions increased the initial turbidity to match the Ref O_2 sample, but the final turbidity was higher than the Ref O_2 sample. In the P series, 4 and 10 µM P did not alter significantly the initial or final turbidity relative to the Ref O_2 sample and the precipitates settled effectively (≈65% turbidity decrease). However, the 16 µM P experiment resulted in a colloidally stable suspension. When 1000 µM Ca was added to the 16 µM P solution, the suspension had the highest initial turbidity in the O_2 experiments (14 NTU), with effective turbidity reduction (70%) and good filterability (>99% Fe removed, Table 1).

The settling behavior and filterability of the precipitates formed in the MnO_4 system (Figure 2B, Table 1) differed considerably from those in the O_2 system. The darker Ref and Mn18 suspensions formed in the MnO_4 system were colloidally stable, having initial and final turbidity >5.5 NTU, which contrasts the rapid settling of the Ref O_2 sample. The 150 to 750 µM Si samples in the MnO_4 system were also colloidally stable, but the initial turbidity was slightly lower than the Ref MnO_4 sample. The addition of Ca to the Si solutions produced visually cloudy suspensions that settled more effectively (≈60% turbidity decrease) than the Ca+Si samples in the O_2 system. The 4, 10 and 16 µM P samples in the MnO_4 system were all colloidally stable (turbidity = 3 to 5 NTU) with low filterability (Table 1). Similar to the O_2 system, P16+Ca1000 sample in the MnO_4 system had an higher initial turbidity (≈8 NTU) and improved particle settling (70% turbidity reduction) and filterability (>99% Fe removed).

In the HOCl system (Figure 2C), the initial turbidity of all suspensions (<4 NTU) was systematically lower than the O_2 or MnO_4 systems. The Ref and Mn18 HOCl suspensions were light yellow with visible flocs that settled quickly and were effectively filtered (≈90%), despite their low initial turbidity. The 150 to 750 µM Si samples were colloidally stable, similar to the O_2 and MnO_4 systems. When Ca was added to the Si solutions, turbidity removal improved (20%), but was lower than the Ref HOCl sample. The HOCl experiments in P solutions resembled the O_2 system more than the MnO_4 system, with 46% and 41% decreases in turbidity for P4 and P10 samples, but only 8% for the P16 sample. The impact of Ca in P solutions was similar in all HOCl, O_2 and MnO_4 systems, with the P16+Ca1000 sample displaying increased aggregation and sedimentation (40% turbidity decrease).

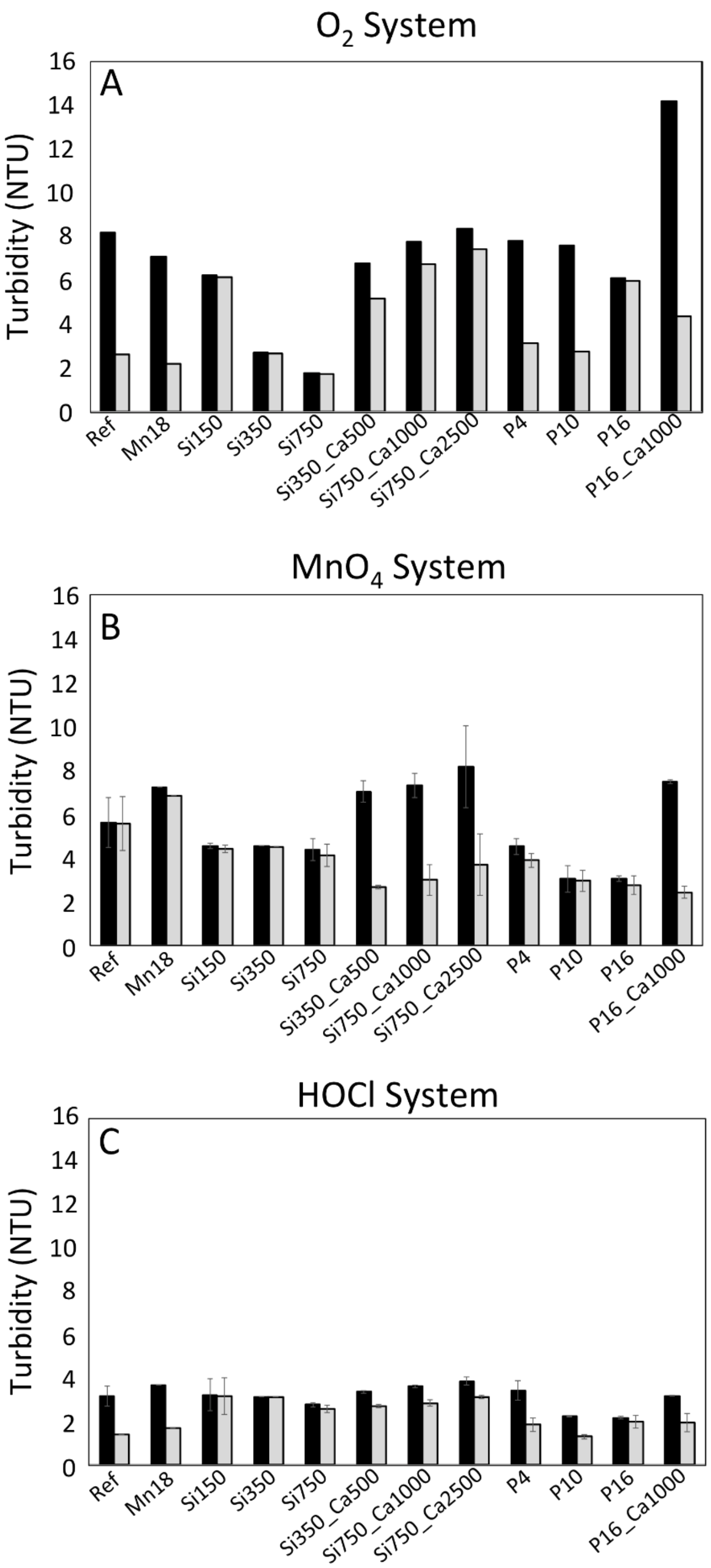

Figure 2. Initial and final turbidity as function of the oxidant used and solution composition. A. O_2 system, B. MnO_4 system, C. HOCl system.

2.3.2 Mn/Fe solid ratios

In the O_2 system, the precipitate Mn/Fe ratio content was low (≤0.05) and varied with solution composition. The Mn/Fe ratio of the Ref experiment was 0.01 mol/mol, which doubled to 0.02 mol/mol in the Mn18 experiment, matching the doubled initial Mn concentration. The presence of Si and P increased the precipitate Mn content, with the Si150 and P16 samples having solids ratios of 0.03 mol/mol and 0.05 mol/mol, respecitvely. By contrast, Ca addition decreased the Mn/Fe ratio. The precipitate Mn content was only 0.02 mol/mol in the P16+Ca1000 sample.

In MnO_4 system the Mn/Fe ratio ranged from 0.5 to 0.55, with no significant trends in the presence of Si, P and Ca. The higher Mn/Fe ratio relative to the O_2 and HOCl systems is attributed to the dosing of MnO_4, which increased the total Mn concentration (not shown in Fig 3).

In the HOCl system, the precipitate Mn/Fe ratio was higher than in the O_2 system, indicating more effective Mn uptake. The Mn/Fe ratio of the Ref and Mn18 experiments was 0.08 and 0.18 mol/mol, which was near the total Mn/Fe ratio dosed into solution. The presence of Si and P did not impact significantly the Mn/Fe ratio in the HOCl system (Table 1), with Mn/Fe ratios of ≈0.08 mol/mol for the Si350 and P16 samples. However, Ca addition decreased Mn uptake, leading to an Mn/Fe solids ratio of 0.05 mol/mol for the Si350+Ca500 and P16+Ca1000 samples.

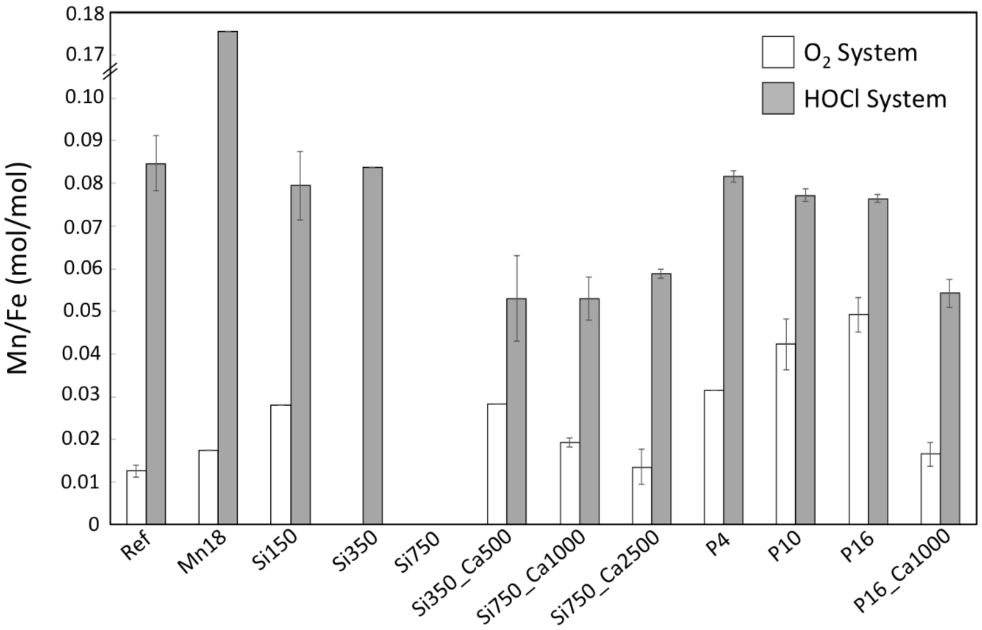

Figure 3. Precipitate Mn/Fe ratio (mol/mol). Samples without data were colloidally stable and could not to be separated with 0.45 µm filters. The Mn/Fe ratio was between 0.5 and 0.55 for all the samples in MnO_4 system and is thus not given. Note the break in the y-axis from 0.10 to 0.17 mol/mol.

2.3.3 Fe K-edge EXAFS spectroscopy

Principal component analysis (PCA) of the Fe K-edge EXAFS spectra of the entire data set (O_2, MnO_4, and HOCl systems) revealed a significant decrease in the indicator function with three independent components and a gradual plateau in the indicator function with increasing components. Based on the PCA results and the experimental conditions, we used three Fe(III) (oxyhydr)oxide standards in the linear combination fits (LCFs) of the experimental spectra: lepidocrocite (γ-FeOOH), 2-line ferrihydrite (2LFh), and an oxyanion-rich hydrous ferric oxide (oxy-HFO) that was produced by Fe(II) oxidation in the presence of P and that contains no Fe-Fe corner-sharing bonds (Van Genuchten et al. 2014b). The LCF output is overlain to the data in Figure 4 and results of the LCFs of the experimental spectra using lepidocrocite, 2LFh, and oxy-HFO are given Figure 5.

The Ref and Mn18 experiments in the O_2 system consisted of dominantly lepidocrocite (>85%). The minor fraction (<15%) of oxy-HFO determined in the LCFs of these samples likely arises from subtle differences in the structure of the lepidocrocite standard and the type of lepidocrocite formed in the experiments (Van Genuchten et al. 2014b, Voegelin et al. 2010). Lepidocrocite formation was largely inhibited in the presence of Si, with the LCFs of all Si series samples returning fractions of 15 to 26% oxy-HFO and 72 to 82% 2LFh without clear trends in the fractions oxy-HFO and 2LFh with increasing Si or presence of Ca. In the P experiments, the LCFs indicated the formation of lepidocrocite, but its fraction depended on the P concentration (i.e. P/Fe ratio). Increasing P from 4 to 16 µM decreased the lepidocrocite fraction from 64 to 27%, which was balanced by an increase in oxy-HFO from 16 to 37% (the 2LFh fraction was stable at ≈30%). The addition of Ca to the P16 solution increased the lepidocrocite fraction from 27 to 55% at the expense of oxy-HFO and 2LFh. This impact of Ca on the Fe(II) oxidation products in the P solutions is consistent with the sequential formation of Ca- and P-rich Fe(III) polymers (Voegelin et al. 2010) which remove P from solution with P/Fe ratios near 1, followed by lepidocrocite formation with excess Fe(II) after P is removed from solution.

In contrast to the O_2 experiments, no sample in the MnO_4 system consisted of lepidocrocite, regardless of solution composition. The LCFs indicated poorly-ordered Fe(III) precipitates formed in MnO_4 experiments, which had average structures consistent with mixtures of 2LFh and oxy-HFO (30 to 73% oxy-HFO, 25 to 69% 2LFh). Increasing the Si concentration from 150 to 750 µM increased the fraction of oxy-HFO from 32 to 60%, with 2LFh making up the remainder. The Fe(III) precipitates formed from Fe(II) oxidation by MnO_4 in P solutions were similar to those in Si solutions, with the LCFs yielding mixtures of 2LFh and oxy-HFO without clear trends in the presence of Ca.

In the HOCl system, lepidocrocite was not detected in any sample. The LCFs of the Ref sample yielded 53% oxy-HFO and 40% 2LFh, whereas the Mn18 sample consisted of 40% oxy-HFO and 54% 2LFh. Although P and Si increased the fraction of poorly-ordered Fe(III) precipitates in the O_2 system, the analogous trend was not observed in the HOCl system. No trends in the fractions of 2LFh and oxy-rich HFO with increasing Si or P were observed in the HOCl samples. Comparing the LCFs across all oxidants (i.e. O_2, MnO_4, and HOCl) reveals that Si and P impacted Fe(III) speciation in the O_2 experiments more than in MnO_4 and HOCl experiments.

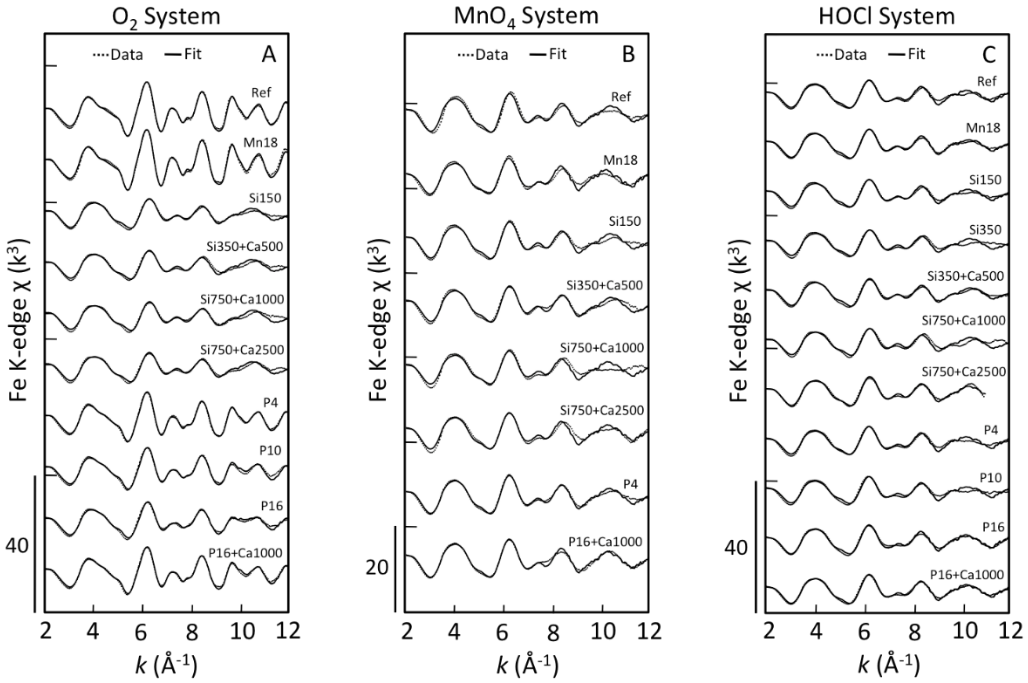

Figure 4. Fe K-edge EXAFS spectra of precipitate samples (dotted lines) and output of linear combination fits (solid lines) using lepidocrocite, 2-line ferrihydrite, and oxyanion-rich hydrous ferric oxide.

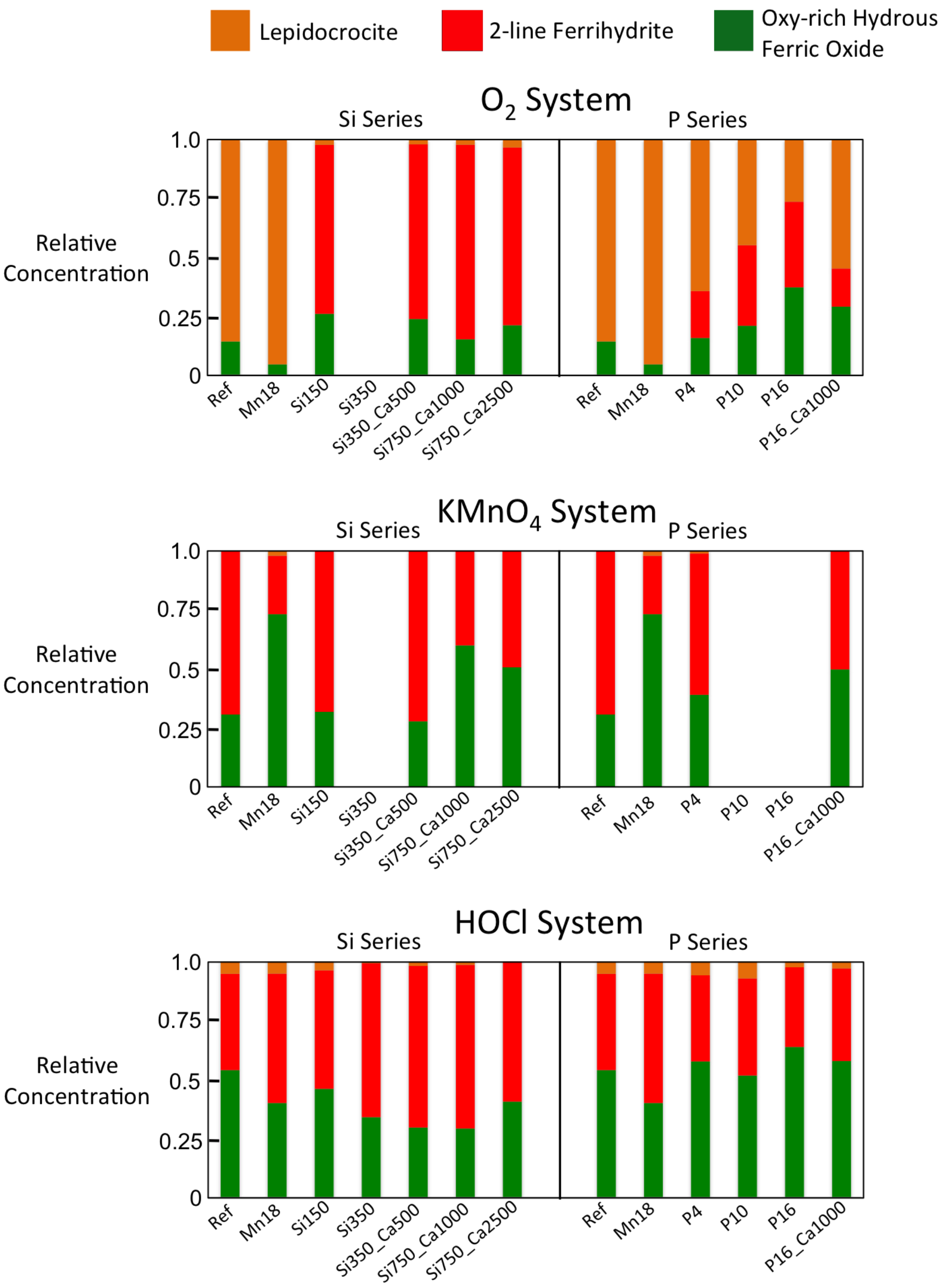

Figure 5. Relative concentrations of lepidocrocite (brown bars), 2-line ferrihydrite (red bars), and oxyanion-rich hydrous ferric oxide (green bars) derived by linear combination fits for each precipitate sample. Samples without data were colloidally stable and could not to be separated with 0.45 µm filters. (For interpretation of the references to color in this figure legend, the reader is referred to the Web version of this article.)

2.3.4 Mn K-edge XANES spectroscopy

The Mn K-edge XANES LCFs of the Ref O_2 sample (Figure 6, Table 2) indicated that Mn(III) was the dominant species (96±3%) in the solids, consistent with the absorption maximum near 6556 eV. However, the Si150 sample displayed an absorption maximum at lower X-ray energy (6552 eV) and the LCFs indicated Mn(II) was the dominant species (Mn(II) = 75±2%, Mn(III) = 26±4%). The trend in increased Mn(II) in the presence of oxyanions was also observed in the P16 experiment, which consisted of 85±3% Mn(II), with Mn(III) making up the remainder. When Ca was added to the P16 electrolyte, the LCFs indicated a significant decrease in solid-associated Mn(II) (52±3%) and an increase in Mn(III) (45±5%). The presence of Mn(IV) was not supported by the LCFs of any O_2 samples.

The XANES spectra of the MnO_4 samples were largely independent of solution chemistry, with >98% Mn(IV) detected by the LCFs in all samples (absorption maximum near 6558 eV). While the LCFs returned a small fraction of Mn(III) in some samples (<20%), the standard deviation was nearly as high as the fit-derived value (Table 2). No clear trends in the Mn oxidation state with Si, P, or Ca were detected in the LCFs of the MnO_4 samples. The presence of residual, unreacted Mn(VII), which has a prominent pre-edge peak near 6541 eV, was not supported by the XANES spectra.

Co-oxidation of Fe(II) and Mn(II) by HOCl produced primarily Mn(III) in the Ref and Mn18 samples, with a slight increase in the Mn(IV) fraction from 15±10% in the Ref sample to 23±11% in the Mn18 sample. The LCFs of the Si150 sample indicated that Mn(III) remained the dominant solid-phase Mn species (>85%). At P concentrations of 4 and 16 µM, the solid-phase Mn(II) fraction increased from 9±5 to 41±4%. When Ca was added to the P16 solution, the solid-phase Mn(II) fraction decreased from 41±4 to 14±5%. A similar decrease in Mn(II) fraction in favor of Mn(III) was observed in the O_2 experiments when Ca was added to the P16 solution.

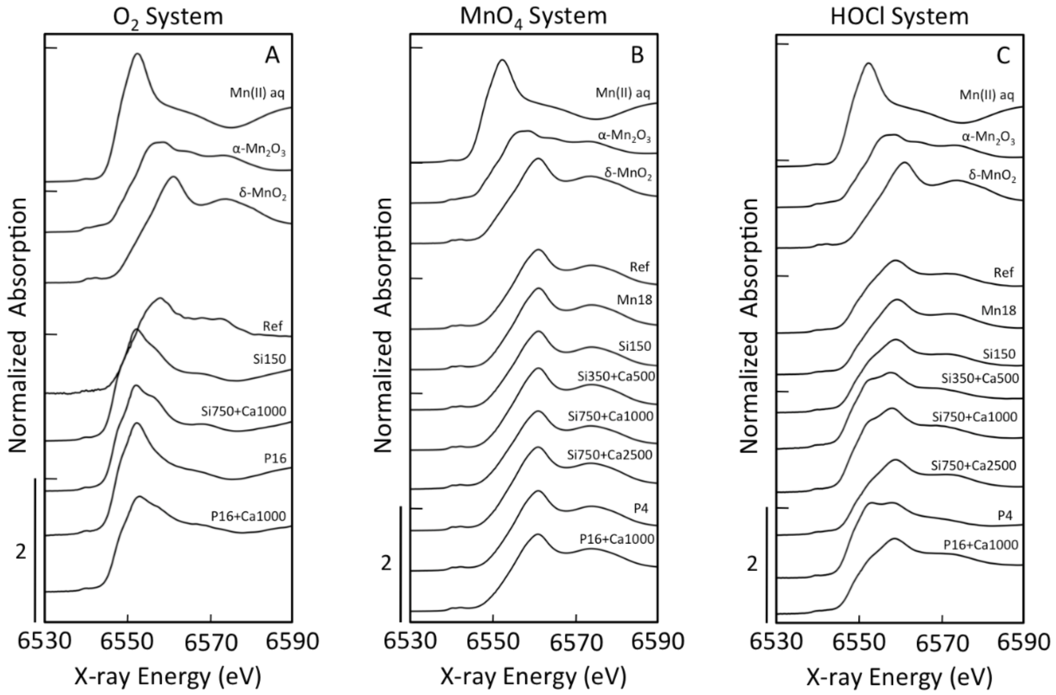

Figure 6. Mn K-edge XANES spectra for precipitate samples formed in the O_2 (left panel), MnO_4 (middle panel) and HOCl (right panel) experiments. The experimental data is plotted below Mn(II), Mn(III), and Mn(IV) standards.

Table 2: Summary of XANES LCF Results

Oxidant	Experiment Code	% Mn^{2+}	% Mn^{3+}	% Mn^{4+}
O_2 System	Ref	<1	96 ± 3	<1
	Si150	75 ± 2	26 ± 4	<1
	Si750 + Ca1000	65 ± 3	35 ± 5	<1
	P16	85 ± 3	20 ± 4	<1
	P16 + Ca1000	52 ± 3	45 ± 5	<1
MnO_4 System	Ref	<1	8 ± 8	106 ± 15
	Mn18	<1	6 ± 7	109 ± 15
	Si150	<1	7 ± 8	105 ± 14
	Si350 + Ca500	<1	8 ± 9	108 ± 14
	Si750 + Ca1000	<1	16 ± 6	99 ± 16
	Si750 + Ca2500	<1	17 ± 8	102 ± 14
	P4	<1	10 ± 7	104 ± 15
	P16 + Ca1000	<1	13 ± 6	98 ± 15
HOCl System	Ref	5 ± 4	84 ± 16	15 ± 10
	Mn18	<1	79 ± 15	23 ± 11
	Si150	11 ± 5	85 ± 18	10 ± 11
	Si750 + Ca1000	33 ± 8	85 ± 12	<1
	Si750 + Ca2500	27 ± 6	95 ± 11	<1
	P4	9 ± 5	87 ± 18	11 ± 12
	P16	41 ± 4	63 ± 11	3 ± 4
	P16 + Ca1000	14 ± 5	88 ± 18	10 ± 11

2.3.5 Mn K-edge EXAFS spectroscopy

2.3.5.1 O_2 experiments

In Figure 7, the Mn K-edge EXAFS spectra of samples produced in the O_2, MnO_4, and HOCl experiments are shown alongside the spectra of Mn standards. The Ref O_2 sample, which was found by the LCFs to be dominantly Mn(III), differed relative to the other spectra in Figure 7, including the aqueous Mn(II), bixbyite (α-Mn_2O_3) and δ-MnO_2 standards. In particular, the first oscillation from 3 to 5.5 $Å^{-1}$ became a doublet, which is not present in other Mn(III)-bearing material (e.g. groutite, manganite, feitnechtite) (Manceau et al. 2012). Furthermore, the next major peaks at 6.2 and 7.5 $Å^1$ in the Ref O_2 sample are out of phase with the standards, which suggests a unique Mn coordination environment. In the presence of P and Si, the EXAFS oscillations for the O_2 samples match more closely those of aqueous Mn(II), which is consistent with the XANES-derived predominance of Mn(II) in these samples.

Shell-by-shell fits of the Fourier-transformed Mn K-edge EXAFS spectrum of the Ref O_2 sample (Figure 8, Table 3) returned an Mn-O interatomic distance ($R_{Mn\text{-}O}$) of 1.93±0.02 Å and an Mn-O coordination number ($CN_{Mn\text{-}O}$) of 1.9±0.5, which is lower than the theoretical CN of 6 for octahedrally coordinated Mn(III). These fit-derived $R_{Mn\text{-}O}$ and $CN_{Mn\text{-}O}$ values matched the first shell fits of bixbyite ($R_{Mn\text{-}O}$ = 1.92±0.02 Å, $CN_{Mn\text{-}O}$ = 2.4±0.5) and are consistent Jahn-Teller distorted Mn(III) octahedra. Fits of the second shell of the Ref O_2 sample resulted in a $CN_{Mn\text{-}Mn/Fe}$ = 2.8±1.1 and $R_{Mn\text{-}Mn/Fe}$ = 3.04±0.02 Å. This $R_{Mn\text{-}Mn/Fe}$ is significantly shorter than the edge-sharing Mn-Mn bond in bixbyite (Table 3) and longer than the edge-sharing Mn-Mn bond in groutite (Wyckoff 1963). However, the fit-derived $R_{Mn\text{-}Mn/Fe}$ value for this sample is in good agreement with the edge-sharing Fe-Fe bond length in the Fe(III) precipitates that formed in this sample (i.e. lepidocrocite, $R_{Fe\text{-}Fe}$ = 3.07±0.01 Å).

2.3.5.2 MnO_4 experiments

The Mn K-edge EXAFS spectra of MnO_4 samples were similar regardless solution composition, with all samples resembling the EXAFS spectrum of the δ-MnO_2 standard. All experimental EXAFS spectra contained the characteristic staircase feature from 4 to 6 $Å^{-1}$ indicative of MnO_2 minerals (Manceau et al. 2012), which implies that Mn(II) and Fe(II) co-oxidation by MnO_4 in a variety of solutions leads to solid-phase Mn in a MnO_2-like bonding environment.

Shell-by-shell fits of the Ref MnO_4 sample, which contained <10% Mn(III) (Table 2), indicated a Mn-O coordination shell of $CN_{Mn\text{-}O}$ = 5.2±0.9 and $R_{Mn\text{-}O}$ = 1.91±0.01 Å. These fit-derived values are in excellent agreement with the first shell fits of the δ-MnO_2 standard (Table 3) and are representative of Mn(IV) in octahedral coordination. The second shell fit of the Ref MnO_4 sample returned values of $CN_{Mn\text{-}Mn/Fe}$ = 3.2±0.4 and $R_{Mn\text{-}Mn/Fe}$ = 2.89±0.01 Å, which also matches the fits δ-MnO_2 standard (Table 3) and is consistent with edge-sharing MnO_6 octahedra. Furthermore, this fit-derived $R_{Mn\text{-}Mn/Fe}$ value is considerably shorter than the fit-derived $R_{Mn\text{-}Mn\text{-}Fe}$ of the Ref O_2 sample and is also shorter than the edge-sharing Fe-Fe bond in Fe(III) (oxyhydr)oxide minerals (Manceau and Combes 1988). Interestingly, the shell-by-shell fits of the Ref MnO_4 sample and the MnO_4 sample generated in the highest oxyanion solution (i.e. Si750+Ca2500) were identical within fit-derived standard errors (Table 3). This result suggests that oxyanions do not modify the structure of MnO_2 solids as much as Fe(III) precipitates, which is attributed to the lower affinity of oxyanions for MnO_2 surfaces than Fe(III) (oxyhydr)oxides (van Genuchten and Peña 2016a).

2.3.5.3 HOCl experiments

The EXAFS spectra of the Ref and Mn18 samples in the HOCl system, which consisted of primarily Mn(III) (Table 3), were nearly identical. Both Ref and Mn18 spectra displayed a split oscillation from 3 to 5 Å^{-1}, which is similar to that of the Ref O_2 sample, but the split in this oscillation was less prominent in the HOCl samples. The Ref and Mn18 HOCl samples also exhibited an asymmetric oscillation near 6.5 Å^{-1} that was less pronounced or absent from the EXAFS spectra of other samples and standards (Figure 7). In the presence of P and Si, some features in the EXAFS spectra changed, including the disappearance of the assymetric oscillation near 6.5 Å, but the first oscillation from 3 to 5 Å^{-1} was still split. The similarity of key EXAFS features across all HOCl samples regardless of the presence (e.g. Si150, P4) or absence (Ref, Mn18) of oxyanions is consistent with the XANES LCFs, which identified Mn(III) as the predominant Mn oxidation state in all HOCl samples (Table 2).

Shell-by-shell fits of the Fourier-transformed EXAFS spectrum of the Ref HOCl sample (Table 3) revealed a first shell Mn-O coordination environment similar to the Ref O_2 sample, with $CN_{Mn\text{-}O}$ = 2.4±0.4 and $R_{Mn\text{-}O}$ = 1.91±0.01 Å, which is consistent with Jahn-Teller distorted Mn(III) octahedra. Fits of the second shell of the Ref HOCl sample returned values of 1.7±0.4 for $CN_{Mn\text{-}Mn/Fe}$ and 3.01±0.02 Å for $R_{Mn\text{-}Mn/Fe}$. Similar to the O_2 system, the second shell fits of the Ref HOCl sample produced a $R_{Mn\text{-}Mn/Fe}$ value that is shorter than the edge-sharing Mn-Mn bond in Mn(III)-bearing minerals. However, the $R_{Mn\text{-}Mn/Fe}$ for the HOCl sample is in good agreement with the Fe-Fe bond length for edge-sharing FeO_6 octahedra in Fe(III) precipitates that formed in this sample (i.e. hydrous ferric oxide, $R_{Fe\text{-}Fe}$ = 3.05±0.01 Å).

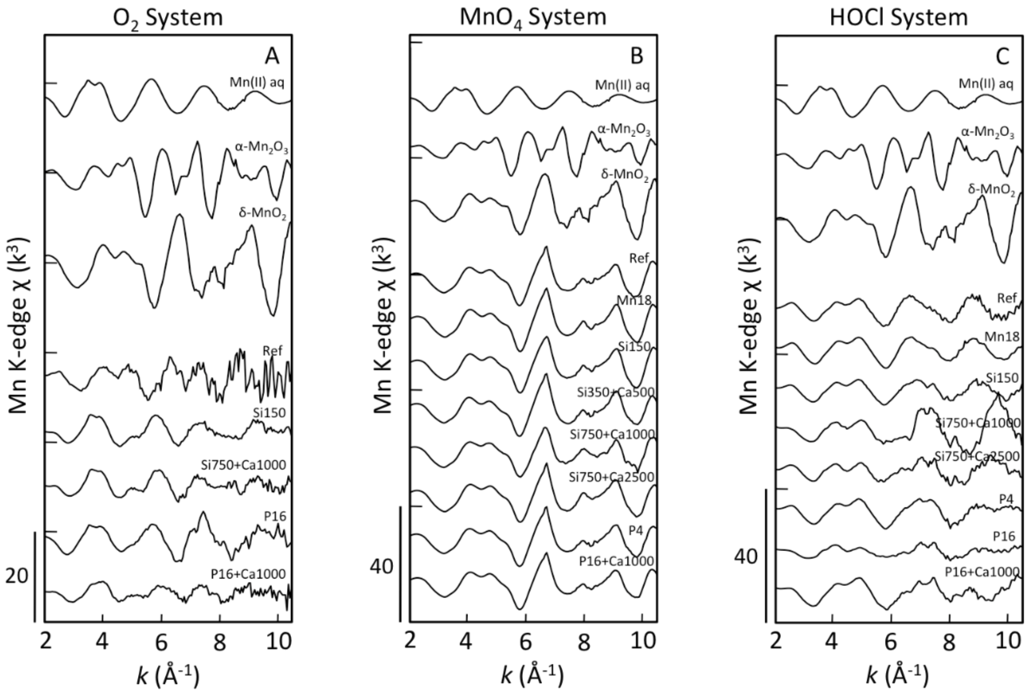

Figure 7. Mn K-edge EXAFS spectra for precipitate samples formed in the O_2 (left panel), MnO_4 (middle panel) and HOCl (right panel) experiments. The experimental data is plotted below Mn(II), Mn(III), and Mn(IV) standards.

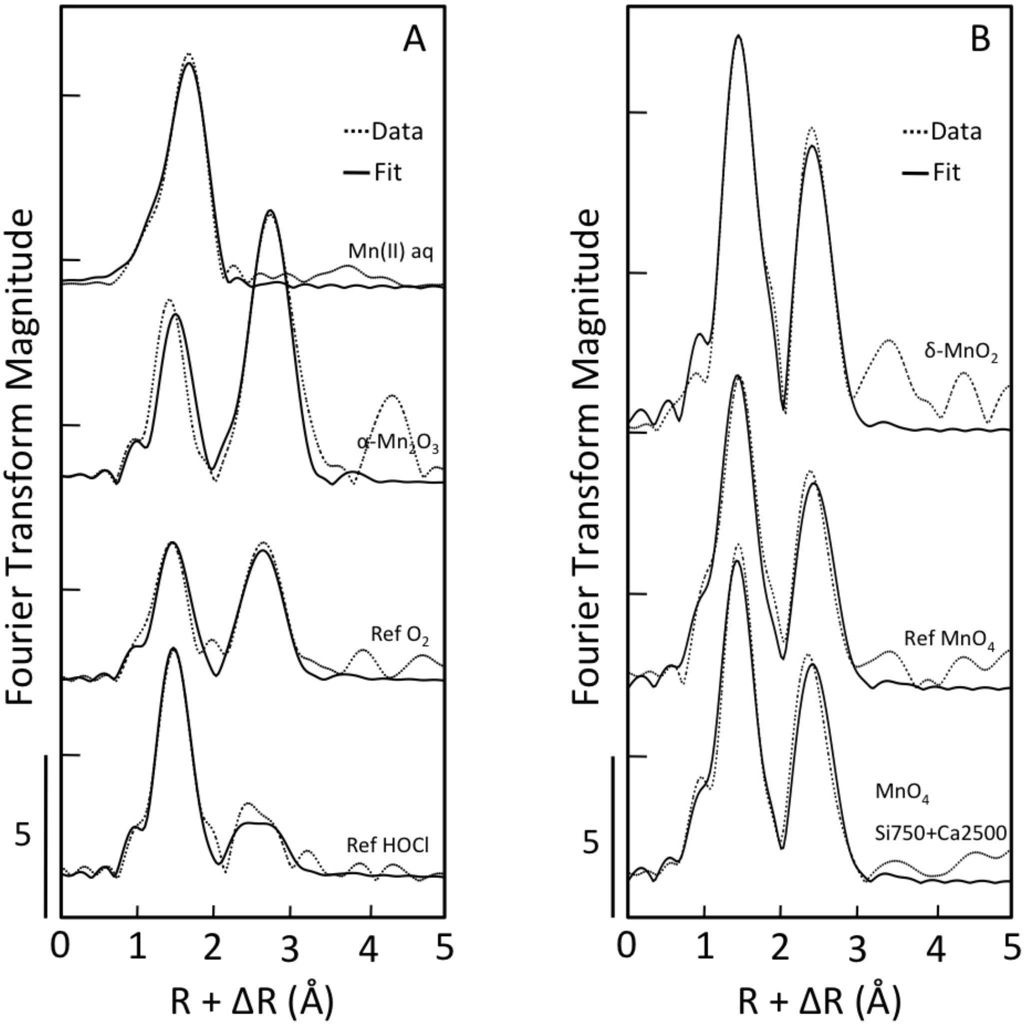

Figure 8. Fourier-transformed Mn K-edge EXAFS spectra of precipitate samples (dotted lines) overlain to the output of shell-by-shell fits.

Table 3: Summary of Shell Fits of Mn-bearing Standards and Precipitate Samples

Experiment Code	Atomic Pairs	CN	R (Å)	σ^2 (Å^2)	ΔE_0 (eV)	R-Factor
Aqueous Mn(II)	Mn-O	7.0 (0.6)	2.18 (0.01)	0.010 (0.001)	-11.0 (1.0)	0.015
α-Mn_2O_3	Mn-O	2.4 (0.7)	1.92 (0.02)	0.004 (0.002)	-16.7 (1.8)	0.041
	Mn-Mn1	4.8 (2.3)	3.10 (0.03)	0.009 (0.004)		
	Mn-Mn2	3.4 (1.7)	3.53 (0.04)	σ^2 (Mn-Mn1)		
δ-MnO_2	Mn-O	4.4 (1.0)	1.90 (0.01)	0.001 (0.001)	-17.6 (2.7)	0.047
	Mn-Mn	4.3 (0.6)	2.88 (0.02)	0.007		
Ref O_2	Mn-O	1.9 (0.5)	1.93 (0.02)	0.004 (0.003)	-11.4 (3.0)	0.067
	Mn-Mn/Fe	2.8 (1.1)	3.04 (0.02)	0.009 (0.003)		
Ref HOCl	Mn-O	2.4 (0.4)	1.91 (0.01)	0.002 (0.001)	-10.0 (2.1)	0.032
	Mn-Mn/Fe	1.7 (0.4)	3.01 (0.02)	0.01		
Ref MnO_4	Mn-O	5.2 (0.9)	1.91 (0.01)	0.005 (0.002)	-16.7 (2.1)	0.031
	Mn-Mn/Fe	3.2 (0.4)	2.89 (0.01)	0.007		
MnO_4 Si750 + Ca1000	Mn-O	4.9 (0.7)	1.90 (0.01)	0.004 (0.001)	-17.3 (1.7)	0.020
	Mn-Mn/Fe	3.3 (0.3)	2.87 (0.01)	0.007		

CN represents the coordination number. R the interatomic distance. σ^2 the mean squared atomic displacement and ΔE_0 represents the change in threshold energy. The passive electron reduction factor. S_0^2. was fixed at 0.7. Fitting parameters allowed to float are accompanied by fit-determined standard errors in parenthesis. while constrained parameters appear without a parenthesis. All fits were carried out from 1 to 3.5 Å in R+ΔR-space. The number of independent point (N_{IDP}) in the fits was 13.4 and the number of variables (N_{Var}) was 4 to 9.

2.4 Discussion

2.4.1 Effect of oxidant and solution chemistry on Fe(III) speciation and particle aggregation

2.4.1.1 Fe(II) oxidation in O_2, MnO_4, and HOCl Ref experiments

Comparison of the Ref experiments across all oxidants shows that Fe(II) and Mn(II) co-oxidation by O_2 and HOCl produced suspensions that aggregated rapidly and that can be separated by gravitational settling or filtering easily, whereas the MnO_4 Ref experiment generated a colloidally stable suspension. However, Fe(III) speciation differed between Ref O_2 and Ref HOCl experiments, with O_2 producing lepidocrocite and both HOCl and MnO_4 producing poorly-crystalline Fe(III) precipitates. These differences in aggregation and Fe(III) speciation with oxidant can be explained by the different Fe(II) reaction rates with O_2, HOCl, and MnO_4 and the different end-products of each reaction. The Fe(II) oxidation rate by O_2 depends strongly on pH (van Beek et al. 2016, Van Beek et al. 2012, Vries et al. 2017), but at circumneutral pH is orders of magnitude lower than HOCl and MnO_4 (Ghurye and Clifford 2001, Knocke et al. 1991, Stumm and Morgan 1996). Although our experiments were designed to allow for complete Fe(II) oxidation in the O_2 experiments, Fe(II) reactions with O_2 are not instantaneous, which ensures that freshly-oxidized Fe(III) precursors form in the presence of Fe(II). Aqueous Fe(II) catalyzes the rapid transformation of poorly-ordered Fe(III) precipitates into lepidocrocite, which was the dominant Fe(III) phase of the Ref O_2 experiment (Pedersen et al. 2005). By contrast, the reaction rate of HOCl and MnO_4 with Fe(II) is high enough that aqueous Fe(II) is too unstable to catalyze the transformation of freshly-formed Fe(III) to lepidocrocite, leading instead to the persistence of poorly-ordered Fe(III) precipitates. Although Fe(III) speciation was similar in the Ref HOCl and MnO_4 experiments, the Ref MnO_4 solids contained a major fraction of MnO_2 that did not form in the O_2 and HOCl experiments. The presence of MnO_2 likely enhances the colloidal stability of the MnO_4 samples because of the much lower point of zero charge of MnO_2 (≈2-3) compared to lepidocrocite and poorly-ordered Fe(III) precipitates (≈7-8) (Sposito 2008). At circumneutral pH, suspensions containing MnO_2 will have a strong negative charge, preventing aggregation, whereas suspensions of Fe(III) precipitates will be near the optimum pH to induce aggregation (Sposito 2008).

2.4.1.2 Impact of ionic composition

Solution chemistry was found to alter both the suspension stability and Fe(III) speciation, with different impacts depending on the Fe(II) oxidant and ionic composition. The Fe(III) speciation in the O_2 samples was impacted the most by solution composition, but similar trends were observed in the MnO_4 and HOCl experiments. The presence of oxyanions in the O_2 samples decreased particle aggregation and resulted in a transition from lepidocrocite to poorly-ordered Fe(III) precipitates. Oxyanions, such as Si and P, bind strongly to Fe(III) precipitate surfaces during Fe(III) polymerization, which modifies two key properties of the suspension. First, by binding strongly to crystal growth sites on the Fe(III) precipitate surface, oxyanions inhibit the formation of crystalline Fe(III) minerals (i.e. lepidocrocite), leading to the persistence of poorly-ordered Fe(III) precipitates with a large specific surface area (Van Genuchten et al. 2014b, Voegelin et al. 2010). Second, sorption of oxyanions leads to negatively charged Fe(III) precipitate surfaces, even in the case of Si, which is uncharged in solution circum-neutral pH (Delaire et al. 2016, Kanematsu et al. 2013a). Therefore, oxyanion sorption generates particles with highly negative surface charge that are less likely to aggregate. Both consequences of co-occurring oxyanions during Fe(III) precipitation (i.e. changes in suspension aggregation and Fe(III) speciation) were observed in the O_2 experiments. These effects were less pronounced in the MnO_4 experiments since the Ref MnO_4 suspension was already colloidal stable and consisted of poorly-ordered Fe(III) precipitates even in the absence of Si and P.

The presence of Ca can counteract some of the oxyanion effects, particularly with respect to particle surface charge. Ca addition enhanced aggregation (i.e. settling and filterability) in nearly every O_2, HOCl and MnO_4 experiment, with stronger impact in P solutions than Si. The pronounced impact of Ca in P solutions is attributed to the formation of Ca-O-P linkages during Fe(III) polymerization that enhance particle aggregation by neutralizing more effectively the negative surface charge of P-rich Fe(III) precipitates (Senn et al. 2015, van Genuchten et al. 2014a, Voegelin et al. 2010). The presence of Ca was also important to enhancing the aggregation of MnO_4 suspensions, which is explained by positively charged Ca neutralizing the negatively charged MnO_2 produced in the MnO_4 experiments.

2.4.2 **Behavior of Mn(II) during co-oxidation with Fe(II)**

2.4.2.1 Mn(II) removal in O_2, MnO_4, and HOCl Ref experiments

A visual representation of the structure and composition of the solids formed in the Ref experiments is given in Figure 9. The Ref O_2, MnO_4 and HOCl experiments were performed in solutions with the least ionic complexity and form the baseline for comparing Mn(II) removal in the simulated groundwater solutions. In the Ref O_2 experiment, the Mn/Fe solids ratio was ≈0.01 mol/mol (i.e. ≈10% Mn(II) removal) and the XANES LCFs indicated solid-phase Mn was dominantly Mn(III). Shell-by-shell fits of the Ref O_2 sample were consistent with a first shell Mn(III)-O coordination environment and a second shell that consisted of Mn-Mn/Fe atomic pairs at $R = 3.04 \pm 0.02$ Å. This R-value matches that of edge-sharing FeO_6 octahedra in the Fe(III) precipitates formed in this sample. Therefore, Mn(II) removal in the Ref O_2 experiment likely occurs via Mn(II) oxidation to Mn(III) by the reactive Fenton-type oxidants produced during Fe(II) oxidation by O_2 ($^*O_2^-$, Fe(IV)) and subsequent (partial) incorporation into the resulting Fe(III) precipitate. This Mn(II) removal mechanism has been observed in experiments that dosed Fe(II) slowly by Fe(0) electrolysis into air-saturated solutions of Mn(II), allowing Fe(II) and Mn(II) co-oxidize by O_2 (van Genuchten and Pena 2017a).

The Ref MnO_4 experiment had a high Mn/Fe solids ratio of >0.5 mol/mol, which matches the total Mn/Fe ratio dosed into the initial solution. The XANES LCFs of the Ref MnO_4 sample indicated Mn was present as Mn(IV). The line shape and position of the Mn K-edge EXAFS spectrum and the shell-by-shell fitting output of the Ref MnO_4 sample indicated an Mn coordination environment similar to the δ-MnO_2 standard. The formation of nanoscale MnO_2 by reaction of Mn(II) and MnO_4 has been well documented in many studies (Knocke et al. 1991, Lee et al. 2011) and our results suggest that the presence of Fe(II) and other background ions in the Ref MnO_4 experiment did not alter this reaction pathway.

Effective removal of approximately 80% of the initial Mn(II) was observed in the Ref HOCl, leading to an Mn/Fe solids ratio of ≈0.08 mol/mol, which was significantly higher than the Ref O_2 sample. The XANES LCFs of the Ref HOCl sample indicated that solid-phase Mn was dominantly Mn(III). Similar to the O_2 system, the shell-by-shell fits of the Ref HOCl sample were consistent with a first shell Mn(III)-O coordination environment and second shell that consisted of Mn-Mn/Fe atomic pairs at an R-value (3.01±0.02 Å) that is not found in Mn(III) (oxyhydr)oxide minerals. However, this R-value is similar to that of the edge-sharing Fe octahedra in the Fe(III) precipitates that formed in this sample (3.05±0.01 Å). Therefore, we propose that Mn(II) removal in the Ref HOCl experiment proceeds by a single electron transfer from Mn(II) to Mn(III), with Mn(III) stabilized by co-precipitating Fe(III) (oxyhydr)oxides. While a similar Mn(II) removal pathway has been documented for Mn(II) and Fe(II) co-oxidation by H_2O_2, this pathway is inconsistent with previous research investigating Mn(II) removal by chlorination, which report the formation of Mn(IV) species (Allard et al. 2013, Hao et al. 1991). In our experiments, the precipitation of Fe(III) during Mn(II) oxidation likely stabilizes the initial Mn(III) product by incorporation into the solid phase, which prevents subsequent Mn(III) oxidation to Mn(IV).

2.4.2.2 Impact of ionic composition

A visual representation of the impact of oxyanions and bivalent cations on the structure and composition of the precipitates formed by Fe(II) and Mn(II) co-oxidation is given in Figure 9. Solution composition modified the uptake and removal mechanism of Mn(II) in many experiments, with the most pronounced impacts in the O_2 and HOCl systems. Based on the XANES LCFs and Mn K-edge EXAFS spectra, Mn(II) was removed by reaction with MnO_4 to form nanoscale MnO_2 in every experiment in the MnO_4 system, regardless of solution composition. However, in the O_2 and HOCl experiments, Si and P increased the fraction of solid-phase Mn(II). For example, whereas <5% Mn(II) was present in the Ref O_2 and HOCl samples, the P16 samples in the O_2 and HOCl systems consisted of 85±3 and 41±4% Mn(II), respectively. The impact of Si was weaker than P, but still increased the Mn(II) fraction in the Si150 sample in the O_2 system to 75±2%. Furthermore, the increased fraction of sorbed Mn(II) in the O_2 experiments coincided with an increase in Mn/Fe solids ratio, particularly in the P experiment (Mn/Fe_{Ref} = 0.01 mol/mol, Mn/Fe_{P16} = 0.05 mol/mol). These results indicate that P, and Si to a lesser extent, can enhance Mn(II) sorption when Mn(II) oxidation is incomplete. The enhanced Mn(II) removal in the presence of oxyanions can be explained by the interaction between positively charged Mn(II) and negatively charged surfaces of oxyanion-rich Fe(III) precipitates. The more pronounced impact of P relative to Si could arise from direct Mn(II)-O-P bonding on the Fe(III) precipitate surface (i.e. ternary complexes), analogous to Ca-O-P linkages.

In contrast to the effect of oxyanions, the presence of Ca in Si and P solutions systematically decreased the fraction of solid-phase Mn(II) in both O_2 and HOCl experiments. The impact of Ca was most pronounced in the P16 solutions, with decreases in the Mn(II) fraction from 85±3 to 20±4% in the O_2 system and from 41±4 and 14±5% in the HOCl system. The Ca-induced decrease in sorbed Mn(II) was coupled to a decrease in the Mn/Fe solids ratio (Figure 3), which suggests that Ca can compete effectively with Mn(II) for sorption sites, especially in the case of P-rich Fe(III) precipitates. This conclusion is consistent with the similar ionic potential (charge/ionic radius) of Mn(II) ($IP_{Mn(II)} \approx 24$) and Ca ($IP_{Ca} \approx 20$) ions, which suggests similar sorption reactivity between Mn(II) and Ca.

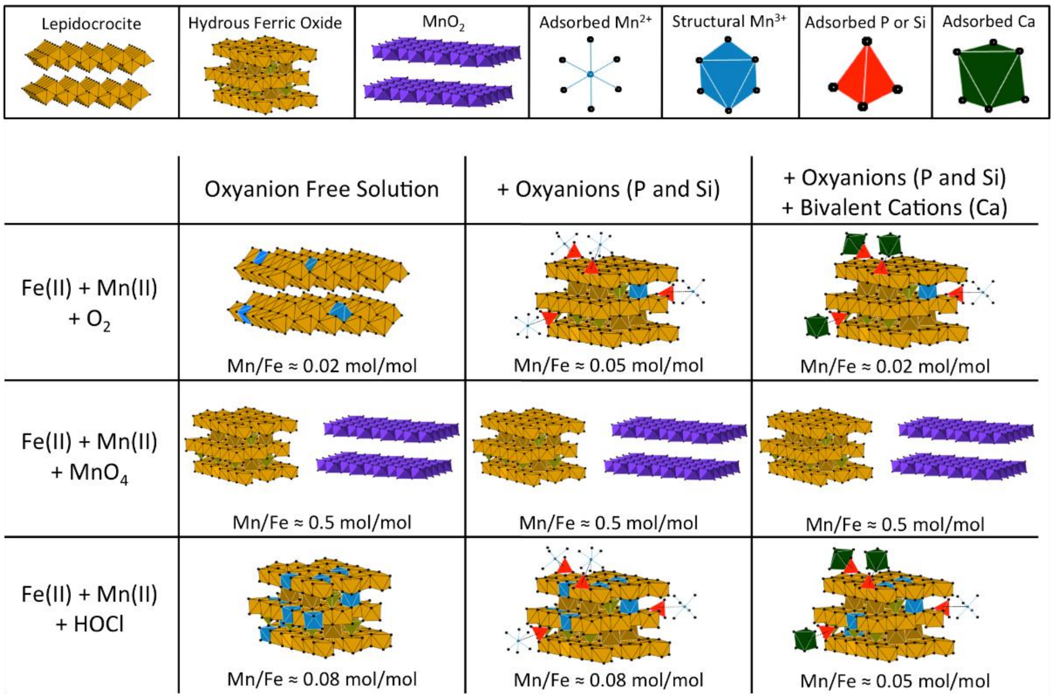

Figure 9. Visual representations and Mn/Fe ratios of the experimental solids derived from the wet chemical measurements and XAS analyses. We expect that sorbed Mn(II) increased in the oxyanion experiments due to Mn(II) interactions with P and Si bound to the Fe(III) precipitate. We did not include P or Si oxyanions bound to the Fe(III) precipitates in the MnO_4 panels since Mn(II) was not detected in these samples.

2.5 Conclusions and implications for water treatment

We found that the ion composition of water and the identity of the oxidant strongly determines the macroscopic and molecular-scale characteristics of Fe and Mn bearing precipitates generated by Fe(II) and Mn(II) co-oxidation. The higher Mn/Fe ratio of the precipitates produced with MnO_4 or HOCl indicates that the Mn removal mechanism will differ between the typical aeration—rapid sand filtration type groundwater treatment systems that rely on bacteria and surface catalysts for Mn(II) removal (Bruins et al. 2015) and the ones that use strong oxidants such as $KMnO_4$ and NaOCl. In the prior case, Mn removal will take place deeper in the filter bed, whereas Mn is expected to precipitate in the supernatant storage with $KMnO_4$ and NaOCl, resulting in accumulation of Mn bearing solids in the top sand filter layer.

Our study shows that the addition of Ca counteracts the negative effect of oxyanions and enhances the settling and filterability of Fe and Mn bearing precipitates. Thus, water treatment utilities that plan to implement softening at Fe/Mn removal plants should consider placing softening reactors after Fe/Mn removal to avoid colloidally stable suspensions arising from solutions low in bivalent cations. If colloidally stable suspensions are unavoidable, low pressure membrane systems (microfiltration/ultrafiltration) may replace rapid sand filters for effective removal of colloidal precipitates, but the fouling of membranes will be a critical issue. Precipitates can foul the membranes in different ways, depending on particle size. Particle sizes larger than the membrane pores will deposit on membrane surfaces, resulting in cake layer formation, which is often easily reversible (Floris et al. 2016). However, smaller particles can deposit in the membrane internal structure, resulting in undesirable pore entrapment and pore narrowing, which severely decreases the flux over time (irreversible fouling).

With respect to contaminant removal during treatment, the formation of MnO_2 by MnO_4 addition should not be overlooked. The characterization data in the MnO_4 experiments indicated that the Mn solids were structurally similar to δ-MnO_2, a nanoscale MnO_2 mineral. These types of Mn(IV) oxides have remarkable reactivity with respect to sorption of a wide variety of toxic heavy metals (e.g. Cd(II), Pb(II), Cu(II), Ni(II)) (Peña et al. 2015, Pena et al. 2010, Villalobos 2015). For example, the Pb/Mn solids ratio for δ-MnO_2 can reach 0.4 mol/mol (Villalobos et al. 2005), which is partly due to highly reactive Mn(IV) vacancies in MnO_2 sheets (Lanson et al. 2002). In our study, MnO_4 was investigated primarily because it improves the kinetics of Fe(II), Mn(II) and As(III) oxidation. However, our results suggest that Fe(II) oxidation by MnO_4 and the production of mixtures of Fe(III) and MnO_2 would be ideal for concurrent treatment of As(III) and heavy metals. This result is particularly important for the co-removal of As(III) and Cd(II), which can often occur simultaneously in polluted environments (Perera et al. 2016), since Cd(II) removal by Fe(III) precipitates is much less effective than MnO_2 (van Genuchten and Peña 2016b).

References

Ahmad, A., Cornelissen, E., van de Wetering, S., van Dijk, T., van Genuchten, C., Bundschuh, J., van der Wal, A. and Bhattacharya, P. (2018) Arsenite removal in groundwater treatment plants by sequential Permanganate—Ferric treatment. Journal of Water Process Engineering 26, 221-229.

Ahmad, A., Kools, S., Schriks, M., Stuyfzand, P. and Hofs, B. (2015) Arsenic and chromium concentrations and their speciation in groundwater resources and drinking water supply in the Netherlands p. 78, KWR Water Cycle Research Institute, Nieuwegein, The Netherlands.

Allard, S., Fouché, L., Dick, J., Heitz, A. and von Gunten, U. (2013) Oxidation of Manganese(II) during Chlorination: Role of Bromide.

Borsboom, M., Bras, W., Cerjak, I., Detollenaere, D., van Loon, D., Goedtkindt, P., Konijnenburg, M., Lassing, P., Levine, Y., Munneke, B., Oversluizen, M., van Tol, R. and Vlieg, E. (1998) The Dutch-Belgian beamline at the ESRF. Journal of Synchrotron Radiation 5, 518-520.

Bruins, J.H., Petrusevski, B., Slokar, Y.M., Kruithof, J.C. and Kennedy, M.D. (2015) Manganese removal from groundwater: Characterization of filter media coating. Desalination and Water Treatment 55(7), 1851-1863.

de Moel, P.J., Verberk, J.Q.J.C. and van Dijk, J.C. (2006) Drinking Water: Principles and Practices, Delft, The Netherlands.

Delaire, C., van Genuchten, C., Amrose, S. and Gadgil, A. (2016) Bacteria attenuation by iron electrocoagulation governed by interactions between bacterial phosphate groups and Fe(III) precipitates. Water Research 103, 74-82.

Diem, D. and Stumm, W. (1984) Is dissolved Mn^{+2} being oxidized by O_2 in absence of Mn-bacteria and surface catalysts? Geochimica et Cosmochimica Acta 48, 1571-1573.

Floris, R., Nijmeijer, K. and Cornelissen, E.R. (2016) Removal of Aqueous nC_{60} Fullerene from Water by Low Pressure Membrane Filtration. Water Research 91, 115-125.

Ghurye, G. and Clifford, D. (2001) Laboratory Study on the Oxidation of Arsenic III to As V, p. 87, Unites States Environmental Protection Agency, Washington DC.

Gude, J.C.J., Rietveld, L.C. and van Halem, D. (2016) Fate of low arsenic concentrations during full-scale aeration and rapid filtration. Water Research 88, 566-574.

Hao, O., P. Davis, A. and H. Chang, P. (1991) Kinetics of Manganese(II) Oxidation with Chlorine.

Hug, S.J. and Leupin, O. (2003) Iron-Catalyzed Oxidation of Arsenic(III) by Oxygen and by Hydrogen Peroxide: pH-Dependent Formation of Oxidants in the Fenton Reaction. Environmental Science & Technology 37(12), 2734-2742.

Kaegi, R., Voegelin, A., Folini, D. and Hug, S.J. (2010) Effect of phosphate, silicate, and Ca on the morphology, structure and elemental composition of Fe(III)-precipitates formed in aerated Fe(II) and As(III) containing water. Geochimica et Cosmochimica Acta 74(20), 5798-5816.

Kanematsu, M., Young, T., Fukushi, K., Green, P. and Darby, J. (2013) Arsenic(III, V) adsorption on a goethite-based adsorbent in the presence of major co-existing ions: Modeling competitive adsorption consistent with spectroscopic and molecular evidence. Geochimica Et Cosmochimica Acta 106, 404-428.

Kelly, S.D., Hesterberg, D. and Ravel, B. (2008) Analysis of soils and minerals using X-ray absorption spectroscopy. In *Methods of Soil Analysis. Part 5. Mineralogical Methods. SSA Book Series No.5.*

Knocke, W.R., Van Benschoten, J.E., Kearney, M.J., Soborski, A.W. and Reckhow, D.A. (1991) Kinetics of Manganese and Iron Oxidation by Potassium Permanganate and Chlorine Dioxide. AWWA 83(6), 80-87.

Lan, S., Wang, X., Xiang, Q., Yin, H., Tan, W., Qiu, G., Liu, F., Zhang, J. and Feng, X. (2017) Mechanisms of Mn(II) catalytic oxidation on ferrihydrite surfaces and the formation of manganese (oxyhydr)oxides.

Lanson, B., Drits, V., Feng, Q. and Manceau, A. (2002) Structure of synthetic Na-birnessite: Evidence for a triclinic one-layer unit cell. American Mineralogist 87(11-12), 1662-1671.

Lee, G., Song, K. and Bae, J. (2011) Permanganate oxidation of arsenic (III): Reaction stoichiometry and the characterization of solid product

Manceau, A. and Combes, J.M. (1988) Structure of Mn and Fe oxides and oxyhydroxides: A topological approach by EXAFS. Physics and Chemistry of Minerals 15(3), 283-295.

Manceau, A., Marcus, M. and Grangeon, S. (2012) Determination of Mn valence states in mixed-valent manganates by XANES spectroscopy.

McArthur, J.M., Sikdar, P.K., Nath, B., Grassineau, N., Marshall, J.D. and Banerjee, D.M. (2012) Sedimentological Control on Mn, and Other Trace Elements, In Groundwater of the Bengal Delta. Environmental Science & Technology 46(2), 669-676.

Newville, M. (2001) IFEFFIT: interactive XAFS analysis and FEFF fitting. Journal of Synchrotron Radiation, 322-324.

Nikitenko, S., Beale, A., van der Eerden, A., Jacques, S., Leynaud, O., O'Brien, M., Detollenaere, D., Kaptein, R., Weckhuysen, B. and Bras, W. (2008) Implementation of a combined SAXS/WAXS/QEXAFS set-up for time-resolved in situ experiments. Journal of Synchrotron Radiation 15, 632-640.

Pedersen, H.D., Postma, D., Jakobsen, R. and Larsen, O. (2005) Fast transformation of iron oxyhydroxides by the catalytic action of aqueous Fe(II). Geochimica et Cosmochimica Acta 69(16), 3967-3977.

Peña, J., Bargar, J.R. and Sposito, G. (2015) Copper sorption by the edge surface of synthetic birnessite nanoparticles. Chemical Geology.

Pena, J., Kwon, K., Refson, K., Bargar, J. and Sposito, G. (2010) Mechanisms of nickel sorption by a bacteriogenic birnessite. Geochimica Et Cosmochimica Acta 74(11), 3076-3089.

Perera, P.A.C.T., Sundarabarathy, T.V., Sivananthawerl, T., Kodithuwakku, S.P. and Edirisinghe, U. (2016) Arsenic and Cadmium Contamination in Water, Sediments and Fish is a Consequence of Paddy Cultivation: Evidence of River Pollution in Sri Lanka. Achievements in the Life Sciences 10(2), 144-160.

Rehr, J., Albers, R. and Zabinsky, S. (1992) High-order multiple-scattering calculations of X-ray absorption fine structure. Physical Review Letters, 3397-3400.

Rossberg, A., Reich, T. and Bernhard, G. (2003) Complexation of uranium(VI) with protocatechuic acid - application of iterative transformation factor analysis to EXAFS spectroscopy. Analytical and Bioanalytical Chemistry 376(5), 631-638.

Scheinost, A., Rossberg, A., Vantelon, D., Xifra, I., Kretzschmar, R., Leuz, A., Funke, H. and Johnson, C. (2006) Quantitative antimony speciation in shooting-range soils by EXAFS spectroscopy. Geochimica Et Cosmochimica Acta 70(13), 3299-3312.

Senn, A.-C., Hug, S.J., Kaegi, R., Hering, J.G. and Voegelin, A. (2017) Arsenate co-precipitation with Fe(II) oxidation products and retention or release during precipitate aging. Water Research.

Senn, A.-C., Kaegi, R., Hug, S.J., Hering, J.G., Mangold, S. and Voegelin, A. (2015) Composition and structure of Fe(III)-precipitates formed by Fe(II) oxidation in water at near-neutral pH: Interdependent effects of phosphate, silicate and Ca. Geochimica et Cosmochimica Acta 162, 220-246.

Sorlini, S. and Gialdini, F. (2010) Conventional oxidation treatments for the removal of arsenic with chlorine dioxide, hypochlorite, potassium permanganate and monochloramine. Water Research 44(19), 5653-5659.

Sposito, G. (2008) The Chemistry of Soils, Oxford University Press, New York.

Stumm, W. and Morgan, J.J. (1996) Aquatic Chemistry, Chemical Equilibria and Rates in Natural Waters, John Wiley & Sons, Inc., New York.

Tebo, B.M., Johnson, H.A., McCarthy, J.K. and Templeton, A.S. (2005) Geomicrobiology of manganese(II) oxidation. Trends in Microbiology 13(9), 421-428.

van Beek, C.G.E.M., Dusseldorp, J., Joris, K., Huysman, K., Leijssen, H., Schoonenberg Kegel, F., de Vet, W.W.J.M., van de Wetering, S. and Hofs, B. (2016) Contributions of homogeneous, heterogeneous and biological iron(II) oxidation in aeration and rapid sand filtration (RSF) in field sites. Journal of Water Supply: Research and Technology—AQUA 65(3), 195-207.

Van Beek, C.G.E.M., Hiemstra, T., Hofs, B., Bederlof, M.M., van Paassen, J.A.M. and Reijnen, G.K. (2012) Homogeneous, heterogeneous and biological oxidation of iron(II) in rapid sand filtration. Journal of Water Supply: Research and Technology—AQUA 61(1), 1-2012.

van Genuchten, C., Addy, S., Pena, J. and Gadgil, A. (2012) Removing arsenic from synthetic groundwater with iron electrocoagulation: An Fe and As K-edge EXAFS study. Environmental Science & Technology 46(2), 986-994.

van Genuchten, C., Behrends, T., Kraal, P., Stipp, S. and Dideriksen, K. (2018) Controls on the formation of Fe(II,III) (hydr)oxides by Fe(0) electrolysis. Electrochimica Acta 286, 324-338.

van Genuchten, C. and Pena, J. (2017) Mn(II) Oxidation in Fenton and Fenton Type Systems: Identification of Reaction Efficiency and Reaction Products. Environmental Science & Technology 51(5), 2982-2991.

van Genuchten, C.M., Gadgil, A.J. and Peña, J. (2014a) Fe(III) Nucleation in the Presence of Bivalent Cations and Oxyanions Leads to Subnanoscale 7 Å Polymers. Environmental Science & Technology 48(20), 11828-11836.

van Genuchten, C.M. and Peña, J. (2016a) Antimonate and arsenate speciation on reactive soil minerals studied by differential pair distribution function analysis. Chemical Geology 429, 1-9.

van Genuchten, C.M. and Peña, J. (2016b) Sorption selectivity of birnessite particle edges: a d-PDF analysis of Cd(ii) and Pb(ii) sorption by δ-MnO2 and ferrihydrite. Environmental Science: Processes & Impacts 18(8), 1030-1041.

Van Genuchten, C.M., Pena, J., Amrose S, E. and Gadgil, A.J. (2014b) Structure of Fe(III) precipitates genberated by the electrolytric dissolution of Fe(0) in the presence of groundwater ions. Geochimica et Cosmochimica Acta 127, 285-304.

Villalobos, M. (2015) Advances in the Environmental Biogeochemistry of Manganese Oxides. Feng, X., Li, W., Zhu, M. and Sparks, D. (eds), American Chemical Society.

Villalobos, M., Bargar, J. and Sposito, G. (2005) Mechanisms of Pb(II) sorption on a biogenic manganese oxide. Environmental Science & Technology 39(2), 569-576.

Voegelin, A., Kaegi, R., Frommer, J., Vantelon, D. and Hug, S.J. (2010) Effect of phosphate, silicate, and Ca on Fe(III)-precipitates formed in aerated Fe(II)- and As(III)-containing water studied by X-ray absorption spectroscopy. Geochimica et Cosmochimica Acta 74(1), 164-186.

Vries, D., Bertelkamp, C., Schoonenberg Kegel, F., Hofs, B., Dusseldorp, J., Bruins, J.H., de Vet, W. and van den Akker, B. (2017) Iron and manganese removal: Recent advances in modelling treatment efficiency by rapid sand filtration. Water Research 109, 35-45.

Webb, S. (2005) SIXPACK: a graphical user interface for XAS analysis using IFEFFIT. Physica Scripta T115, 1011-1014.

Wyckoff, R.W.G. (1963) Crystal Structures, Wiley.

3 Impact of phosphate, silicate and natural organic matter on the size of Fe(III) precipitates and arsenate co-precipitation efficiency in calcium containing water

This chapter has been published as:

Ahmad, A., Rutten, S., Eikelboom, M., de Waal, L., Bruning, H., Bhattacharya, P., & van der Wal, A. (2020). Impact of phosphate, silicate and natural organic matter on the size of Fe(III) precipitates and arsenate co-precipitation efficiency in calcium containing water. Separation and Purification Technology. 235 (116117)

3.1 Introduction

The co-precipitation of arsenic (As) with *in situ* produced Fe(III)(oxyhydr)oxides is a widely used As removal technique in water treatment (Fuller et al. 1993, Roberts et al. 2004, van Genuchten et al. 2012b). Typically, an Fe(III) coagulant such as ferric chloride ($FeCl_3$) is dosed which, in contact with water, undergoes hydrolysis to form Fe(III)(oxyhydr)oxide precipitates. Arsenic adsorbs onto the surface of the Fe(III) precipitates, at an early stage of the precipitate growth (Hering et al. 1996, Jain et al. 1999, Qiao et al. 2012, van Genuchten et al. 2012b, Waychunas et al. 1993). The As bearing Fe(III) precipitates (i.e. co-precipitated As and Fe(III)) can be removed from water in a downstream granular media filter or e.g. with low-pressure membranes (Choi and Dempsey 2004, Jessen et al. 2005). At pH relevant to most natural waters (6.5–8.5), As(V) is negatively charged and therefore exhibits a higher affinity for the surface of Fe(III) precipitates than As(III) which is uncharged (Hering et al. 1996, Lakshmanan et al. 2008, Smedley and Kinniburgh 2002). Therefore, in order to effectively remove As from ground water, oxidizing As(III) to As(V) e.g. by adding potassium permanganate ($KMnO_4$) before co-precipitation with Fe(III)(oxyhydr)oxides has previously been suggested (Ahmad et al. 2018, Guan et al. 2009a, Guan et al. 2009b, Sorlini and Gialdini 2010). Recent studies have shown that As(III) also oxidizes rapidly to As(V) during rapid sand filtration (RSF), a treatment step commonly used at water treatment plants (Ahmad et al. 2018, Gude et al. 2018a, Gude et al. 2016). Thus, the use of $KMnO_4$ in water treatment can be avoided by treating the RSF effluent for As(V) removal instead of treating the raw groundwater for As(III) removal.

The removal efficiency of As(V) with Fe(III) based co-precipitation is sensitive to the ionic composition of water (Davis and Edwards 2017, Dong et al. 2011, Guan et al. 2009a, Guan et al. 2009b, Kanematsu et al. 2010, 2013b, Qiao et al. 2012). The most abundant oxyanions that may impact As(V) removal are silicate (i.e.H_4SiO_4) and phosphate (i.e. $H_2PO_4^-$ or HPO_4^{2-}), denoted further as Si and P respectively (Meng et al. 2000, van Genuchten et al. 2012b, Van Genuchten et al. 2014b). Moreover, natural organic matter (NOM), especially humic substances (HS), can adversely affect As(V) removal (Davis and Edwards 2017, Sharma et al. 2010, Weng et al. 2009). These inorganic and organic solutes can modify the structure, composition and identity of the Fe(III) precipitates, thereby affecting their size and As(V) uptake behaviour (Sposito 2008, Van Genuchten et al. 2014b). Moreover, these solutes compete with As(V) for adsorption sites on Fe(III) precipitates (Chen et al. 2014, Dixit and Hering 2003, Hering et al. 1996, Meng et al. 2000, Su and Puls 2001, Weng et al. 2009, Wilkie and Hering 1996, Youngran et al. 2007). On the other hand, natural waters often contain calcium ions (Ca) which can increase As(V) removal during Fe(III) based co-precipitation. It has been shown that Ca increases the size of Fe(III) precipitates (Ahmad et al. 2019a) and also results in an increased uptake of As(V) by Fe(III) precipitates. Several mechanisms have been proposed to explain these observations, such as neutralization of the Fe(III) precipitate surface charge by Ca (Wilkie and Hering 1996), suppression of electrostatic repulsion (Masue et al. 2007) and the formation of ternary complexes between Fe(III), As(V) and Ca (Kanematsu et al. 2013b, van Genuchten et al. 2014a).

So far, most of the available studies have focused on the interactions between As(V) and Fe(III) precipitates in simple solutions (Laky and Licskó 2011, Weng et al. 2008, Weng et al. 2009), whereas systematic studies providing understanding of the As(V)–Fe(III) interactions in complex multi-solute solutions are lacking. In this study, we aim to provide more insights into the independent and combined effects of Si, P, NOM and Ca on As(V) co-precipitation efficiency and the size of formed Fe(III) precipitates.

3.2 Materials and methods

3.2.1 Chemicals and stock solutions

All chemicals were reagent grade and used without any purification. The stock solutions of 1.4 g/L $FeCl_3$, 92.9 g/L $NaHCO_3$, 15 g/L NaCl, and 30.2 g/L Na_2SiO_3 were prepared by dissolving the required amounts of $FeCl_3 \cdot 6H_2O$ (CAS: 10025-77-1, 97% purity, J.T Baker The Netherlands), $NaHCO_3$ (CAS: 144-55-8, >99% purity, J.T Baker The Netherlands), NaCl (CAS: 7647-14-5, 99% purity, J. T Baker The Netherlands) and $Na_2SiO_3 \cdot 5H_2O$ (CAS: 10213-79-3, 99% purity, Sigma-Aldrich) respectively in ultrapure water (Mill-Q, produced by purifying distilled water with a Purelab Chorus provided by Veolia). The stock solutions of 73.8 g/L $CaCl_2$, 39.2 g/L $MgCl_2$ and 0.45 g/L NaH_2PO_4 were prepared by dissolving $CaCl_2$ anhydrous (CAS: 10043-52-4, 96% purity, J. T Baker), $MgCl_2 \cdot 6H_2O$ (CAS: 7791-18-6, 99% purity, Boom B.V.) and $NaH_2PO_4 \cdot H_2O$ (CAS: 10049-21-5, >98% purity, J.T Baker) respectively in 0.1 M HCl. The NOM stock solution of 2.4 g DOC/L was prepared by diluting a primary stock (HumVi, Vitens, The Netherlands, 117.4 g DOC/L) that contained ca. 75% HS. Arsenate was dosed using a stock solution of 1.0 g/l As_2O_5 (CAS: 12044-50-7, 99% purity, Inorganic Ventures). pH was adjusted with 0.1 M HCl or 0.1 M NaOH.

3.2.2 Composition of initial solutions

The experiments were performed with synthetic solutions and real RSF effluent collected from WTP Ouddorp (Table 1). The ionic composition of the synthetic initial solutions in the experiments (Table 1) was based on the yearly variation recorded in the quality of RSF effluent at the WTP. The synthetic initial solution in the reference experiment contained 0.07 µM As(V) and 2000 µM Ca, without Si, P and NOM. The rest of the experiments are identified by the ions added in µM to the reference solution (i.e. 70Si consists of 70 µM Si, 0.07 µM As(III) and 2000 µM Ca). All the synthetic initial solutions also contained 4.1 mM $NaHCO_3$ and 0.6 mM NaCl to provide alkalinity and ionic strength.

The experiments with the RSF effluent were performed with and without pre-treatment with anion exchange (AEX) or cation exchange (CEX). The objective of the AEX or CEX pre-treatment was to remove the naturally present anions or cations from the RSF effluent before use as initial solution in the experiments, to determine the impact of natural anions or cations on Fe(III) precipitation and As(V) removal. The AEX was performed with Amberlite® IRA-400 chloride form resin (CAS: 60177-39-1) and the CEX was carried out with Amberlite® IR120 N^+ form (CAS: 68441-33-8), both were obtained from Sigma Aldrich, Zwijndrecht, The Netherlands. Each IEX treatment was performed in a glass column with a contact time of 1 min and bed volumes of 78 cm^3. The RSF effluent based initial solutions were spiked with As(V) to achieve As concentration of 0.07 µmol/L (i.e. similar As concentration as synthetic initial solutions). The AEX effluent samples were dosed with $NaHCO_3$ to compensate for the loss of HCO_3 during AEX.

Table 1. Nomenclature and composition of the initial solutions used in the co-precipitation experiments. In all the initial solutions the concentration of Fe(III) was 5 µmol/L, As(V) was 0.07 µmol/L (As/Fe=0.014) and HCO_3 was 4100 µmol/L. The concentration of Ca was 2000 µmol/L in all the synthetic initial solutions (Ca/Fe=400). In RSF effluent the concentration of Ca was 2200 µmol/L (Ca/Fe=440), which was reduced to <1 µmol/L after CIEX treatment.

Experiment code	Si	P	DOC	Si/Fe	P/Fe	DOC/Fe
	µmol/L			mol/mol		
Reference (Ref)	–	–	–	–	–	–
Si70	70	–	–	14	–	–
Si140	140	–	–	28	–	–
Si280	280	–	–	56	–	–
P1.3	–	1.3	–	–	0.26	–
P2.5	–	2.5	–	–	0.5	–
P3.3	–	3.3	–	–	0.66	–
DOC165	–	–	165	–	–	33
DOC330	–	–	330	–	–	66
DOC500	–	–	500	–	–	100
Si0 + P1.3+ DOC165	–	1.3	165	–	0.26	33
Si140 + P1.3 + DOC165	140	1.3	165	28	0.26	33
Si280 + P1.3 + DOC165	280	1.3	165	56	0.26	33
Si140 + P2.5 + DOC165	140	2.5	165	28	0.5	33
Si140 + P3.3 + DOC165	140	3.3	165	28	0.66	33
Si140 + P1.3 + DOC330	140	1.3	330	28	0.26	66
Si140 + P1.3 + DOC500	140	1.3	500	28	0.26	100
Effluent RSF+	153	1.5	172	31	0.3	34
Effluent RSF after CIEX+	159	1.5	175	32	0.3	35
Effluent RSF after AIEX+ *	160	BDL	59	32	–	12

*HCO_3 was compensated after the AIEX treatment

+ As(V) was spiked using a stock solution

BDL: below detection limit (<0.2 µmol/L)

3.2.3 Co-precipitation experiments

The experiments were performed with a 5 L glass reactor connected to a controller (ez-Control, Applikon® Biotechnology) for adjusting, maintaining and logging (BioXpertV2 software) reaction parameters, including the pH, temperature, oxidant supply and stirring speed (Figure 1). The reactor was connected to a Mastersizer 2000 (Malvern Instruments, UK). The experiments were carried out at pH 7.5 and 20ºC, with stirring set to 100 rpm. The experimental procedure included: (i) preparation of the initial solutions in the reaction vessel and collection of solution samples for control, (ii) dosing the $FeCl_3$ stock to result in Fe(III) concentration of 5 µmol/L and allowing the hydrolysis and precipitation of Fe(III) to take place while the suspension was stirred at 100 rpm and (iii) collection of suspension samples after 1 and 60 min of $FeCl_3$ addition, which were filtered over 0.45 µm filters to determine the removal of Fe(III) precipitates. The samples were preserved for subsequent analysis. The unfiltered samples without conservation were collected for zeta-potential measurements.

For the filtration of samples Spartan$^{\text{TM}}$ 30/0.45 RC 0.45 µm syringe filters (GE Healthcare, Buckinghamshire, UK) were used. Samples for Fe, As, Si, Ca and P were conserved by addition of 50 µL 60% HNO_3 solution to 50 mL of sample and stored at 4 °C. The removal of As and Fe were determined from the difference between the measured values of the initial solution and final filtered solution. Samples for DOC analysis were conserved by adding 200 µL 40% HCl solution to 100 ml of sample which was closed off airtight and stored at 4 °C.

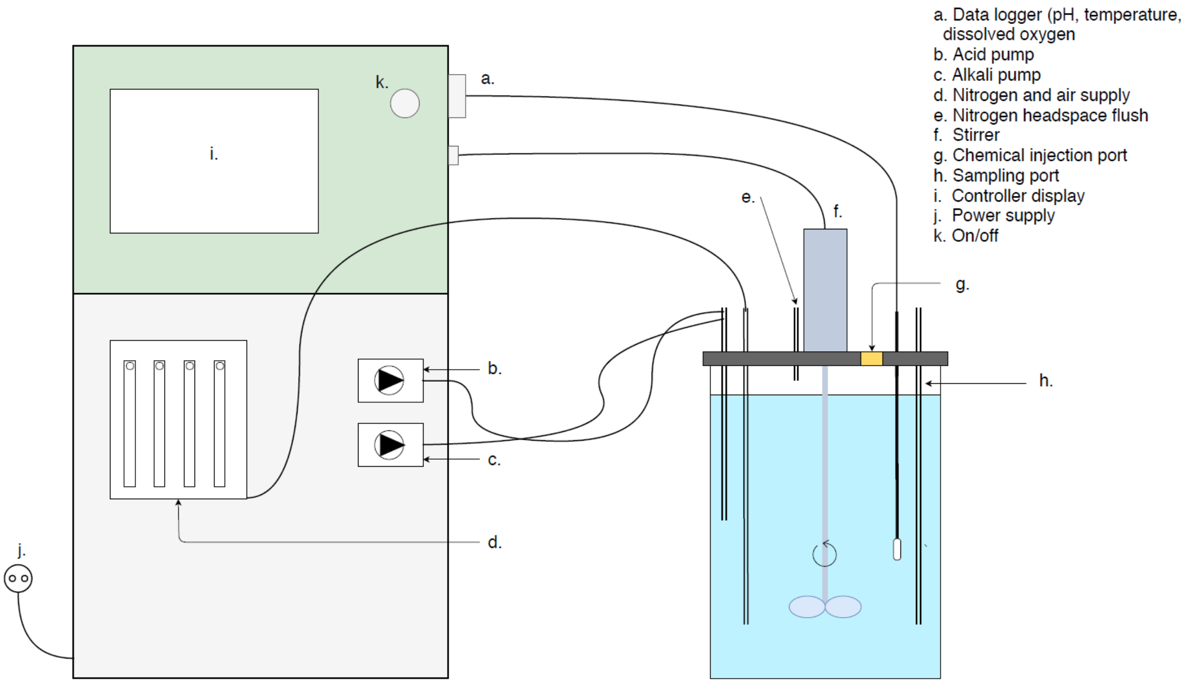

Fig 1. A schematic overview of the laboratory setup.

3.2.4 Wet analysis

Arsenic, Fe, Ca, Si, P were measured in water samples by Inductively Coupled Plasma Mass Spectrometry (ICP-MS) (XSERIES 2, Thermo Fisher Scientific, The Netherlands). The analysis of DOC in water samples was carried out with a Shimadzu TOC-V_{CPH} total organic carbon analyzer (Shimadzu Benelux, 's-Hertogenbosch, The Netherlands). Bicarbonate was analyzed by titration (HI-3811, Hanna Instruments).

3.2.5 Particle characterization

The size distribution of the Fe(III) precipitates was determined by Multiple Light Scattering (MLS) using the Mastersizer 2000 (Malvern Instruments, UK). The Mastersizer was connected to the co-precipitation reactor and the suspension was fed to the Mastersizer at a constant flow of 216 mL/min through a masterflex easy-load II peristaltic pump combination (Metrohm Nederland B.V. The Netherlands). Malvern instruments mastersizer 2000 software v5.61 recorded the particle size distribution every 20 seconds for 5 min. The Zetasizer Nano-ZS (Malvern Instruments) was used for the determination of electrophoretic mobility and the calculated zeta-potential of the particles in a sub-set of samples collected after 60 min of $FeCl_3$ dosing. Each sample was equilibrated at 20 °C for 300 seconds prior to measurement which were obtained in duplicate. The measurement cell (cuvette) was rinsed with ethanol and demineralized water and dried between the measurements.

3.3 Results and discussion

3.3.1 Size distribution and filterability of Fe(III) precipitates

3.3.1.1 Impact of independent Si, P and NOM addition

The particle size distribution and the removal efficiency of Fe(III) precipitates by 0.45 µm filters as a function of the composition of initial solution are given in Figure 2 and 3 respectively. For the reference experiment, (initial solution free of Si, P and NOM), the particles were in the range of 5–180 µm with the mode of the distribution (d_m, the most commonly occurring particle diameter) at 70 µm. The precipitates in both 1 min and 60 min samples were completely removed (≈100% removal) by 0.45 µm filtration, indicating a rapid growth of Fe(III) precipitates within the first minute. When different concentrations of Si or P were added, the size distribution of the precipitates was not significantly affected, although a slightly lower d_m (≈ 50 µm) was noted for the highest Si and P additions (i.e. 280 Si µM and 3.3 µM P) compared to the reference (d_m ≈ 70 µm). Nevertheless, the precipitates were completely removed by 0.45 µm filtration in all the samples, indicating yet effective and rapid Fe(III) precipitate growth. Silicate and P oxyanions bind to the surface of Fe(III) precipitates and result in colloidally stable suspensions (Doelsch et al. 2000, Rose et al. 1996). On the other hand, it has been shown that in the presence of Ca the electrostatic repulsion between the particles is reduced, which can result in coagulation/destabilization of colloidal Fe(III) precipitates. For example, Mayer and Jarrell (1996) reported an improved flocculation, settling and filtration of Fe(III) precipitates in a solution where the molar Si/Fe and Ca/Fe ratio was 4.5 and 20 (Ca/Si =0.2). In our study, however, the molar Ca/Si ratio was much higher (Ca/Si=7–28) than in the study of Mayer and Jarrell (1996). Similarly, Van Genuchten et al. (2014b), in their co-precipitation experiments, noticed a stabilization of Fe(III) suspensions at molar P/Fe ratio of 0.3 and destabilization of the colloids was observed when Ca was present at Ca/Fe=2.0 (Ca/P=6.7). In our study the molar Ca/P was 570–1300, thus much higher than Van Genuchten et al. (2014b). From this we conclude that in our study the large size and highly efficient removal of the Fe(III) precipitates by 0.45 µm filtration with the independent additions of Si and P was due to the presence of high Ca concentration in water (Table 1).

Unlike the Si and P additions, the independent NOM addition altered the particle size distribution significantly (Figure 2). The particle size distribution was bimodal for 330 and 500 µM DOC additions, consisting of a larger contribution from particles in the non-colloidal size range (i.e. ≥1 µm) and a relatively small contribution in the colloidal range (<1 µm) for each case (please note that the precipitate size distribution was not measured for 165 µM DOC addition). Moreover, Fe(III) removal by 0.45 µm filtration was significantly reduced (e.g. with the additions of 165, 330 and 500 µM DOC, Fe(III) removal after 60 min was ≈ 40, 30 and 20% respectively, Figure 3). These observations are in agreement with several previous studies which also report a similar reduction in the removal of Fe(III) in the presence NOM. The suppression of Fe(III) removal by filtration has been attributed to formation of soluble Fe(III)–NOM complexes, as well as formation of Fe(III)–NOM and Fe(III)(oxyhydr)oxide–NOM colloids (Davis and Edwards 2017, Kim et al. 2015, Sharma et al. 2010). These different Fe(III)–NOM complexes, which can be soluble and/or colloidal, are not removed from water by 0.45 µm filtration due to their small size. Although the exact mechanism for the decreased Fe(III) removal in the presence of NOM in our study is not clarified, it is proposed that the mobility of Fe(III) was affected by the formation of soluble and colloidal Fe(III)–NOM complexes.

To study further the precipitate aggregation, we characterized the particles from a subset of experiments by zeta-potential measurements. The zeta-potential of the reference sample was low (-2.6 mV, Table 2) and no considerable decrease was observed with the addition of 3.3 µM P (-2.8 mV). This is in agreement with the yet effective aggregation of Fe(III) precipitates with the independent P addition, similar to the reference. In the presence of 165 µM DOC the zeta-potential decreased somewhat (-11.1 mV), which is in agreement with the restricted growth of the precipitates in the presence of 165 µM DOC, due to electrostatic repulsion between the Fe(III) particles.

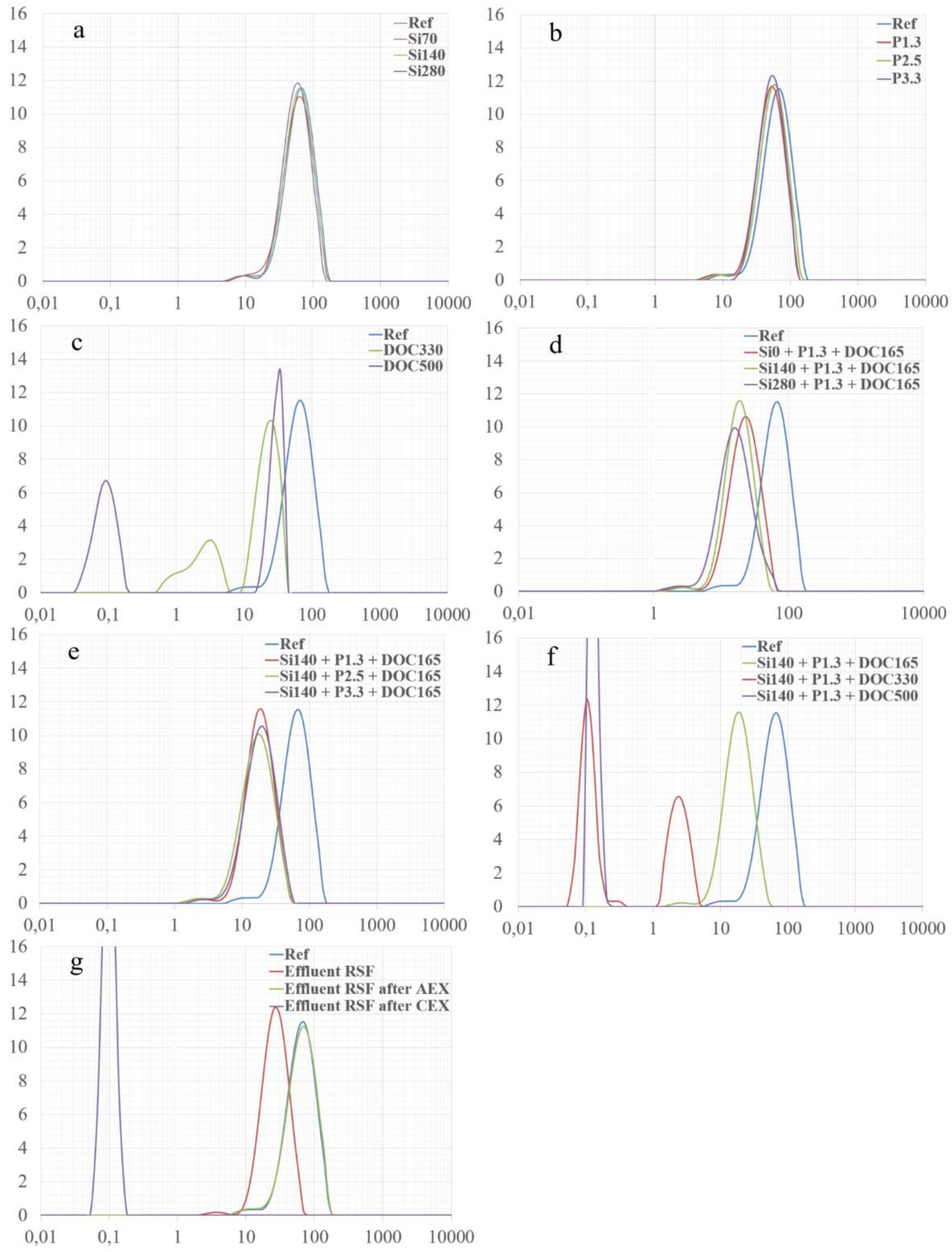

Fig 2. Independent and combined effects of silicate, phosphate and natural organic matter on Fe(III) precipitate size. X-axis: particle size (µm). Y-axis: abundance (%). Ref refers to the reference experiment performed in the absence of Si, P and NOM.In (Fig 2f & 2g) complete Y-axis is not shown. In Figure 2f the abundance peak of Si140+P1.3+DOC 500 is at 35.4%. In Figure 2g the abundance peak of Effluent RSF after CEX is at 25.5%.

3.3.1.2 Impact of combined Si, P and NOM addition

In experiments where P and NOM were present with and without Si, the Fe(III) particles were smaller than in the reference (Figure 2). Moreover, the removal of Fe(III) precipitates by 0.45 µm filtration was lower than the reference (≤80% compared to 100%) (Figure 3). Minor changes in the precipitate size were observed with the variation in solution composition. For example, in the absence of Si when 1.3 µM P was present with 165 µM DOC, particles in the range of 1.4–70 µm were observed with d_m of ≈ 20 µm. The addition of 140 to 280 µM Si in this solution resulted in a very slight decrease in the removal of Fe(III) precipitates by 0.45 µm filtration (≈ 10%). Moreover, the precipitate size range was similar to the solution that did not contain Si (i.e. 1.3 µM P and165 µM DOC). Similarly, the precipitate size distribution and the removal efficiency of Fe(III) was not significantly affected in the experiments where the concentration of P was increased from 1.3 to 3.3 µM, keeping Si and DOC fixed at 140 and 165 µM respectively. Thus, the studied variations in Si and P concentrations with fixed concentrations of NOM and Ca in water, did not severely impact the size of Fe(III) precipitates.

Compared to when only NOM (165 µM DOC) was present, the Fe(III) removal by 0.45 µm filtration was higher when NOM was present with P and Si (Figure 3). Also, the zeta-potential with the independent NOM addition was -11.1 mV, which was lower relative to the experiments in which NOM was present with Si and P (Table 2). The higher zeta-potential obviously is in agreement with the large size and higher removal of Fe(III) precipitates in the complex NOM bearing solutions (Figure 2 and 3). However, the exact mechanism responsible for the higher zeta-potential when NOM co-occurred with Si and P is not clarified. Nevertheless, we note that the interactions between NOM and Fe(III) in the absence and presence of P and Si appear to follow different mechanisms.

When the concentration of NOM was increased (from 165 to 330 µM DOC), keeping Si and P (140 and 1.3 µM respectively) fixed, the Fe(III) removal by 0.45 µm filtration was reduced significantly. A further increase in NOM concentration (to 500 µM DOC) resulted in no Fe(III) removal (Figure 3). This increasing mobility of Fe(III) may be attributed to the formation of soluble and colloidal Fe(III)–NOM complexes that were not removed with the 0.45 µm membrane filters. The presence of colloidal particles is also confirmed with the particle size distribution measurements (Figure 2). However, the identity of the particles (Fe(III)–NOM or Fe(III)(oxyhydr)oxide–NOM colloids) was not investigated. Moreover, the properties of the soluble fraction of Fe(III)–NOM complexes remain unclear. Nevertheless, our results indicate that the variations in NOM concentrations, in solution with fixed concentrations of Si, P and Ca exhibit a strong impact on the size of Fe(III) precipitates and their removal.

3.3.1.3 Impact of removing anions and cations from RSF effluent

In the RSF effluent, the Fe(III) precipitate size ranged from 2–80 µm with the d_m at 25 µm (Figure 2). The Fe(III) precipitates were effectively removed (≈ 95% removal) by 0.45 µm filtration in both 1 min and 60 min samples (Figure 3). The removal of Fe(III) precipitates in the RSF effluent was slightly higher than the synthetic solutions that contained Si, P and NOM in comparable concentrations. This can be explained by a higher charge neutralization due to the higher Ca concentration and an additional presence of ≈ 10 mg/L magnesium (Mg) in the RSF effluent compared to the synthetic solutions. When the RSF effluent was pre-treated with AEX, P and a major portion of the NOM (negatively charged) was removed from water (Table 1). The AEX did not remove Si (H_4SiO_4) because it is not disassociated at the given pH of 7.5 (de Ridder et al. 2018). Interestingly, the precipitate size distribution was quite similar to the reference (i.e. in the absence of Si, P, NOM) and in solutions where we added Si. The removal efficiency of Fe(III) in the AEX treated RSF effluent was clearly higher than the untreated RSF effluent (Figure 3) which can be attributed to a lower charge repulsion between the particles in the absence of surface sorbed (negatively charged) P and NOM ions.

When the CEX treated RSF effluent, which lacked Ca and Mg ions (Table 1), was used as the initial solution in the co-precipitation experiments, the particle size decreased and the removal of Fe(III) precipitates by 0.45 µm filtration strongly depleted (Fe(III) removal <10%). It has been shown previously that the presence of cations in solutions result in neutralization of Fe(III) precipitate surface charge and a lower electrostatic repulsion which promotes growth of Fe(III) precipitates (Ahmad et al. 2019a, van Genuchten et al. 2014a, Van Genuchten et al. 2014b). In this study, when Ca and Mg were removed from water by CEX, the sorption of Si, P and NOM on Fe(III) precipitate surface resulted in a negatively charged precipitate surface with high electrostatic repulsion which hindered the precipitate growth (de Ridder et al. 2018).

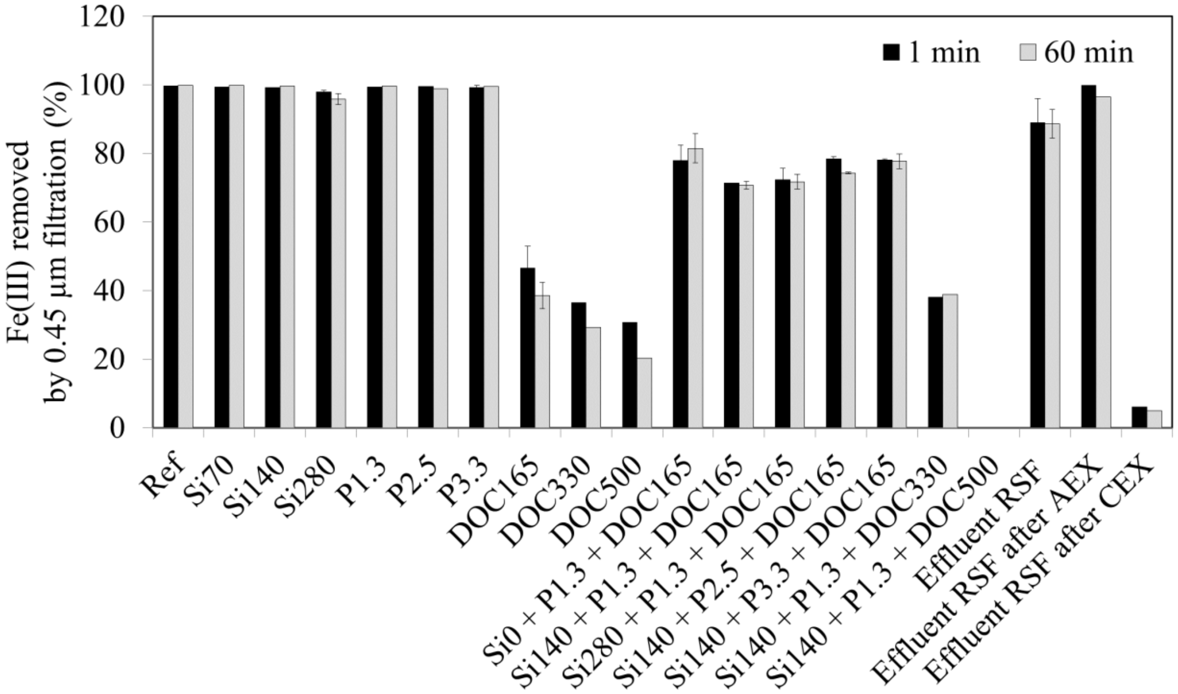

Figure 3. Percentage Fe(III) removed by 0.45 µm filtration as a function of the composition of the initial solution and time. Ref refers to the reference experiment performed in the absence of Si, P and NOM.

3.3.2 Arsenic removal

3.3.2.1 Impact of independent Si, P and NOM additions

Arsenate removal was the highest in the reference experiment (i.e. in the absence of Si, P and NOM), with As(V) removal efficiency of 65% and ≈ 90% after 1 min and 60 min respectively (Figure. 4A). This represents a ≈ 75% of the total As(V) removed in the first minute, indicating a rapid adsorption of As(V) to Fe(III) precipitate surfaces. Since Fe(III) precipitates were completely removed by 0.45 µm filtration after both 1 min and 60 min (Figure 3), the ≈ 25% increase in As(V) removal in reference experiment was attributed to the diffusion-controlled mass transfer of As to adsorption sites located in the internal porosity of Fe(III) precipitates (Figure 4). The similar time-dependent As(V) adsorption kinetics observed in the presence of Si, P and NOM can also be explained by the slow transfer of As towards the internal adsorption sites (Figure 4B). The independent additions of Si, P and NOM resulted in a lower As(V) removal efficiency compared to the reference (Figure 4A). The addition of 70 µM Si resulted in As(V) removal efficiency of 45% and 75% after 1 min and 60 min, which decreased to ≈ 40% and 60% respectively, with the independent addition of the highest concentration of (280 µM Si). The addition of 1.3 µM P resulted in an As(V) removal efficiency of 25% and 44% after 1 min and 60 min, which decreased to ≈ 20% and 30% respectively, with the independent addition of the highest concentration of P (3.3 µM P). As the removal of Fe(III) precipitates by 0.45 µm filtration was (nearly) complete (Figure 3), we conclude that the reduced As(V) removal was due to a reduced adsorption of As(V) onto the surface of Fe(III) precipitates, similar to the reference (Dixit and Hering 2003, Meng et al. 2000).

Figure 4B shows that the independent P additions, though much smaller compared to Si (Table 1), results in a lower As(V) adsorption efficiency than with Si additions. These results can be explained by the pH dependent affinity of As(V), P and Si for the adsorption sites on Fe(III) precipitates (Ahmad et al. 2019a, Van Genuchten et al. 2014b, Voegelin et al. 2010) and the concentration differences between Si and P relative to As(V). The adsorption of As(V), Si and P onto the surface of Fe(III) precipitates is competitive. However, at pH 7.5 (this study), As(V) and P exhibit a similarly high affinity for adsorption sites on Fe(III) precipitates due to their negative charge and similar chemical properties. Silicate, on the other hand, is uncharged at pH 7.5 and the adsorption onto Fe(III) precipitates is much lower than As(V) and P. Thus, the greater reduction in As(V) adsorption due to lower P concentrations than Si is rationalized.

The As(V) removal efficiency was the lowest with the independent NOM additions. For example, the addition of 165 µM DOC resulted in As(V) removal efficiency of ≈ 20% and 35% after 1 min and 60 min, which decreased to 10% and 15% respectively with the independent addition of 500 µM DOC. The lower As(V) removal efficiency (Figure 4A) compared to the reference was due to i) the lower adsorption of As(V) onto the surface of Fe(III) precipitates, as reflected in the lower As/Fe solids ratio for NOM additions (Figure 4B), and ii) a higher mobility of Fe(III) due to the formation of Fe(III)–NOM complexes that were not removed by 0.45 µm filtration (Figure 3). With NOM additions, the As/Fe solid ratio was higher than the As/Fe solid ratio with P additions. This indicates a stronger competition with As(V) for adsorption sites by P than NOM (Figure 4B). Compared to the Si additions, the As/Fe solid ratio was slightly lower in case of NOM additions. This indicates a stronger competition with As(V) for adsorption sites by NOM than Si (Figure 4B). Thus, in the given conditions, P competed with As(V) for adsorption sites on Fe(III) precipitates most strongly and reduced the As(V) adsorption followed by NOM, whereby Si showed had the least negative impact on As(V) adsorption.

From these results it can be concluded that the removal of As(V) in the presence of Si and P was affected mainly because of the reduced adsorption of As(V), whereas in the presence of NOM a reduced adsorption and a reduced Fe(III) removal both were responsible. Phosphate reduced As(V) adsorption the most, mainly because of its similar affinity for adsorption sites and higher concentration than As(V). But, the overall As(V) removal efficiency was reduced the most with the variations in NOM concentrations, mainly because NOM rendered a large portion of Fe(III) mobile in the solution.

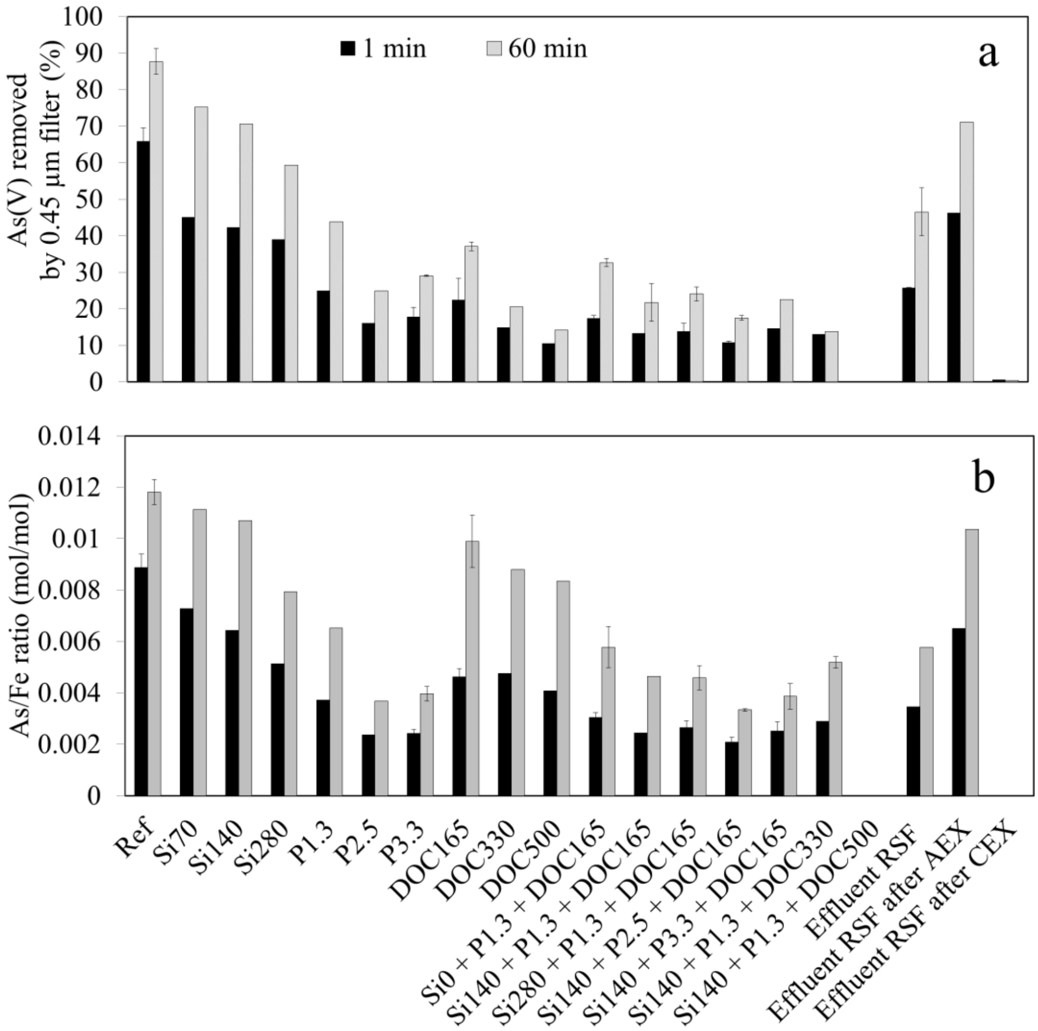

Fig 4. (a) Percentage As(V) removed by 0.45 µm filtration and (b) As(V) uptake by Fe(III) precipitates as a function of the composition of the initial solution and time. Ref refers to the reference experiment performed in the absence of Si, P and NOM.

3.3.2.2 Impact of combined Si, P and NOM additions

In the experiments where 165 µM DOC was fixed and P and Si concentrations were varied, the As(V) removal efficiency was lower than the reference experiment and the experiments with the corresponding independent Si, P and NOM additions (Figure 4A). For example, with 165 µM DOC fixed, the addition of 1.3 µM P resulted in As(V) removal efficiency of 17 and 32% after 1 min and 60 min. This was lower than the As(V) removal efficiencies observed for the independent 1.3 µM P (25% and 44% after 1 min and 60 min) and 165 µM DOC (22% and 37% after 1 min and 60 min) additions. The lower As removal can be attributed to i) a greater competition for the adsorption of As(V) onto Fe(III) precipitates due to the presence of multiple inorganic and organic ions, as also confirmed by the lower As/Fe solid ratios, and ii) a NOM-induced higher mobility of Fe(III) (Figure 3), as discussed previously.

At fixed P and NOM concentrations (1.3 µM P and 165 µM DOC), the addition of Si up to 280 µM resulted in only a slight reduction in As(V) removal efficiency compared to the absence of Si. Similarly, the removal efficiency of As(V) was reduced only slightly when P concentrations were increased up to 3.3 µM in the presence of 140 and 165 µM Si and DOC respectively. The subtle decrease in As(V) removal was attributed to a stronger competition for As(V) adsorption onto Fe(III) precipitates which resulted in a lower As/Fe solid ratio (Figure 4B). Arsenate removal efficiency was majorly reduced with an increase in NOM concentration, with Si and P also present in water at fixed concentrations. For example, when 500 µM DOC was added along with 140 µM Si and 1.3 µM P, As(V) removal was reduced to zero. The absence of As(V) removal (Figure 4A) was due to formation of Fe–NOM complexes that could not be filtered, as discussed previously.

Overall, it can be concluded that in complex solutions, containing Si, P, NOM and Ca, As(V) removal appears to be most sensitive to variations in NOM concentration, with NOM- Fe(III) complexation a key determinant.

3.3.2.3 Impact of removing anions and cations from RSF effluent

In the RSF effluent, the As(V) removal was lower than the reference experiment, i.e. As(V) removal was 46% in the RSF effluent compared to ≈ 90% for the reference solution after 60 min (Figure 4A). The lower As(V) removal in RSF effluent compared to the reference was largely due to competition for As(V) adsorption from the anions such as Si, P and NOM. This was also confirmed by pre-treating the RSF effluent by AEX which showed that As(V) removal significantly increased with the removal of P and NOM (Table 1). The removal of Si with AEX treatment was not effective and therefore Si competed with As(V) for the adsorption sites, resulting in As/Fe solid ratio that matched the experiments where independent Si additions were investigated (Figure 4B).

Arsenate removal was absent when the CEX-pre-treated RSF effluent was used as initial solution. The fact that no removal was observed in the absence of Ca and Mg is mainly due to the high mobility of Fe(III), which can be attributed to the highly negative surface of Fe(III) precipitates that hinders the growth of Fe(III) precipitates to become larger particles. The mechanistic understanding of how cations like Ca interact with Fe(III) precipitates in multi-anionic solutions has been presented in previous studies. It has been reported that when Ca is present during co-precipitation of Fe(III) and (oxy)anions such as Si, P, As(V) and NOM, it is incorporated in the structure of the growing Fe(III) precipitates due to chemical bonding with the surface-sorbed oxyanions (van Genuchten et al. 2014a). Moreover, Ca interacts electrostatically with the surface of Fe(III) precipitates. Magnesium ions have also been shown to enhance aggregation of Fe(III) precipitates, but the effect is less pronounced than Ca (Senn et al. 2015, Van Genuchten et al. 2014b).

Table 2. The zeta-potential of Fe(III) precipitates in a sub-set of experiments.

Experiment code	Zeta-potential [mV]
Reference	-2.6 ± 0.9
P3.3	-2.8 ± 0.6
DOC165	-11.1 ± 1.5
P1.3 + DOC165	-5.5 ± 1.9
Si140 + P1.3 + DOC165	-5.7 ± 0.9
Si280 + P1.3 + DOC165	-7.6 ± 0.2
Si140 + P2.5 + DOC165	-7.1 ± 0.6
Si140 + P1.3 + DOC330	-13.1 ± 0.3
RSF effluent	-7.0 ± 1.2

3.4 Conclusions and implications for water treatment

This study shows that As(V) removal in Fe(III) based co-precipitation is sensitive to the composition of water matrix. In complex solutions containing multiple solutes and high levels of Ca, (variations in) Si and P concentrations reduce As(V) removal to some extent, mainly due to a decreased adsorption of As(V) onto Fe(III) precipitates. On the other hand, NOM concentrations reduce As(V) removal quite drastically, which we attribute largely to the formation of soluble and colloidal Fe(III)–NOM complexes.

The findings presented in this study have a great significance for predicting As removal at water treatment plants where water quality changes may take place, e.g. due to seasonal effects. Surface complexation modeling (Dzombak and Morel 1990, Hiemstra and Van Riemsdijk 1999, Kanematsu et al. 2010, 2013b, Stachowicz et al. 2008) is useful in gaining further insights in the As uptake by Fe(III) precipitates, but its application to real water treatment systems is limited. In water treatment plants, the effectiveness of As removal also depends on the separation of Fe(III) precipitates from water. Calcium effectively counteracts the negative effect of oxyanions and promotes the growth of Fe(III) precipitates, which can be easily separated from water by gravitation settling and rapid sand filtration. Thus, hardness of water should be carefully considered in designing As removal processes that rely on the co-precipitation of As and Fe. Obviously, effective separation of the colloidal particles can also be achieved by employing low-pressure membrane filtration (MF/UF) instead of the conventional rapid sand filtration for effective separation of the colloidal particles. Nevertheless, also in this case, the charge and size distribution of Fe(III) precipitates will remain crucial in determining the membrane fouling mechanisms.

References

Ahmad, A., Cornelissen, E., van de Wetering, S., van Dijk, T., van Genuchten, C., Bundschuh, J., van der Wal, A. and Bhattacharya, P. (2018) Arsenite removal in groundwater treatment plants by sequential Permanganate—Ferric treatment. Journal of Water Process Engineering 26, 221-229.

Ahmad, A., van der Wal, B., Bhattacharya, P. and van Genuchten, C.M. (2019) Characteristics of Fe and Mn bearing precipitates generated by Fe(II) and Mn(II) co-oxidation with O2, MnO4 and HOCl in the presence of groundwater ions. Water Research.

Chen, C., Dynes, J.J., Wang, J., Karunakaran, C. and Sparks, D.L. (2014) Soft X-ray Spectromicroscopy Study of Mineral-Organic Matter Associations in Pasture Soil Clay Fractions. Environmental Science & Technology 48(12), 6678-6686.

Choi, K.Y.-j. and Dempsey, B.A. (2004) In-line coagulation with low-pressure membrane filtration. Water Research 38(19), 4271-4281.

Davis, C.C. and Edwards, M. (2017) Role of Calcium in the Coagulation of NOM with Ferric Chloride. Environmental Science & Technology 51(20), 11652-11659.

de Ridder, D.J., van de Wetering, S., van Dijk, T. and van Halem, D. (2018) Influence of HPO4 2- , H4SiO4 , Ca2+ , Mg2+ on Fe floc growth and As(III) removal in aerated, natural groundwater.

Dixit, S. and Hering, J.G. (2003) Comparison of arsenic(V) and arsenic(III) sorption onto iron oxide minerals: Implications for arsenic mobility. Environmental Science and Technology 37(18), 4182-4189.

Doelsch, E., Rose, J., Masion, A., Bottero, J.Y., Nahon, D. and Bertsch, P.M. (2000) Speciation and Crystal Chemistry of Iron(III) Chloride Hydrolyzed in the Presence of SiO4 Ligands. 1. An Fe K-Edge EXAFS Study. Langmuir 16(10), 4726-4731.

Dong, H.R., Guan, X.H., Wang, D.S. and Ma, J. (2011) Individual and combined influence of calcium and anions on simultaneous removal of chromate and arsenate by Fe(II) under suboxic conditions

Separation and Purification Technology 80, 284-292.

Dzombak, D.A. and Morel, F.M.M. (1990) Surface Complexation Modeling: Hydrous Ferric Oxide, John Wiley & Sons, New York, New York.

Fuller, C.C., Davis, J.A. and Waychunas, G.A. (1993) Surface chemistry of ferrihydrite: Part 2. Kinetics of arsenate adsorption and coprecipitation. Geochimica et Cosmochimica Acta 57(10), 2271-2282.

Guan, X., Dong, H., Ma, J. and Jiang, L. (2009a) Removal of arsenic from water: Effects of competing anions on As(III) removal in KMnO4–Fe(II) process. Water Research 43(15), 3891-3899.

Guan, X., Ma, J., Dong, H. and Jiang, L. (2009b) Removal of arsenic from water: Effect of calcium ions on As(III) removal in the KMnO4–Fe(II) process. Water Research 43(20), 5119-5128.

Gude, J.C.J., Joris, K., Huysman, K., Rietveld, L.C. and van Halem, D. (2018) Effect of supernatant water level on As removal in biological rapid sand filters. Water Research X 1, 100013.

Gude, J.C.J., Rietveld, L.C. and van Halem, D. (2016) Fate of low arsenic concentrations during full-scale aeration and rapid filtration. Water Research 88, 566-574.

Hering, J.G., Chen, P.-Y., Wilkie, J.A., Elimelech, M. and Liang, S. (1996) Arsenic removal by ferric chloride. American Water Works Association 88(4), 155-167.

Hiemstra, T. and Van Riemsdijk, W.H. (1999) Surface structural ion adsorption modeling of competitive binding of oxyanions by metal (Hydr)oxides. Journal of Colloid and Interface Science 210(1), 182-193.

Jain, A., Raven, K. and R.H., L. (1999) Arsenite and Arsenate Adsorption on Ferrihydrite: Surface Charge Reduction and Net OH- Release Stoichiometry.

Jessen, S., Larsen, F., Koch, C.B. and Arvin, E. (2005) Sorption and Desorption of Arsenic to Ferrihydrite in a Sand Filter. Environmental Science & Technology 39(20), 8045-8051.

Kanematsu, M., Young, T.M., Fukushi, K., Green, P.G. and Darby, J.L. (2010) Extended Triple Layer Modeling of Arsenate and Phosphate Adsorption on a Goethite-based Granular Porous Adsorbent. Environmental Science & Technology 44(9), 3388-3394.

Kanematsu, M., Young, T.M., Fukushi, K., Green, P.G. and Darby, J.L. (2013) Arsenic(III, V) adsorption on a goethite-based adsorbent in the presence of major co-existing ions: Modeling competitive adsorption consistent with spectroscopic and molecular evidence. Geochimica et Cosmochimica Acta 106, 404-428.

Kim, E.J., Hwang, B.-R. and Baek, K. (2015) Effects of natural organic matter on the coprecipitation of arsenic with iron. Environmental Geochemistry and Health 37(6), 1029-1039.

Lakshmanan, D., Clifford, D. and Samanta, G. (2008) Arsenic Removal by Coagulation with Aluminum, Iron, Titanium, and Zirconium. American Water Works Association 100(2), 76-88.

Laky, D. and Licskó, I. (2011) Arsenic removal by ferric-chloride coagulation – effect of phosphate, bicarbonate and silicate. Water Science and Technology 64(5), 1046-1055.

Masue, Y., Loeppert, R.H. and Kramer, T.A. (2007) Arsenate and Arsenite Adsorption and Desorption Behavior on Coprecipitated Aluminum:Iron Hydroxides. Environmental Science & Technology 41(3), 837-842.

Mayer, T.D. and Jarrell, W.M. (1996) Formation and stability of iron(II) oxidation products under natural concentrations of dissolved silica. Water Research 30(5), 1208-1214.

Meng, X., Bang, S. and Korfiatis, G.P. (2000) Effects of silicate, sulfate, and carbonate on arsenic removal by ferric chloride. Water Research 34(4), 1255-1261.

Qiao, J., Jiang, Z., Sun, B., Sun, Y., Wang, Q. and Guan, X. (2012) Arsenate and arsenite removal by FeCl3: Effects of pH, As/Fe ratio, initial As concentration and co-existing solutes. Separation and Purification Technology 92, 106-114.

Roberts, L.C., Hug, S.J., Ruettimann, T., Billah, M.M., Khan, A.W. and Rahman, M.T. (2004) Arsenic Removal with Iron(II) and Iron(III) in Waters with High Silicate and Phosphate Concentrations. Environmental Science & Technology 38(1), 307-315.

Rose, J., Manceau, A., Bottero, J.-Y., Masion, A. and Garcia, F. (1996) Nucleation and Growth Mechanisms of Fe Oxyhydroxide in the Presence of PO 4 Ions. 1. Fe KEdge EXAFS Study.

Senn, A.-C., Kaegi, R., Hug, S.J., Hering, J.G., Mangold, S. and Voegelin, A. (2015) Composition and structure of Fe(III)-precipitates formed by Fe(II) oxidation in water at near-neutral pH: Interdependent effects of phosphate, silicate and Ca. Geochimica et Cosmochimica Acta 162, 220-246.

Sharma, P., Ofner, J. and Kappler, A. (2010) Formation of Binary and Ternary Colloids and Dissolved Complexes of Organic Matter, Fe and As. Environmental Science & Technology 44(12), 4479-4485.

Smedley, P.L. and Kinniburgh, D.G. (2002) A review of the source, behaviour and distribution of arsenic in natural waters. Applied Geochemistry 17(5), 517-568.

Sorlini, S. and Gialdini, F. (2010) Conventional oxidation treatments for the removal of arsenic with chlorine dioxide, hypochlorite, potassium permanganate and monochloramine. Water Research 44(19), 5653-5659.

Sposito, G. (2008) The Chemistry of Soils, Oxford University Press, New York.

Stachowicz, M., Hiemstra, T. and van Riemsdijk, W.H. (2008) Multi-competitive interaction of As(III) and As(V) oxyanions with Ca(2+), Mg(2+), PO(3-)(4), and CO(2-)(3) ions on goethite. J Colloid Interface Sci 320(2), 400-414.

Su, C. and Puls, R.W. (2001) Arsenate and Arsenite Removal by Zerovalent Iron: Effects of Phosphate, Silicate, Carbonate, Borate, Sulfate, Chromate, Molybdate, and Nitrate, Relative to Chloride. Environ. Sci. Technol. 35(22), 4562-4568.

van Genuchten, C.M., Addy, S.E.A., Peña, J. and Gadgil, A.J. (2012) Removing Arsenic from Synthetic Groundwater with Iron Electrocoagulation: An Fe and As K-Edge EXAFS Study. Environmental Science & Technology 46(2), 986-994.

van Genuchten, C.M., Gadgil, A.J. and Peña, J. (2014a) Fe(III) Nucleation in the Presence of Bivalent Cations and Oxyanions Leads to Subnanoscale 7 Å Polymers. Environmental Science & Technology 48(20), 11828-11836.

Van Genuchten, C.M., Pena, J., Amrose S, E. and Gadgil, A.J. (2014b) Structure of Fe(III) precipitates genberated by the electrolytric dissolution of Fe(0) in the presence of groundwater ions. Geochimica et Cosmochimica Acta 127, 285-304.

Voegelin, A., Kaegi, R., Frommer, J., Vantelon, D. and Hug, S.J. (2010) Effect of phosphate, silicate, and Ca on Fe(III)-precipitates formed in aerated Fe(II)- and As(III)-containing water studied by X-ray absorption spectroscopy. Geochimica et Cosmochimica Acta 74(1), 164-186.

Waychunas, G.A., Rea, B.A., Fuller, C.C. and Davis, J.A. (1993) Surface chemistry of ferrihydrite: Part 1. EXAFS studies of the geometry of coprecipitated and adsorbed arsenate. Geochimica et Cosmochimica Acta 57(10), 2251-2269.

Weng, L., Van Riemsdijk, W.H. and Hiemstra, T. (2008) Humic nanoparticles at the oxide-water interface: Interactions with phosphate ion adsorption. Environmental Science and Technology 42(23), 8747-8752.

Weng, L., Van Riemsdijk, W.H. and Hiemstra, T. (2009) Effects of Fulvic and Humic Acids on Arsenate Adsorption to Goethite: Experiments and Modeling. Environmental Science & Technology 43(19), 7198-7204.

Wilkie, J.A. and Hering, J.G. (1996) Adsorption of arsenic onto hydrous ferric oxide: effects of adsorbate/adsorbent ratios and co-occurring solutes. Colloids and Surfaces A: Physicochemical and Engineering Aspects 107, 97-110.

Youngran, J., Fan, M., Van Leeuwen, J. and Belczyk, J.F. (2007) Effect of competing solutes on arsenic(V) adsorption using iron and aluminum oxides. Journal of Environmental Sciences 19(8), 910-919.

4 Arsenite removal in groundwater treatment plants by sequential permanganate—ferric treatment

This chapter has been published as:

Ahmad, A., Cornelissen, E., van de Wetering, S., van Dijk, T., van Genuchten, C., Bundschuh, J., van der Wal, A. Bhattacharya, P. (2018). Arsenite removal in groundwater treatment plants by sequential Permanganate—Ferric treatment. Journal of Water Process Engineering, 26, 221-229.

4.1 Introduction

Arsenic in drinking water is one of the largest human health risks known at the present time, with well over 200 million people around the world being exposed to high As concentrations (McCarty et al. 2011, Murcott 2012, Naujokas et al. 2013). Arsenic can be released from the Earth's crust into drinking water sources by both natural (e.g. leaching from rocks and sediments, volcanism) and anthropogenic processes (e.g. mining, agrochemicals, wood preservatives) (Bhattacharya et al. 2002, Borba et al. 2003, Bundschuh et al. 2017, Gunduz et al. 2010, MacDonald et al. 2016, Marszałek and Wąsik 2000, Nriagu et al. 2007, Woo and Choi 2001). In aqueous environments As may occur in organic and inorganic forms, whereby the latter is known to predominate in fresh water (Bhattacharya et al. 2007, Pontius et al. 1994, Smedley and Kinniburgh 2002). Inorganic As predominantly occurs in two oxidation states; +3 and +5, with varying level of protonation, depending on the pH (Ferguson and Gavis 1972, Pontius et al. 1994, Smedley and Kinniburgh 2002, Wang and Mulligan 2006).

Arsenic can cause a number of carcinogenic and non-carcinogenic adverse effects on human health (Schuhmacher-Wolz et al. 2009, Smith et al. 1992, Vahter 2008, Vahter et al. 2012), however, its mode of action and dose-response characteristics allowing for the identification of a safe exposure level are still not well-understood (Kozisek 2017, Pontius et al. 1994, Schmidt 2014, WHO 2011). This leads to considerable uncertainties about the actual risks of As exposure, especially at low concentrations (Kozisek 2017). Following a preventive approach, the Dutch drinking water sector is actively investigating treatment options to reduce trace levels of As from drinking water to <1 µg/L (Van der Wens et al. 2016). Groundwater is the main source of drinking water in the Netherlands and As concentration in raw groundwater ranges between <0.5-70 µg/L (Ahmad et al. 2015, Stuyfzand et al. 2008). In drinking water, produced at approximately 180 centralized Water Treatment Plants (WTPs), the concentration of As ranges between <0.5-6.2 µg/L (Ahmad et al. 2015, Stuyfzand et al. 2008) which shows that As is removed with varying efficiencies during treatment and the resulting concentrations in drinking water are well below the WHO guideline (10 µg/L).

Most groundwater treatment plants in the Netherlands typically apply aeration followed by rapid sand filtration to accomplish the removal of dissolved iron [Fe(II)], manganese [Mn(II)] and ammonium (NH_4^+) from water through distinct removal pathways (de Moel et al. 2006). Iron(II) may oxidize homogeneously, heterogeneously and biologically, or by a combined mechanism involving these processes, leaving hydrous ferric oxide (HFO) precipitates (Fe(III)-precipitates) in the supernatant, in the pores and on the surface of the filter media (Jessen et al. 2005, Van Beek et al. 2012, Vries et al. 2017). Direct oxidation of Mn(II) by oxygen (O_2) is generally negligible (Diem and Stumm 1984, Lytle et al. 2005) and bacteria and surface catalysts on the filter media grains are known to transform Mn(II) to insoluble hydrous manganese oxide (MnO_2) (Bruins et al. 2015, Katsoyiannis et al. 2008). Ammonium is removed by nitrification which takes place in the filter bed, mediated by different bacterial species (de Moel et al. 2006, De Vet

2011). These treatment plants also remove As, attributed to adsorption to the precipitated HFO (Ahmad et al. 2015, Gude et al. 2016), as observed by McNeill and Edwards (1995) and Lytle et al. (2007) in several groundwater treatment plants in the United States, by Sorlini et al. (2014) in Italy and by Katsoyiannis et al. (2008) in Greece. The presence of anions in groundwater e.g. phosphate, sulfate, carbonate, silicate, as well as the natural organic matter may reduce the adsorption of As to Fe(III)-precipitates due to their competition for adsorption sites (Dixit and Hering 2003, Hering et al. 1996, Qiao et al. 2012, Su and Puls 2001, Wilkie and Hering 1996, Youngran et al. 2007), sometimes rendering the amount of natural Fe in raw water insufficient to achieve the target effluent As concentration. The concentration of Fe nevertheless can be increased by dosing an Fe(III) or Fe(II) based coagulant such as ferric chloride ($FeCl_3$) or ferrous sulfate ($FeSO_4$). The As removal efficiency may differ when Fe(II) or Fe(III) is dosed, per equal concentration of precipitated Fe (Gude et al. 2017, Roberts et al. 2004). In The Netherlands, $FeCl_3$ is the most widely used coagulant in drinking water production and for this reason we chose it as the source of Fe in this study.

The adsorption of As to Fe(III)-precipitates is also sensitive to As species in water (Jain and Ali 2000, Pierce and Moore 1982, Raven et al. 1998, Wilkie and Hering 1996). The adsorption of As(V) to Fe(III)-precipitates at low As/Fe molar ratios and pH relevant for most groundwater (6.5-8.5) is more efficient compared to As(III) (Hering et al. 1996, Hsu et al. 2008, Lakshmanan et al. 2008, Lytle et al. 2005, Qiao et al. 2012), mainly because of the anionic character of As(V). Therefore, at WTPs where As(III) is a dominant species in source water, (pre-)oxidation of As(III) to As(V) could increase As removal. Oxidation of As(III) by dissolved O_2 alone is thermodynamically possible, however the reaction proceeds very slowly (Frank and Clifford 1986, Kim and Nriagu 2000), rendering the traditional aeration techniques, e.g. spray or cascade aeration, inefficient in oxidizing As(III) (Jessen et al. 2005, Katsoyiannis et al. 2008, Lytle et al. 2007). Chemical oxidants, such as chlorine, ozone, hydrogen peroxide, permanganate (MnO_4^-) etc. have been shown to achieve rapid oxidation of As(III) (Bissen and Frimmel 2003). In this study MnO_4^- was used for As(III) oxidation because it has the ability to oxidize As(III) over a broad pH range and within time frame of seconds to one minute (Ghurye and Clifford 2001, Lihua et al. 2009, Sorlini and Gialdini 2010). Furthermore, MnO_4^- does not form harmful by-products such as chlorination in the presence of humic substances (Smeets et al. 2009) and ozonation with bromide present (Von Gunten 2003) and is easy to dose and affordable (Borho and Wilderer 1996, Guan et al. 2009b).

Arsenic removal from water involving MnO_4^- and Fe(III) dosing has been previously investigated. Borho and Wilderer (1996) demonstrated at pilot scale that MnO_4^- dosing followed by Fe(III) dosing could lead to very low residual As concentration, provided the As containing Fe(III)-precipitates were sufficiently removed from water. Lihua et al. (2009) studied the MnO_4^- and Fe(III) dosing in water with the aim of developing a small system for rural populations in low income countries. They used tap water spiked with As(III) in their experiments and filtration was accomplished through a sand filter followed by ultrafiltration (UF). It was shown that when water was pre-treated with MnO_4^- for As(III) oxidation, lower and more stable effluent As concentrations were achieved and the sand filtration was mainly responsible for the removal of As-laced Fe(III)-precipitates. Bordoloi et al. (2013) studied As(III) removal from groundwater water by MnO_4^- and Fe(III) dosing at mild alkaline pH that was achieved through the addition of $NaHCO_3$ in water. Their study was also aimed at developing a process for rural application in low income countries. With laboratory and field experiments, Bordoloi et al. (2013) showed that As(III) could be efficiently removed to meet the WHO guideline for As in drinkingwater (10 µg/L).

All these studies show that MnO_4^-—Fe(III) dosing is a promising method to increase the As(III) removal efficiency at typical aeration—rapid sand filtration type groundwater treatment facilities where As(III) is present in the raw water, however As removal to <1 µg/L, as aimed in this study, has never been a goal of any of the previous studies. The effects of adopting MnO_4^-—Fe(III) dosing on the existing removal efficiencies of Fe(II), Mn(II) and NH_4^+ at typical aeration—rapid sand filtration type groundwater treatment facilities are also not well documented in literature. Moreover, the influence on settling characteristics of filter backwash water, which is an important parameter affecting the design and operation of backwash water treatment at WTPs, has not been studied before. Consequently, the aim of this study was (1) to achieve <1 µg/L As by MnO_4^-—Fe(III) dosing at a typical aeration—rapid sand filtration facility (2) to study the influence of MnO_4^-—Fe(III) dosing on the removal of As, Fe, Mn and NH_4^+

in rapid sand filtration and (3) to study the influence of MnO_4^-—Fe(III) dosing on the settling and molecular scale structural properties of the filter backwash solids. The study, including batch, pilot and full-scale experiments, was carried out at a groundwater treatment facility (WTP Dorst) in the Netherlands with typical aeration—rapid sand filtration based treatment scheme.

4.2 Materials and methods

4.2.1 Treatment layout and water quality of WTP Dorst

WTP Dorst is a typical groundwater treatment facility (10 Mm^3/year production) in the Netherlands which treats anaerobic groundwater in 10 parallel treatment trains, each comprising of a cascade aeration step followed by a submerged rapid sand filter (Figure 1). The surface area and bed height of the sand filters are 27 m^2 and 1.8 m respectively. They contain a single media filter material (silica sand D50=1.3 mm) and are operated at an average (superficial) filtration velocity of 4.6 m/h (filter loading Q=125 m^3/h). Table 1 presents the raw and treated water quality at WTP Dorst.

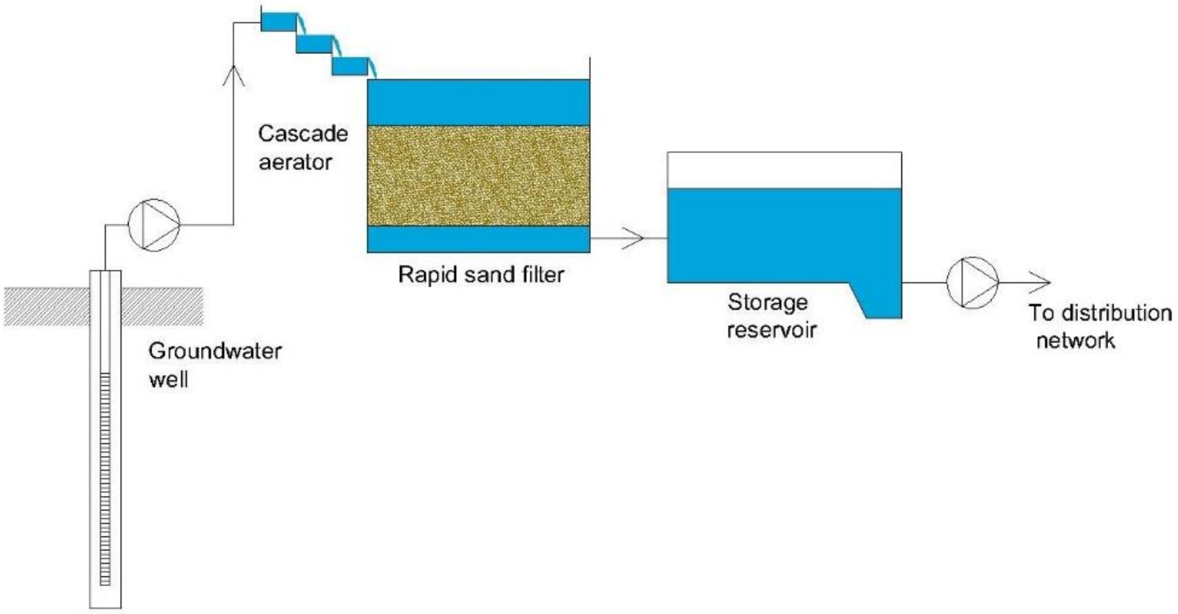

Figure 1. Typical groundwater treatment layout in the Netherlands.

Table 1: Raw and treated water quality of WTP Dorst.

Parameters	Unit	Raw water	Treatment Plant Effluent (Drinking water)	Dutch guidelines for drinking water quality*
pH		7.6 ± 0.1	7.7 ± 0.1	7.0 < pH < 9.5
Temp.	°C	12.2 ± 0.7	12.4 ± 0.6	≤ 25
EC	µS/cm	410 ± 20	406 ± 10	≤ 1250
HCO_3^-	mg/L	251 ± 25	240 ± 10	> 60
Total As$^{\times}$	µg/L	11.9 ± 1.0	6.2 ± 0.7	≤ 10
As(III)$^{¥}$	µg/L	11.7 ± 1.0	0.8 ± 0.1	-
Fe(II)	µg/L	1400 ± 70	<10	≤ 200
Mn(II)	µg/L	40 ± 10	<10	≤ 50
NH_4^+	mg/L	0.55 ± 0.1	<0.03	≤ 0.2
Ca^{+2}	mg/L	65 ± 4	66 ± 3	-
Mg^{+2}	mg/L	6.9 ± 0.4	7.5 ± 0.3	-
TOC	mg C/L	2.4 ± 0.2	2.1 ± 0.2	-

*Drinkwaterbesluit, 2008 (http://wetten.overheid.nl/BWBR0030111/2015-11-28)
$^{\times}$After implementation of MnO_4^-—Fe(III), As=0.6 ± 0.1 µg/L in treatment plant effluent
$^{¥}$ After implementation of MnO_4^-—Fe(III), As(III) <0.5 µg/L in treatment plan effluent.

4.2.2 Optimizing MnO_4 and Fe(III) doses to achieve <1 µg/L As

4.2.2.1 Preliminary batch experiments

To gain preliminary information on MnO_4^- and Fe(III) doses required to remove As to <1 µg/L, a series of batch tests was carried out using the raw water of WTP Dorst (Table 1). The experiments were performed with a jar test apparatus, which comprised a set of six transparent jars (2 L capacity each). Each jar was equipped with a dosing unit to add MnO_4^- and Fe(III), a paddle for mechanical stirring and a sampling point in the bottom. The timing of MnO_4^- and Fe(III) dosing and mixing speed in the jars could be automatically controlled. A 0.03 M $KMnO_4$ (3.6 g/L MnO_4^-) solution was used to dose MnO_4^-. It was prepared by dissolving 948 mg of solid $KMnO_4^-$ (Cairox®, Carus Corporation) in 200 mL deionized (DI) water directly before the start of the batch experiments. A $FeCl_3$ solution (2.0 g Fe(III)/L) was used to dose Fe(III) in water. It was prepared by dissolving 1936 mg solid $FeCl_3.6H_2O$ (J.T. Baker®) in 200 mL DI water directly before the start of the batch experiments.

The jar test procedure was designed to represent the process conditions at the full-scale facility, especially with respect to the residence time of water during aeration and rapid sand filtration. The jar test procedure included the following steps. Firstly, the 6 jars were filled with anaerobic raw groundwater of WTP Dorst (Table 1). Afterwards, a predetermined aliquot of MnO_4^- and/or Fe(III) was dosed in each jar while the solutions were mixed at 300 RPM. In the MnO_4^-—Fe(III) dosing experiments, the interval between MnO_4^- and Fe(III) doses was kept constant at 2 min. This interval was chosen to make sure that complete oxidation of As(III) to As(V) occurred before Fe(III) dosing, though Ghurye and Clifford (2001) and Sorlini and Gialdini (2010) found complete As(III) oxidation within 1 min of MnO_4^- dosing in their experiments with both synthetic and real groundwater samples. After 3 min of mixing at 300 RPM, the mixing speed was reduced to 50 RPM for the next 13.5 min to allow Fe(III) precipitates to grow into larger flocs. Finally, the process water was sampled from the jars by opening the bottom tap and filtering immediately using 0.45 µm filters (GE's GD/XP disposable syringe filters with nylon membrane). The filtered samples were analyzed for As and Fe. During the experiments the jars were kept open to the atmosphere, therefore the agitation caused by stirring at 300 RPM not only accomplished mixing of the chemicals, but also aeration of the raw water.

4.2.2.2 Pilot experiments

Pilot experiments were performed to optimize the dosing of MnO_4^- and Fe(III). The pilot plant, installed at WTP Dorst, was fed with the raw water of WTP Dorst (Table 1). Figure 2 shows a schematic diagram of the pilot setup. The pilot setup consisted of an aeration cascade followed by a filtration column (0.3 m diameter, 2.5 m height) and peristaltic pumps for MnO_4^- and Fe(III) dosing. The column contained filtration media (1.8 m height) obtained from the full-scale filter of WTP Dorst (silica sand D50=1.3 mm) in an attempt to achieve a similar rapid sand filtrate quality as the full-scale facility. Permanganate was dosed using 0.03 M $KMnO_4$ (3.6 g/L MnO_4^-) solution prepared onsite in 20 L jerry cans by dissolving solid $KMnO_4$ (Cairox®) in DI water 2-3 times per week. Ferric was dosed using 40 w/w % $FeCl_3$ solution (Ferralco Nederland BV). MnO_4^- was dosed at the top of the cascade for As(III) oxidation and Fe(III) was dosed for As(V) removal at the bottom, as shown in Figure 2. Two separate membrane pumps (GALA1602, ProMinent®) were used for dosing MnO_4^- and Fe(III).

The pilot experiments were performed under three conditions, based on the outcomes of the preliminary batch experiments and further optimization of chemical dosing to achieve <1 µg/L in pilot filtrate. In the first condition, the pilot plant was operated for 6 weeks without dosing of MnO_4^- and Fe(III) to replicate a filtrate quality similar to that of the full-scale facility. In the second condition, 0.8 mg/L MnO_4^- and 1.8 mg/L Fe(III) were dosed for 4 weeks, and in the third condition, 1.2 mg/L MnO_4^- and 1.8 mg/L Fe(III) were dosed for 4 weeks in the pilot cascade. During all the experiments the pilot was operated at the filtration velocity of 4.6 m/h (filter loading Q=1.3 m^3/h). Unfiltered and 0.45 µm filtered samples were collected from the pilot filtrate during 8-12 runs at each condition and analyzed for the determination of As, Fe, Mn and NH_4^+ concentrations.

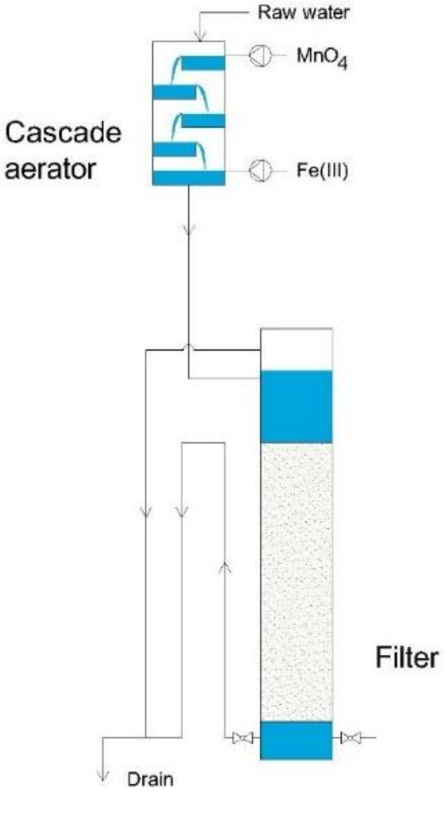

Figure 2. Schematic diagram of the pilot set-up.

4.2.3 Influence of MnO_4—Fe(III) dosing on removal of As, Fe, Mn and NH_4^+

Soon after the completion of the pilot experiments, the full-scale facility received an upgrade with MnO_4^-—Fe(III) dosing. This enabled us to study the influence of MnO_4^-—Fe(III) dose on the removal of As, Fe, Mn and NH_4^+ on full-scale. Reference measurements were obtained before the upgrade, i.e. when the raw water (Table 1) was only treated with aeration—rapid sand filtration. The measurements with MnO_4^-—Fe(III) dosing were obtained one year after the upgrade, with 1.2 mg/L MnO_4^- and 1.8 mg/L Fe(III) dosed (dosing was based on the results of the pilot experiments) to achieve <1 µg/L As in the produced drinking water. In both sampling campaigns, unfiltered and 0.45 µm filtered raw water, supernatant and filtrate samples were collected. Supernatant refers to the water storage on the top of the filter bed. Concentrations of As, Fe and Mn were determined in unfiltered and 0.45 µm filtered samples. Concentrations of NH_4^+ were determined in unfiltered samples only. Dissolved arsenic species were determined in 0.45 µm filtered samples.

4.2.4 Influence of MnO_4—Fe(III) dosage on filter backwash solids characteristics

The influence of MnO_4^-—Fe(III) dosing on the settling and molecular scale structural characteristics of the backwash solids was also studied at the full scale installation. Backwash water samples were collected under 3 conditions: (1) without dosing (no dose), i.e. prior to the upgrade (2) with only dosing 1.2 mg/L MnO_4^- and (3) with dosing 1.2 mg/L MnO_4^- and 1.8 mg/L Fe(III). Under each condition the backwash water sample were collected at the 60th hour of the filter run. To collect each sample during filter backwash, 5 L of backwash water was collected every minute during the first 4 minutes. The samples were subsequently mixed to form a secondary suspension, which was subsequently used for settling experiments and for solids characterization. Unfiltered and 0.45 µm filtered backwash water samples, collected at each setting, were analyzed for Fe and Mn concentration.

4.2.4.1 Settling characteristics of filter backwash solids

The settling characteristics of the filter backwash solids were studied using a method previously used by Van Genuchten et al. (2014b). 1.8 L transparent jars were filled with the backwash water samples, mixed with a magnetic stirrer for 1 min to achieve a homogeneous suspension of filter backwash solids and then allowed to settle under gravity for 1 h. During settling, an aliquot of sample was taken approximately 10 cm below the surface of the suspension, every 15 min between t=0 and 60 min, using a wide-mouthed syringe for turbidity measurements using a Hach 2100 N Turbidimeter. The settling behaviour was also recorded through photographs.

4.2.4.2 Solid phase characterization

Solids were collected on 0.45 µm filters from the backwash water samples under no dose and 1.2 mg/L MnO_4^- dose conditions. The samples were air dried for 24 hours at room temperature and then stored in closed containers at room temperature until analysis in 2 weeks. The solids were characterized by Fe K-edge X-ray absorption spectroscopy (XAS) and X-ray diffraction (XRD). Fe K-edge XAS data were collected at the DUBBLE beam line (BM-26) of the European Synchrotron Radiation Facility (ESRF). Spectra were recorded at room temperature in transmission mode out to k of 13 $Å^{-1}$. X-Ray diffraction measurements (XRD) were performed at the X-Ray facility in Utrecht University, The Netherlands. The Samples for powder XRD measurements, were ground into a powder using an agate mortar and pestle. Powder diffraction patterns were collected with a Bruker D8 Advance diffractometer using Cu K-alpha radiation and a rotating sample stage. Measurements were performed from 5 to 75° 2θ with 0.02° step sizes and total data collection time of approximately 4 h per sample.

4.2.5 Analysis of water samples

Determination of As, Fe and Mn concentrations was carried out by Inductively Coupled Plasma Mass Spectrometry (ICP—MS) (SXERIES 2, Thermo Fisher Scientific) at Aqualab Zuid laboratory in the Netherlands. The detection limits (DLs) for As, Fe, Mn were 0.5, 10 and 10 µg/L respectively. Samples for As, Fe, Mn analysis were preserved immediately after sampling by adding 250 µL of 10% ultra-pure nitric acid (HNO_3). To obtain 0.45 µm filtered samples, GE's GD/XP disposable syringe filters were used. For the determination of Fe and Mn in the backwash water samples, samples were digested in acid and microwaved before ICP—MS. Arsenic speciation (As(III) versus As(V)) was determined using Amberlite® IRA-400 chloride form AIEX resin. The procedure included passing 100 mL of 0.45 µm filtered water through a 30 mL syringe filled with 20 mL of the resin. The As concentration that remained in the effluent after contact with the resin was considered to be uncharged As(III). As(V) was calculated by subtracting As(III) from the As concentration in the column influent (Clifford et al. 1983). NH_4^+ was analyzed by a discrete analyzer spectrophotometry (Aquakem 250, Thermo Scientific) at Aqualab Zuid laboratory (accredited NEN-EN-ISO/IEC 17025:2005). The method DL was 30 µg/L NH_4^+.

4.3 Results and discussion

3.1 Optimizing MnO_4 – and Fe(III) doses to achieve <1 µg/L As

4.3.1.1 Preliminary batch experiments

To gain preliminary information on MnO_4^- and Fe(III) doses required to remove As to <1 µg/L, a series of batch tests was carried out. Figure 3(a) presents the residual As concentration in function of the Fe(III) dose. An As concentration of <1 µg/L was not achieved even with a high dose of Fe(III) (10 mg/L). The residual concentration of As decreased with increasing Fe(III) dose which can be attributed to the increasing amount of Fe(III)-precipitates with each incremental Fe(III) dose (Cornell and Schwertmann 2003, Hering et al. 1996, Wilkie and Hering 1996). The actual raw water of WTP Dorst used in these experiments (Table 1) contained As(III) as the predominant As species. As(III) adsorbs to the Fe(III)-precipitates produced by Fe(III) coagulants in solution (Hering et al. 1996, Lakshmanan et al. 2008). Figure 3(a) shows that the residual As concentration in the absence of Fe(III) dosing was 8.7 µg/L, thus significantly lower than the As concentration in the raw water (11.9 µg/L). This reduction can be attributed to coprecipitation of As with the natural Fe in raw groundwater of WTP Dorst (Edwards 1994, McNeill and Edwards 1995).

The residual As concentration as a function of MnO_4^- and MnO_4^-—Fe(III) dose is presented in Figure 3(b). An As concentration of <1 µg/L As was achieved when ≥1.2 mg/L MnO_4^- was combined with an Fe(III) dose of 2.0 mg/L. Residual As concentrations decreased with increasing MnO_4^- dose for each Fe(III) dose and the curves appear to level-off beyond 1.2 mg/L of MnO_4^- dose indicating ineffectiveness of further increase in MnO_4^- dose for As removal. This result indicates that MnO_4^- dosages of <1.2 mg/L may not be sufficient to completely oxidize As(III) to As(V), thus limiting the As adsorption to Fe(III)-precipitates that were formed in water due to the oxidation and hydrolysis of the natural Fe(II) and dosed Fe (III) (Hering et al. 1996, Hsu et al. 2008, Lakshmanan et al. 2008, Lytle et al. 2005, Qiao et al. 2012). It is worth mentioning that the residual Fe concentration in the entire series of batch experiments was <10 µg/L, indicating the Fe(III) precipitation was not limiting the As removal efficiency.

Comparing the residual As concentrations at 2.0 mg/L Fe(III) dose with and without MnO_4^- (Figure 3(a) and 3(b) respectively), it is evident that a significantly lower residual As was achieved when MnO_4^- and Fe(III) were dosed. The results of the batch experiments indicated that the dosing of around 1.0 mg/L MnO_4^- and 2.0 mg/L Fe(III) would be required to achieve As removal to < 1 µg/L at WTP Dorst. Using these concentrations as a starting point, the next topic is optimizing the MnO_4^-—Fe(III) dose in pilot experiments.

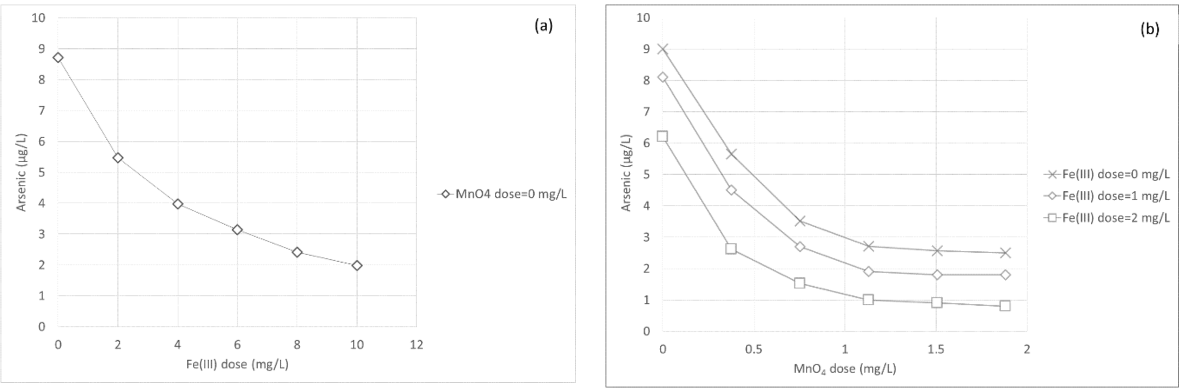

Figure 3. Residual concentration of As (a) as a function of Fe(III) dose and (b) as a function of MnO_4^- and MnO_4^-——Fe(III) dose. Results are based on batch experiments (single trials).

4.3.1.2 Pilot experiments

Arsenic and Fe concentrations in the pilot filtrate are presented in Figure 4(a) and 4(b), respectively. In the absence of MnO_4^-—Fe(III) dosing, the average As concentration in the pilot filtrate was 6.3 µg/L, which was comparable to the full-scale effluent quality (Table 1). However, the pilot filtrate contained a higher Fe concentration (24.4 ± 5.3 µg/L) (Figure 4 (b)) compared to the effluent of the full-scale facility where Fe was undetectable (<10 µg/L) (Table 1). When 0.8 mg/L MnO_4^- and 1.8 mg/L Fe(III) were dosed in the pilot cascade, the As concentration in the filtrate decreased to an average of 1.4 µg/L and the Fe concentration decreased to an average of 21.1 µg/L. When the MnO_4^- dose was increased further to 1.2 mg/L with Fe(III) dose maintained at 1.8 mg/L, the As concentration in the filtrate decreased to an average of 0.9 µg/L and the Fe became undetectable (<10 µg/L).

The increased As removal with increment of MnO_4^- dose may be due to the oxidation of As(III) to As(V) (Bordoloi et al. 2013) and subsequent more efficient uptake of As(V) by Fe(III)-precipitates (Edwards 1994, Qiao et al. 2012, Wilkie and Hering 1996). The Fe speciation (Fe in unfiltered and 0.45 µm filtered samples) in the pilot filtrate showed that the dissolved Fe concentration in the pilot filtrate was consistently <10 µg/L (DL) during the experiments with the three settings. This shows that the precipitation of Fe was not dependent on MnO_4^- . Thus the observed decrease in the Fe concentration in the pilot filtrate with the increase in MnO_4^- dose from 0 to 1.2 mg/L was apparently not related to the oxidizing capacity of MnO_4^-. It may, however, be due to improved aggregation (flocculation) and filterability of Fe(III)-precipitates triggered by MnO_x precipitates that form upon MnO_4^- reduction and oxidation of natural Mn(II) (Lihua et al. 2009).

Under all three experimental conditions, Mn and NH_4^+ concentrations in the pilot filtrate remained below the detection limit (10 µg/L for Mn and 30 µg/L for NH_4^+). This result indicates that the dosing of MnO_4^- and Fe(III) did not decrease the overall removal efficiency of Mn(II) and NH_4^+ in the pilot filter.

It is worth mentioning that the run time of the pilot filter was reduced when MnO_4^- and Fe(III) were dosed. This can be attributed to the increased rate of filter clogging due to increased load of Fe(III)-precipitates and MnO_x-precipitates to the filter compared to the condition when MnO_4^- and Fe(III) were not dosed.

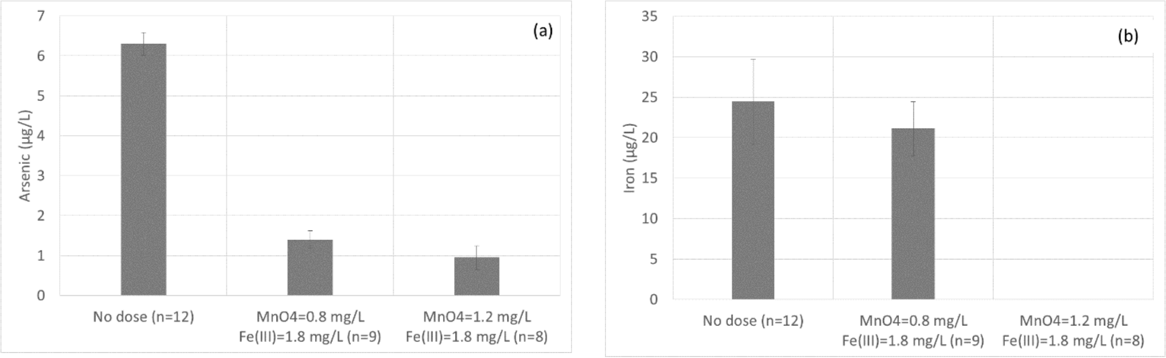

Figure 4. (a) Arsenic and (b) Fe concentrations in the pilot filtrate under three pilot experimental conditions.

4.3.2 Influence of MnO_4—Fe(III) dose on As, Fe, Mn and NH_4^+ removal profiles

Figure 5 (a, b, c and d) presents As, Fe, Mn and NH_4^+ concentrations in the raw, supernatant and filtrate before the upgrade of the full-scale facility (no dose) and after the upgrade when 1.2 mg/L MnO_4^- and 1.8 mg/L Fe(III) were dosed (MnO_4^-—Fe(III)). Figure 5(a) shows that As was approximately 11.5 µg/L in the unfiltered and 0.45 µm filtered raw water samples, indicating the presence of As in dissolved form. In the supernatant, the As concentration in the unfiltered samples was similar to the raw water, indicating that As was not removed during aeration. However, approximately 1 µg/L As (8.7% of the total As) was removed by the 0.45 µm filter in the supernatant with no dose and 11.4 µg/L (99.2% of the total As) As became filterable in the supernatant with MnO_4^-—Fe(III) dose. Figure 5(b) shows that the raw water contained 1400 µg/L Fe, which entirely passed through the 0.45 µm filter. In the supernatant, 942.5 µg/L Fe (66.2% of total Fe) passed through the 0.45 µm filter in the absence of dosing. The As uptake in the supernatant is calculated to be (1/0.942=) 1.1 µg/mg Fe in the absence of MnO_4^-—Fe(III) dosing. The Fe concentration in the supernatant with MnO_4^-—Fe(III) dose was much higher due to Fe(III) dosing in the feed, with 3682.3 µg/L Fe (97.6% of the total Fe) filterable through 0.45 µm filter. The As uptake in the supernatant is calculated to be (11.4/3.37=) 3.3 µg/mg Fe with MnO_4^-—Fe(III) dosing. The 3-fold higher uptake of As in the supernatant with MnO_4^-—Fe(III) dose can be attributed to As(III) oxidation to As(V) by MnO_4^- (Borho and Wilderer 1996, Lihua et al. 2009). In the filtrate, a significant difference in As concentration was observed, with 6.1 µg/L at no dose and 0.54 µg/L with MnO_4^-—Fe(III) dose. In both the cases, As passed through the 0.45 µm filter, indicating its presence as dissolved As. Iron was below the detection limit (10 µg/L) in the filtrate in both the cases. Since most of the Fe was precipitated in the supernatant, homogeneous Fe(II) oxidation followed by flocculative removal can be regarded as the principle Fe removal mechanism both at no dose and with MnO_4^-—Fe(III) dosing. However, a significantly higher concentration of Fe was precipitated in the supernatant when MnO_4^-—Fe(III) was dosed.

Manganese did not pass through 0.45 µm filter in the raw water (Figure 5(c)), indicating its presence in dissolved form. It remained unfilterable in the supernatant at no dose. This showed that the cascade aeration was ineffective in oxidizing Mn(II) and confirmed the previous results (Diem and Stumm 1984, Lytle et al. 2005) that the transformation of Mn(II) to MnO_2 by dissolved O_2 alone is a slow process at pH below 9. At no dose, Mn was below the detection limit (10 µg/L) in the filtrate. This Mn removal can be attributed to the autocatalytic removal mechanism in which dissolved Mn(II) adsorbs to the filter media grains where it is oxidized to form MnO_2 coating (Bruins et al. 2015, Katsoyiannis et al. 2008). On the other hand, the Mn concentration in the supernatant with MnO_4^-—Fe(III) dose, though much higher due to MnO_4^- dosing, was entirely filterable through 0.45 µm filter. Thus, Mn entered the rapid sand filter mainly as particles (MnO_x) and its removal mechanism in the filter bed changed to flocculative.

At no dose, NH_4^+ removal took place entirely in the filter bed (Figure 5(d)), which is consistent with biological nitrification (De Vet 2011). With MnO_4^-—Fe(III) dose, the NH_4^+ concentration in the filtrate remained below the detection limit (30 µg/L), indicating that the nitrification was not affected in the filter bed.

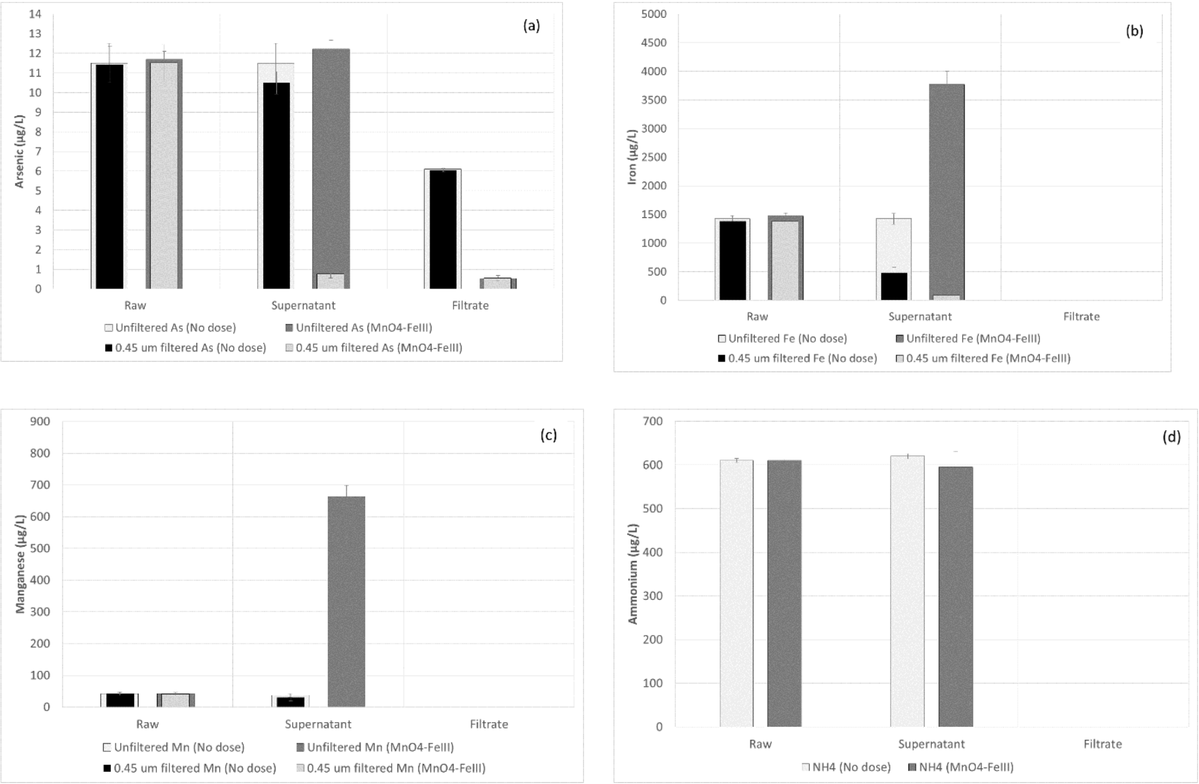

Figure 5. Concentrations of (a) As, (b) Fe, (c) Mn and (d) NH_4^+ in unfiltered and 0.45 µm filtered raw, supernatant and filtrate without and with MnO_4^-—Fe(III) dosing. Supernatant refers the water storage on the top of the filter bed.

Arsenic speciation was carried out in the raw, supernatant and filtrate samples to gain further mechanistic insight of the As removal process. Figure 6(a) presents As(III) and As(V) concentrations in 0.45 µm filtered samples. As(III) was the dominant form of As in the raw water (97.2%). In the supernatant, As(III) remained dominant (89.6%), indicating the inefficiency of the cascade aeration in oxidizing As(III) to a significant level, in agreement with Gude et al. (2016). In the filter effluent, the As concentration was lower than the supernatant due to co-removal with Fe in the filter bed although As(V) dominated (80%). The observed oxidation of As(III) in 9.3 min of rapid sand filtration was higher-than-expected because As(III) oxidation by dissolved oxygen alone proceeds slowly (Frank and Clifford 1986, Kim and Nriagu 2000). Similar rapid oxidation of As(III) during rapid sand filtration was reported by Gude et al. (2016) and Katsoyiannis et al. (2008) and may be attributed to the manganese oxides or microbial activity in the filter bed (Driehaus et al. 1995, Gude et al. 2017, Lytle et al. 2007). With MnO_4^-—Fe(III) dosing, the dissolved As in the supernatant and filtrate consisted entirely of As(V) (Figure 6(b)).

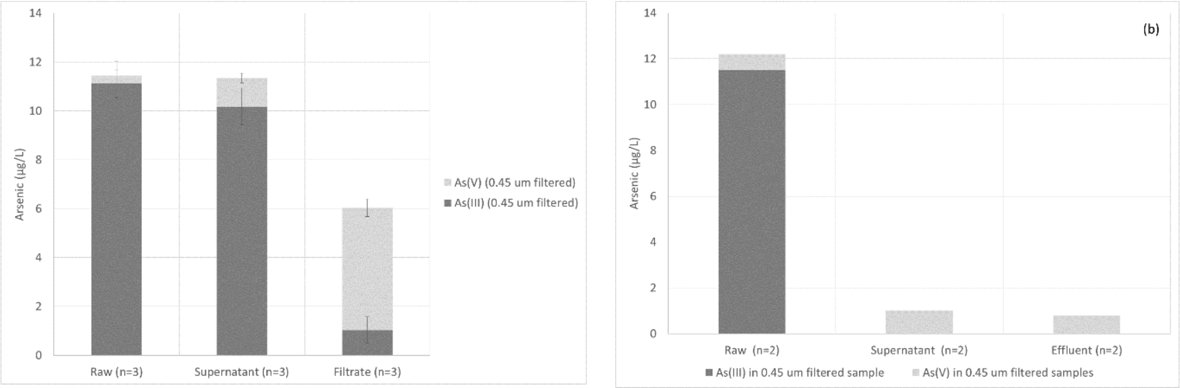

Figure 6. Dissolved As species in raw, supernatant and filtrate (a) without and (b) with MnO_4^-—Fe(III) dosing. Supernatant refers the water storage on the top of the filter bed.

4.3.3 Influence of MnO_4—Fe(III) dosing on filter backwash solids

4.3.3.1 Settling characteristics of filter backwash solids

Figure 7 presents the results of turbidity measurements in the top 10 cm of the backwash water samples as a function of time, as well as a visual comparison of the beginning (t=0) and the end (t=60 min) of settling tests among the backwash water samples that were collected under three conditions: without dosing (no dose), i.e. prior to the upgrade, with only dosing 1.2 mg/L MnO_4^- and with dosing 1.2 mg/L MnO_4^- and 1.8 mg/L Fe(III). The color of the backwash water with MnO_4^- and MnO_4^-—Fe(III) dosing was darker, indicating the presence of solid phase MnO_x. The presence of Mn was also confirmed when backwash water samples were analyzed for Fe and Mn concentration by ICP—MS. The backwash water samples with MnO_4^- and MnO_4^-—Fe(III) dose settled faster than the sample collected at no dose (Figure 7). Thus, the dosing of MnO_4^- and MnO_4^-—Fe(III) improved the settling rate of the filter backwash solids.

The dosing of MnO_4^- might have modified the floc characteristics by altering the molecular-scale structure of the Fe(III)-precipitates in backwash solids. The structure of Fe-oxides depends largely on the synthesis conditions (Cornell and Schwertmann 2003, Van Genuchten et al. 2014b) and since dosing of MnO_4^- oxidized Fe(II) faster than O_2, the molecular-scale structure of the produced Fe(III)-precipitates might also be affected. Therefore, the backwash water solids produced under two conditions: without dosing (no dose), i.e. prior to the upgrade and with only dosing 1.2 mg/L MnO_4^- were characterized by Fe K-edge XAS (XANES and EXAFS) and XRD.

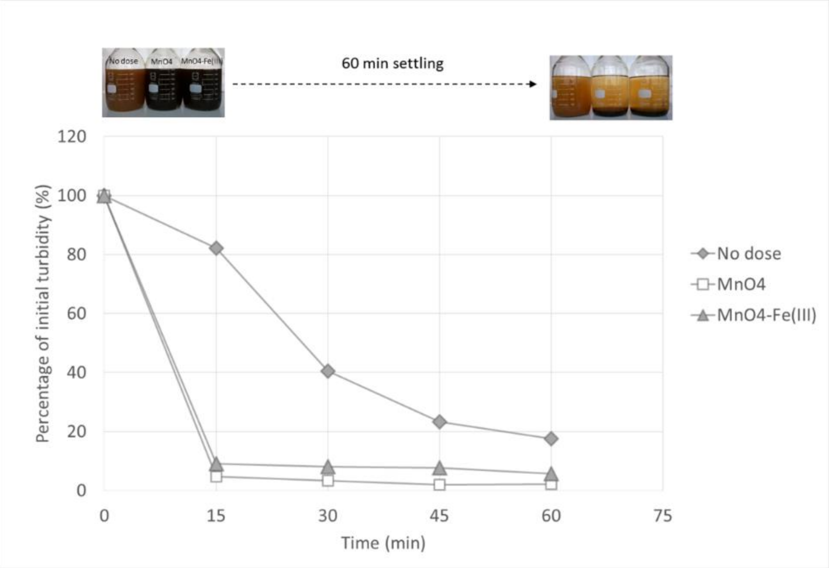

Figure 7. Decrease in backwash water turbidity as a function of time. Photos on top show backwash water samples at the beginning (t = 0) and end (t = 60 min) of the settling test.

4.3.3.2 Characterization of backwash water solids

Figure 8 shows the Fe-K edge XANES and EXAFS spectra of the backwash solids collected from the full scale filter. It can be observed that the position of the absorption edge in the XANES spectra (Figure 8(a)) of the sample with no dose and with MnO_4^- dose were similar and matched the absorption edge of the lepidocrocite and ferrihydrite XANES spectrum. This result shows that the Fe in both samples was primarily present as Fe(III). The oscillations in the post-edge region of the XANES spectra were similar for both the samples, but showed a slight shoulder (highlighted by the arrows in Figure 8(a)) near the absorption maximum. This oscillation was more pronounced than in the ferrihydrite and lepidocrocite XANES spectra.

The Fe K-edge EXAFS spectra (Figure 8(b)) of the samples showed a roughly symmetric first oscillation from 3.5 to 4.5 $Å^{-1}$, a major fingerprint of poorly-crystalline Fe(III) precipitates. The first oscillation of the samples matches both the 2-line ferrihydrite reference spectrum and the silicate-rich hydrous ferric oxide (Si-HFO) reference spectrum. These two reference spectra represent poorly-ordered Fe(III)-precipitate phases that form via rapid oxidation of Fe(II) or polymerization of Fe(III) salts in the presence of strongly-sorbing oxyanions (e.g. silicate, phosphate) and have been characterized previously (Van Genuchten et al. 2014b). In addition, the small beat near 5.0 – 5.2 $Å^{-1}$ in the ferrihydrite EXAFS spectrum, which is due to the corner-sharing Fe polyhedra, was weakened or absent in the spectra of both the backwash solids samples. The weakened feature indicative of corner-sharing Fe polyhedral in the backwash samples can be explained by the presence of silica in water during Fe(III) precipitation (Van Genuchten et al. 2014b). Finally, the peak near 6.2 $Å^{-1}$ was reduced in the backwash solids and the oscillations at $k > 9$ $Å^{-1}$ in the MnO_4^- sample were broadened relative to lepidocrocite. Therefore, the XAS data showed that Fe in both the backwash solid samples was present as poorly-crystalline Fe(III) precipitates with structures that have slightly less polyhedral connectivity than ferrihydrite, regardless of the presence or absence of MnO_4^-.

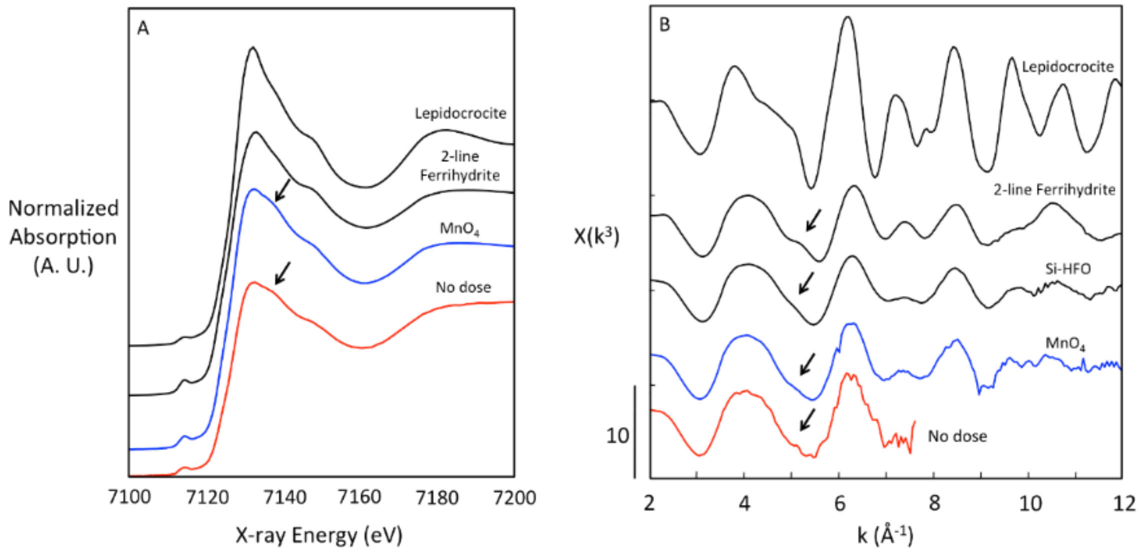

Figure 8. (a) Fe K-edge XANES and (b) EXAFS spectra. Samples without dose (red) and with MnO_4^- (blue).

The XRD data (Figure 9) of both the backwash solids samples were similar and showed only the broad peaks indicative of poorly crystalline hydrous ferric oxide. This result was consistent with the XAS data. Although Mn was present in the samples (much higher concentration in MnO_4^- dosed sample, Mn:Fe > 0.3 g:g), no evidence for any crystalline Mn oxides was observed in the XRD patterns. This result suggests that Mn in the solid phase was present as a nanocrystalline solid, such as poorly-ordered birnessite, or perhaps was incorporated into the structure of the nanocrystalline hydrous ferric oxide, which has been observed previously during the co-precipitation of Mn with Fe(III) precipitates (Ebinger and Schulze 1989, van Genuchten and Pena 2017b). Although neither of these possible Mn coordination environments would produce strong Bragg diffraction peaks, which is consistent with our XRD data, we note that identifying the exact Mn speciation in the solid phase requires additional structural information. Because we observed that MnO_4^- dosing alters substantially the settling characteristics of the backwash solids, and that MnO_4^- dosing did not impact solid phase Fe speciation, it is likely that Mn speciation plays a critical role in determining the macroscopic properties of the backwashed solids. Therefore, further investigation to elucidate the mechanism of Mn incorporation in the flocs, and the subsequent impact on floc size, density, filterability and settling is required.

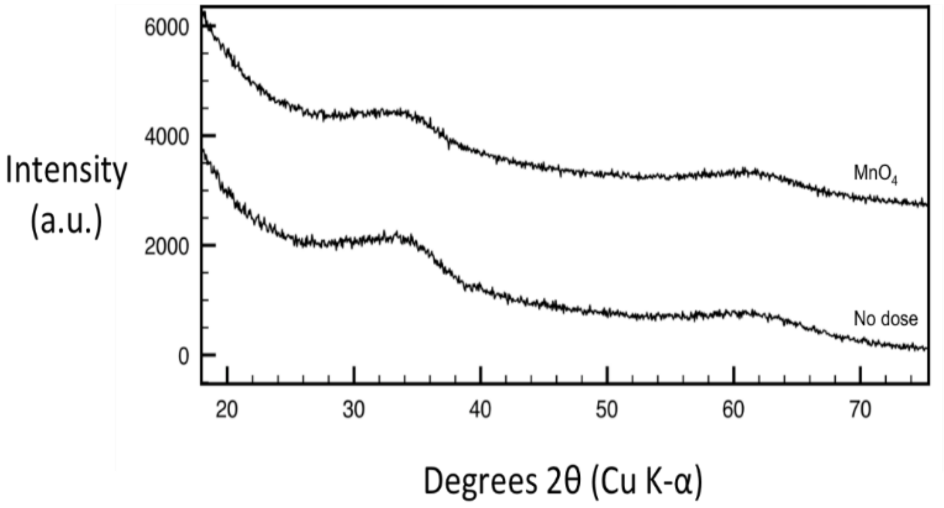

Figure 9. X-ray diffraction patterns of the rapid sand filter backwash solids.

4.4 Conclusions

This study concludes that MnO_4^-—Fe(III) dosing is an effective technique to improve As(III) removal at groundwater treatment facilities that typically use aeration—rapid sand filtration for drinking water production. At WTP Dorst, a typical groundwater treatment facility in the Netherlands, drinking water As concentrations of <1 µg/L were achieved with 1.2 mg/L MnO_4^- and 1.8 mg/L Fe(III), based on the outcomes of systematic batch and pilot study. The optimized combination of MnO_4^- and Fe(III) doses did not decrease the removal efficiency of Fe(II), Mn(II) and NH_4^+, although the removal patterns of Fe(II) and Mn(II) were altered. In the absence of MnO_4^-—Fe(III) dose, a significant part of Fe precipitation and the complete precipitation of Mn occurred in the filter bed whereby with MnO_4^-—Fe(III) dosing, both Fe and Mn were completely precipitated in the supernatant, before entering the filter bed, and resulted in a shortening of the filter run time. The dosing of MnO_4^-—Fe(III) improved the settling rate of backwash solids, which was not attributed to changes in molecular-scale structure of Fe-precipitates that form during treatment, but to the increased Mn concentration in the backwash solids.

References

Ahmad, A. (2017) Towards achieving <1 ug/L arsenic at Katwijk, Ouddorp and Leiduin: Baseline study and batch experiments with $KMnO_4$ and $FeCl_3$ to remove arsenic, p. 44.

Ahmad, A. and Bhattacharya, P. (2019) Arsenic in Drinking Water: Is 10 µg/L a Safe Limit? Current Pollution Reports.

Ahmad, A., Cornelissen, E., van de Wetering, S., van Dijk, T., van Genuchten, C., Bundschuh, J., van der Wal, A. and Bhattacharya, P. (2018) Arsenite removal in groundwater treatment plants by sequential Permanganate—Ferric treatment. Journal of Water Process Engineering 26, 221-229.

Ahmad, A., Kools, S., Schriks, M., Stuyfzand, P. and Hofs, B. (2015) Arsenic and chromium concentrations and their speciation in groundwater resources and drinking water supply in the Netherlands p. 78, KWR Water Cycle Research Institute, Nieuwegein, The Netherlands.

Ahmad, A., Van De Wetering, S., Groenendijk, M. and Bhattacharya, P. (2014) Advanced Oxidation-Coagulation-Filtration (AOCF) - An innovative treatment technology for targeting drinking water with <1 µg/L of arsenic, pp. 817-819.

Ahmad, A., van der Wal, B., Bhattacharya, P. and van Genuchten, C.M. (2019a) Characteristics of Fe and Mn bearing precipitates generated by Fe(II) and Mn(II) co-oxidation with O2, MnO4 and HOCl in the presence of groundwater ions. Water Research.

Ahmad, A., Van der Wens, P., Baken, K., De Waal, L., Bhattacharya, P. and Stuyfzand, P. (2019b) Arsenic reduction to <1 ug/L in Dutch drinking water. Environ Int.

Allard, S., Fouché, L., Dick, J., Heitz, A. and von Gunten, U. (2013) Oxidation of Manganese(II) during Chlorination: Role of Bromide.

Bhattacharya, P., Frisbie, S.H., Smith, E., Naidu, R., Jacks, G. and Sarkar, B. (2002) Handbook of Heavy Metals in the Environment. Sarkar, B. (ed), pp. 145-215, Taylor & Francis Inc., New York.

Bhattacharya, P., Welch, A.H., Stollenwerk, K.G., McLaughlin, M.J., Bundschuh, J. and Panaullah, G. (2007) Arsenic in the environment: Biology and Chemistry. Science of the Total Environment 379(2), 109-120.

Bissen, M. and Frimmel, F.H. (2003) Arsenic - A review. Part II: Oxidation of arsenic and its removal in water treatment. Acta hydrochimica et hydrobiologica 31(2), 97-107.

Borba, R.P., Figueiredo, B.R. and Matschullat, J. (2003) Geochemical distribution of arsenic in waters, sediments and weathered gold mineralized rocks from Iron Quadrangle, Brazil. Environmental Geology 44(1), 39-52.

Bordoloi, S., Nath, S.K., Gogoi, S. and Dutta, R.K. (2013) Arsenic and iron removal from groundwater by oxidation–coagulation at optimized pH: Laboratory and field studies. Journal of Hazardous Materials 260, 618-626.

Borho, M. and Wilderer, P. (1996) Optimized removal of arsenate(III) by adaptation of oxidation and precipitation processes to the filtration step. Water Science and Technology 34(9), 25-31.

Borsboom, M., Bras, W., Cerjak, I., Detollenaere, D., van Loon, D., Goedtkindt, P., Konijnenburg, M., Lassing, P., Levine, Y., Munneke, B., Oversluizen, M., van Tol, R. and Vlieg, E. (1998) The Dutch-Belgian beamline at the ESRF. Journal of Synchrotron Radiation 5, 518-520.

Bruins, J.H., Petrusevski, B., Slokar, Y.M., Kruithof, J.C. and Kennedy, M.D. (2015) Manganese removal from groundwater: Characterization of filter media coating. Desalination and Water Treatment 55(7), 1851-1863.

Bundschuh, J., Maity, J.P., Mushtaq, S., Vithanage, M., Seneweera, S., Schneider, J., Bhattacharya, P., Khan, N.I., Hamawand, I., Guilherme, L.R.G., Reardon-Smith, K., Parvez, F., Morales-Simfors, N., Ghaze, S., Pudmenzky, C.,

Kouadio, L. and Chen, C.Y. (2017) Medical geology in the framework of the sustainable development goals. Science of the Total Environment 581-582, 87-104.
Chen, C., Dynes, J.J., Wang, J., Karunakaran, C. and Sparks, D.L. (2014) Soft X-ray Spectromicroscopy Study of Mineral-Organic Matter Associations in Pasture Soil Clay Fractions. Environmental Science & Technology 48(12), 6678-6686.
Choi, K.Y.-j. and Dempsey, B.A. (2004) In-line coagulation with low-pressure membrane filtration. Water Research 38(19), 4271-4281.
Clifford, D.A., Ceber, L. and Chow, S. (1983) Separation of Arsenic III and AsV by Ion Exchange, AWWA, Denver, Colo.
Cornell, R.M. and Schwertmann, U. (2003) The Iron Oxides: Structure, Properties, Reactions, Occurances and Uses, WILEY-VCH Verlag GmbH & Co. .
Davis, C.C. and Edwards, M. (2017) Role of Calcium in the Coagulation of NOM with Ferric Chloride. Environmental Science & Technology 51(20), 11652-11659.
de Moel, P.J., Verberk, J.Q.J.C. and van Dijk, J.C. (2006) Drinking Water: Principles and Practices, Delft, The Netherlands.
de Ridder, D.J., van de Wetering, S., van Dijk, T. and van Halem, D. (2018) Influence of HPO 4 2- , H 4 SiO 4 , Ca 2+ , Mg 2+ on Fe floc growth and As(III) removal in aerated, natural groundwater.
De Vet, W. (2011) Biological drinking water treatment of anaerobic groundwater in trickling filters, Technical University of Delft, Delft.
Delaire, C., van Genuchten, C., Amrose, S. and Gadgil, A. (2016) Bacteria attenuation by iron electrocoagulation governed by interactions between bacterial phosphate groups and Fe(III) precipitates. Water Research 103, 74-82.
Diem, D. and Stumm, W. (1984) Is dissolved Mn^{+2} being oxidized by O_2 in absence of Mn-bacteria and surface catalysts? Geochimica et Cosmochimica Acta 48, 1571-1573.
Dixit, S. and Hering, J.G. (2003) Comparison of arsenic(V) and arsenic(III) sorption onto iron oxide minerals: Implications for arsenic mobility. Environmental Science and Technology 37(18), 4182-4189.
Doelsch, E., Rose, J., Masion, A., Bottero, J.Y., Nahon, D. and Bertsch, P.M. (2000) Speciation and Crystal Chemistry of Iron(III) Chloride Hydrolyzed in the Presence of SiO4 Ligands. 1. An Fe K-Edge EXAFS Study. Langmuir 16(10), 4726-4731.
Dong, H.R., Guan, X.H., Wang, D.S. and Ma, J. (2011) Individual and combined influence of calcium and anions on simultaneous removal of chromate and arsenate by Fe(II) under suboxic conditions

Separation and Purification Technology 80, 284-292.
Driehaus, W., Seith, R. and Jekel, M. (1995) Oxidation of arsenate(III) with manganese oxides in water treatment. Water Research 29(1), 297-305.
Dzombak, D.A. and Morel, F.M.M. (1990) Surface Complexation Modeling: Hydrous Ferric Oxide, John Wiley & Sons, New York, New York.
Ebinger, M.H. and Schulze, D.G. (1989) Mn-Substituted Goethite and Fe-Substituted Groutite Synthesized at Acid pH. Clays and clay minerals 37(2), 151-156.
Edwards, M. (1994) Chemistry of arsenic removal during coagulation and Fe-Mn oxidation. American Water Works Association, 64-78.
Ferguson, J.F. and Gavis, J. (1972) A review of the arsenic cycle in natural waters. Water Research 6(11), 1259-1274.
Floris, R., Nijmeijer, K. and Cornelissen, E.R. (2016) Removal of Aqueous nC_{60} Fullerene from Water by Low Pressure Membrane Filtration. Water Research 91, 115-125.
Frank, P. and Clifford, D. (1986) Arsenic(III) oxidation and removal from drinking water, p. 69, US Environmental Protection Agency, Cincinnati, OH.
Fuller, C.C., Davis, J.A. and Waychunas, G.A. (1993) Surface chemistry of ferrihydrite: Part 2. Kinetics of arsenate adsorption and coprecipitation. Geochimica et Cosmochimica Acta 57(10), 2271-2282.
Ghurye, G. and Clifford, D.A. (2001) Laboratory Study on the Oxidation of Arsenic III to As V, p. 87, Unites States Environmental Protection Agency, Washington DC.
Guan, X., Dong, H., Ma, J. and Jiang, L. (2009a) Removal of arsenic from water: Effects of competing anions on As(III) removal in KMnO4–Fe(II) process. Water Research 43(15), 3891-3899.
Guan, X., Ma, J., Dong, H. and Jiang, L. (2009b) Removal of arsenic from water: Effect of calcium ions on As(III) removal in the KMnO4–Fe(II) process. Water Research 43(20), 5119-5128.
Gude, J.C.J., Joris, K., Huysman, K., Rietveld, L.C. and van Halem, D. (2018a) Effect of supernatant water level on As removal in biological rapid sand filters. Water Research X 1, 100013.
Gude, J.C.J., Rietveld, L.C. and van Halem, D. (2016) Fate of low arsenic concentrations during full-scale aeration and rapid filtration. Water Research 88, 566-574.
Gude, J.C.J., Rietveld, L.C. and van Halem, D. (2017) As(III) oxidation by MnO2 during groundwater treatment. Water Research 111, 41-51.
Gude, J.C.J., Rietveld, L.C. and van Halem, D. (2018b) As(III) removal in rapid filters: Effect of pH, Fe(II)/Fe(III), filtration velocity and media size. Water Research 147, 342-349.

Gude, J.C.J., Rietveld, L.C. and van Halem, D. (2018c) Biological As(III) oxidation in rapid sand filters. Journal of Water Process Engineering 21, 107-115.
Gunduz, O., Simsek, C. and Hasozbek, A. (2010) Arsenic pollution in the groundwater of Simav Plain, Turkey: Its impact on water quality and human health. Water, Air, and Soil Pollution 205(1-4), 43-62.
Hao, O., P. Davis, A. and H. Chang, P. (1991) Kinetics of Manganese(II) Oxidation with Chlorine.
Herath, I., Vithanage, M., Bundschuh, J., Maity, J.P. and Bhattacharya, P. (2016) Natural Arsenic in Global Groundwaters: Distribution and Geochemical Triggers for Mobilization. Current Pollution Reports 2(1), 68-89.
Hering, J.G., Chen, P.-Y., Wilkie, J.A., Elimelech, M. and Liang, S. (1996) Arsenic removal by ferric chloride. American Water Works Association 88(4), 155-167.
Hiemstra, T. and Van Riemsdijk, W.H. (1999) Surface structural ion adsorption modeling of competitive binding of oxyanions by metal (Hydr)oxides. Journal of Colloid and Interface Science 210(1), 182-193.
Hsu, J.C., Lin, C.J., Liao, C.H. and Chen, S.T. (2008) Removal of As(V) and As(III) by reclaimed iron-oxide coated sands. Journal of Hazardous Materials 153(1-2), 817-826.
Jain, A., Raven, K. and R.H., L. (1999) Arsenite and Arsenate Adsorption on Ferrihydrite: Surface Charge Reduction and Net OH- Release Stoichiometry.
Jain, C.K. and Ali, I. (2000) Arsenic: Occurrence, toxicity and speciation techniques. Water Research 34(17), 4304-4312.
Jessen, S., Larsen, F., Koch, C.B. and Arvin, E. (2005) Sorption and Desorption of Arsenic to Ferrihydrite in a Sand Filter. Environmental Science & Technology 39(20), 8045-8051.
Kaegi, R., Voegelin, A., Folini, D. and Hug, S.J. (2010) Effect of phosphate, silicate, and Ca on the morphology, structure and elemental composition of Fe(III)-precipitates formed in aerated Fe(II) and As(III) containing water. Geochimica et Cosmochimica Acta 74(20), 5798-5816.
Kanematsu, M., Young, T., Fukushi, K., Green, P. and Darby, J. (2013a) Arsenic(III, V) adsorption on a goethite-based adsorbent in the presence of major co-existing ions: Modeling competitive adsorption consistent with spectroscopic and molecular evidence. Geochimica Et Cosmochimica Acta 106, 404-428.
Kanematsu, M., Young, T.M., Fukushi, K., Green, P.G. and Darby, J.L. (2010) Extended Triple Layer Modeling of Arsenate and Phosphate Adsorption on a Goethite-based Granular Porous Adsorbent. Environmental Science & Technology 44(9), 3388-3394.
Kanematsu, M., Young, T.M., Fukushi, K., Green, P.G. and Darby, J.L. (2013b) Arsenic(III, V) adsorption on a goethite-based adsorbent in the presence of major co-existing ions: Modeling competitive adsorption consistent with spectroscopic and molecular evidence. Geochimica et Cosmochimica Acta 106, 404-428.
Katsoyiannis, I.A., Zikoudi, A. and Hug, S.J. (2008) Arsenic removal from groundwaters containing iron, ammonium, manganese and phosphate: A case study from a treatment unit in northern Greece. Desalination 224(1-3), 330-339.
Kelly, S.D., Hesterberg, D. and Ravel, B. (2008) Analysis of soils and minerals using X-ray absorption spectroscopy. In *Methods of Soil Analysis. Part 5. Mineralogical Methods. SSA Book Series No.5.*
Kim, E.J., Hwang, B.-R. and Baek, K. (2015) Effects of natural organic matter on the coprecipitation of arsenic with iron. Environmental Geochemistry and Health 37(6), 1029-1039.
Kim, M.-J. and Nriagu, J. (2000) Oxidation of arsenite in groundwater using ozone and oxygen. Science of the Total Environment 247(1), 71-79.
Knocke, W.R., Van Benschoten, J.E., Kearney, M.J., Soborski, A.W. and Reckhow, D.A. (1991) Kinetics of Manganese and Iron Oxidation by Potassium Permanganate and Chlorine Dioxide. AWWA 83(6), 80-87.
Kozisek, F. (2017) Best Practice Guide on the Control of Arsenic in Drinking Water. . Bhattacharya, P., Polya, D.A. and Jovanovic, D. (eds), IWA Publishing, London, UK.
Lakshmanan, D., Clifford, D. and Samanta, G. (2008) Arsenic Removal by Coagulation with Aluminum, Iron, Titanium, and Zirconium. American Water Works Association 100(2), 76-88.
Laky, D. and Licskó, I. (2011) Arsenic removal by ferric-chloride coagulation – effect of phosphate, bicarbonate and silicate. Water Science and Technology 64(5), 1046-1055.
Lan, S., Wang, X., Xiang, Q., Yin, H., Tan, W., Qiu, G., Liu, F., Zhang, J. and Feng, X. (2017) Mechanisms of Mn(II) catalytic oxidation on ferrihydrite surfaces and the formation of manganese (oxyhydr)oxides.
Lanson, B., Drits, V., Feng, Q. and Manceau, A. (2002) Structure of synthetic Na-birnessite: Evidence for a triclinic one-layer unit cell. American Mineralogist 87(11-12), 1662-1671.
Lee, G., Song, K. and Bae, J. (2011) Permanganate oxidation of arsenic (III): Reaction stoichiometry and the characterization of solid product
Lihua, S., Ruiping, L., Shengji, X., Yanling, Y. and Guibai, L. (2009) Enhanced As(III) removal with permanganate oxidation, ferric chloride precipitation and sand filtration as pretreatment of ultrafiltration. Desalination 243(1), 122-131.
Lytle, D.A., Chen, A.S., Sorg, T.J., Phillips, S. and French, K. (2007) Microbial As(III) oxidation in water treatment plant filters. American Water Works Association 99(12), 72-86.

Lytle, D.A., Sorg, T.J. and Snoeyink, V.L. (2005) Optimizing arsenic removal during iron removal: Theoretical and practical considerations. Journal of Water Supply: Research and Technology - AQUA 54(8), 545-560.
MacDonald, A.M., Bonsor, H.C., Ahmed, K.M., Burgess, W.G., Basharat, M., Calow, R.C., Dixit, A., Foster, S.S.D., Gopal, K., Lapworth, D.J., Lark, R.M., Moench, M., Mukherjee, A., Rao, M.S., Shamsudduha, M., Smith, L., Taylor, R.G., Tucker, J., Van Steenbergen, F. and Yadav, S.K. (2016) Groundwater quality and depletion in the Indo-Gangetic Basin mapped from in situ observations. Nature Geoscience 9(10), 762-766.
Manceau, A. and Combes, J.M. (1988) Structure of Mn and Fe oxides and oxyhydroxides: A topological approach by EXAFS. Physics and Chemistry of Minerals 15(3), 283-295.
Manceau, A., Marcus, M. and Grangeon, S. (2012) Determination of Mn valence states in mixed-valent manganates by XANES spectroscopy.
Marszałek, H. and Wąsik, M. (2000) Influence of arsenic-bearing gold deposits on water quality in Zloty Stok mining area (SW Poland). Environmental Geology 39(8), 888-892.
Masue, Y., Loeppert, R.H. and Kramer, T.A. (2007) Arsenate and Arsenite Adsorption and Desorption Behavior on Coprecipitated Aluminum:Iron Hydroxides. Environmental Science & Technology 41(3), 837-842.
Mayer, T.D. and Jarrell, W.M. (1996) Formation and stability of iron(II) oxidation products under natural concentrations of dissolved silica. Water Research 30(5), 1208-1214.
McCarty, K.M., Hanh, H.T. and Kim, K.W. (2011) Arsenic geochemistry and human health in South East Asia. Rev Environ Health 26(1), 71-78.
McNeill, L.S. and Edwards, M. (1995) Soluble arsenic removal at water treatment plants. American Water Works Association 87(4), 105-113.
Meng, X., Bang, S. and Korfiatis, G.P. (2000) Effects of silicate, sulfate, and carbonate on arsenic removal by ferric chloride. Water Research 34(4), 1255-1261.
Mukherjee, A., Sengupta, M.K., Hossain, M.A., Ahamed, S., Das, B., Nayak, B., Lodh, D., Rahman, M.M. and Chakraborti, D. (2006) Arsenic contamination in groundwater: A global perspective with emphasis on the Asian scenario. Journal of Health, Population and Nutrition 24(2), 142-163.
Murcott, S. (2012) Arsenic Contamination in the World, IWA Publishing, London, UK.
Naujokas, M.F., Anderson, B., Ahsan, H., Aposhian, H.V., Graziano, J.H., Thompson, C. and Suk, W.A. (2013) The broad scope of health effects from chronic arsenic exposure: update on a worldwide public health problem. Environ Health Perspect 121(3), 295-302.
Newville, M. (2001) IFEFFIT: interactive XAFS analysis and FEFF fitting. Journal of Synchrotron Radiation, 322-324.
Nikitenko, S., Beale, A., van der Eerden, A., Jacques, S., Leynaud, O., O'Brien, M., Detollenaere, D., Kaptein, R., Weckhuysen, B. and Bras, W. (2008) Implementation of a combined SAXS/WAXS/QEXAFS set-up for time-resolved in situ experiments. Journal of Synchrotron Radiation 15, 632-640.
Nriagu, J.O., Bhattacharya, P., Mukherjee, A.B., Bundschuh, J., Zevenhoven, R. and Loeppert, R.H. (2007) Trace Metals and other Contaminants in the Environment, pp. 3-60.
Pedersen, H.D., Postma, D., Jakobsen, R. and Larsen, O. (2005) Fast transformation of iron oxyhydroxides by the catalytic action of aqueous Fe(II). Geochimica et Cosmochimica Acta 69(16), 3967-3977.
Peña, J., Bargar, J.R. and Sposito, G. (2015) Copper sorption by the edge surface of synthetic birnessite nanoparticles. Chemical Geology.
Pena, J., Kwon, K., Refson, K., Bargar, J. and Sposito, G. (2010) Mechanisms of nickel sorption by a bacteriogenic birnessite. Geochimica Et Cosmochimica Acta 74(11), 3076-3089.
Perera, P.A.C.T., Sundarabarathy, T.V., Sivananthawerl, T., Kodithuwakku, S.P. and Edirisinghe, U. (2016) Arsenic and Cadmium Contamination in Water, Sediments and Fish is a Consequence of Paddy Cultivation: Evidence of River Pollution in Sri Lanka. Achievements in the Life Sciences 10(2), 144-160.
Pierce, M.L. and Moore, C.B. (1982) Adsorption of arsenite and arsenate on amorphous iron hydroxide. Water Research 16(7), 1247-1253.
Pontius, F.W., Brown, K.G. and Chen, C.-J. (1994) Health Implications of Arsenic in Drinking Water. American Water Works Association 86(9), 52-63.
Qiao, J., Jiang, Z., Sun, B., Sun, Y., Wang, Q. and Guan, X. (2012) Arsenate and arsenite removal by FeCl3: Effects of pH, As/Fe ratio, initial As concentration and co-existing solutes. Separation and Purification Technology 92, 106-114.
Raven, K.P., Jain, A. and Loeppert, R.H. (1998) Arsenite and arsenate adsorption on ferrihydrite: Kinetics, equilibrium, and adsorption envelopes. Environmental Science and Technology 32(3), 344-349.
Rehr, J., Albers, R. and Zabinsky, S. (1992) High-order multiple-scattering calculations of X-ray absorption fine structure. Physical Review Letters, 3397-3400.
Roberts, L.C., Hug, S.J., Ruettimann, T., Billah, M.M., Khan, A.W. and Rahman, M.T. (2004) Arsenic Removal with Iron(II) and Iron(III) in Waters with High Silicate and Phosphate Concentrations. Environmental Science & Technology 38(1), 307-315.

Rose, J., Manceau, A., Bottero, J.-Y., Masion, A. and Garcia, F. (1996) Nucleation and Growth Mechanisms of Fe Oxyhydroxide in the Presence of PO 4 Ions. 1. Fe KEdge EXAFS Study.
Rossberg, A., Reich, T. and Bernhard, G. (2003) Complexation of uranium(VI) with protocatechuic acid - application of iterative transformation factor analysis to EXAFS spectroscopy. Analytical and Bioanalytical Chemistry 376(5), 631-638.
Saint-Jacques, N., Brown, P., Nauta, L., Boxall, J., Parker, L. and Dummer, T.J.B. (2018) Estimating the risk of bladder and kidney cancer from exposure to low-levels of arsenic in drinking water, Nova Scotia, Canada. Environ Int 110, 95-104.
Scheinost, A., Rossberg, A., Vantelon, D., Xifra, I., Kretzschmar, R., Leuz, A., Funke, H. and Johnson, C. (2006) Quantitative antimony speciation in shooting-range soils by EXAFS spectroscopy. Geochimica Et Cosmochimica Acta 70(13), 3299-3312.
Schmidt, C.W. (2014) Low-Dose Arsenic: In Search of a Risk Threshold. Environ Health Perspect 122(5), A131-134.
Schuhmacher-Wolz, U., Dieter, H.H., Klein, D. and Schneider, K. (2009) Oral exposure to inorganic arsenic: evaluation of its carcinogenic and non-carcinogenic effects. Critical reviews in toxicology 39(4), 271-298.
Senn, A.-C., Hug, S.J., Kaegi, R., Hering, J.G. and Voegelin, A. (2017) Arsenate co-precipitation with Fe(II) oxidation products and retention or release during precipitate aging. Water Research.
Senn, A.-C., Kaegi, R., Hug, S.J., Hering, J.G., Mangold, S. and Voegelin, A. (2015) Composition and structure of Fe(III)-precipitates formed by Fe(II) oxidation in water at near-neutral pH: Interdependent effects of phosphate, silicate and Ca. Geochimica et Cosmochimica Acta 162, 220-246.
Sharma, P., Ofner, J. and Kappler, A. (2010) Formation of Binary and Ternary Colloids and Dissolved Complexes of Organic Matter, Fe and As. Environmental Science & Technology 44(12), 4479-4485.
Smedley, P.L. and Kinniburgh, D.G. (2002) A review of the source, behaviour and distribution of arsenic in natural waters. Applied Geochemistry 17(5), 517-568.
Smeets, P., Medema, G. and Dijk, J. (2009) The Dutch secret: How to provide safe drinking water without chlorine in the Netherlands.
Smith, A.H., Hopenhayn-Rich, C., Bates, M.N., Goeden, H.M., Hertz-Picciotto, I., Duggan, H.M., Wood, R., Kosnett, M.J. and Smith, M.T. (1992) Cancer risks from arsenic in drinking water. Environ Health Perspect 97, 259-267.
Sorlini, S. and Gialdini, F. (2010) Conventional oxidation treatments for the removal of arsenic with chlorine dioxide, hypochlorite, potassium permanganate and monochloramine. Water Research 44(19), 5653-5659.
Sorlini, S., Gialdini, F. and Collivignarelli, M.C. (2014) Survey on full-scale drinking water treatment plants for arsenic removal in Italy. Water Practice and Technology 9(1), 42-51.
Sposito, G. (2008) The Chemistry of Soils, Oxford University Press, New York.
Stachowicz, M., Hiemstra, T. and van Riemsdijk, W.H. (2008) Multi-competitive interaction of As(III) and As(V) oxyanions with Ca(2+), Mg(2+), PO(3-)(4), and CO(2-)(3) ions on goethite. J Colloid Interface Sci 320(2), 400-414.
Stumm, W. and Morgan, J.J. (1996) Aquatic Chemistry, Chemical Equilibria and Rates in Natural Waters, John Wiley & Sons, Inc., New York.
Stuyfzand, P., van Rossum, P. and Mendizabal, I. (2008) Arsenic in groundwater - A world problem. Appelo, T. (ed), pp. 102-125, Netherlands National Committee of the IAH, Utrecht, The Netherlands.
Su, C. and Puls, R.W. (2001) Arsenate and Arsenite Removal by Zerovalent Iron: Effects of Phosphate, Silicate, Carbonate, Borate, Sulfate, Chromate, Molybdate, and Nitrate, Relative to Chloride. Environ. Sci. Technol. 35(22), 4562-4568.
Tebo, B.M., Johnson, H.A., McCarthy, J.K. and Templeton, A.S. (2005) Geomicrobiology of manganese(II) oxidation. Trends in Microbiology 13(9), 421-428.
Vahter, M. (2008) Health effects of early life exposure to arsenic. Basic and Clinical Pharmacology and Toxicology 102(2), 204-211.
Vahter, M., Gardner, R., Ahmed, S., Kippler, M., Hamadani, J.D., Tofail, F. and Raqib, R. (2012) Effects of early-life arsenic exposure on child health and development, pp. 173-174.
van Beek, C.G.E.M., Dusseldorp, J., Joris, K., Huysman, K., Leijssen, H., Schoonenberg Kegel, F., de Vet, W.W.J.M., van de Wetering, S. and Hofs, B. (2016) Contributions of homogeneous, heterogeneous and biological iron(II) oxidation in aeration and rapid sand filtration (RSF) in field sites. Journal of Water Supply: Research and Technology—AQUA 65(3), 195-207.
Van Beek, C.G.E.M., Hiemstra, T., Hofs, B., Bederlof, M.M., van Paassen, J.A.M. and Reijnen, G.K. (2012) Homogeneous, heterogeneous and biological oxidation of iron(II) in rapid sand filtration. Journal of Water Supply: Research and Technology—AQUA 61(1), 1-2012.
Van der Wens, P., Baken, K. and Schriks, M. (2016) Arsenic at low concentrations in Dutch drinking water: assessment of removal costs and health benefits. . Bhattacharya, P., Vahter, M., Jarsjö, J., Kumpiene, J., Ahmad, A., Sparrenbom, C., Jacks, G., Donselaar, M.E., Bundschuh, J. and Naidu, R. (eds), pp. 563-564, CRC Press, Stockholm, Sweden.

van Genuchten, C., Addy, S., Pena, J. and Gadgil, A. (2012a) Removing arsenic from synthetic groundwater with iron electrocoagulation: An Fe and As K-edge EXAFS study. Environmental Science & Technology 46(2), 986-994.
van Genuchten, C., Behrends, T., Kraal, P., Stipp, S. and Dideriksen, K. (2018) Controls on the formation of Fe(II,III) (hydr)oxides by Fe(0) electrolysis. Electrochimica Acta 286, 324-338.
van Genuchten, C. and Pena, J. (2017a) Mn(II) Oxidation in Fenton and Fenton Type Systems: Identification of Reaction Efficiency and Reaction Products. Environmental Science & Technology 51(5), 2982-2991.
van Genuchten, C.M., Addy, S.E.A., Peña, J. and Gadgil, A.J. (2012b) Removing Arsenic from Synthetic Groundwater with Iron Electrocoagulation: An Fe and As K-Edge EXAFS Study. Environmental Science & Technology 46(2), 986-994.
van Genuchten, C.M., Gadgil, A.J. and Peña, J. (2014a) Fe(III) Nucleation in the Presence of Bivalent Cations and Oxyanions Leads to Subnanoscale 7 Å Polymers. Environmental Science & Technology 48(20), 11828-11836.
van Genuchten, C.M. and Pena, J. (2017b) Mn(II) Oxidation in Fenton and Fenton Type Systems: Identification of Reaction Efficiency and Reaction Products. Environ. Sci. Technol. 51(5), 2982-2991.
van Genuchten, C.M. and Peña, J. (2016a) Antimonate and arsenate speciation on reactive soil minerals studied by differential pair distribution function analysis. Chemical Geology 429, 1-9.
van Genuchten, C.M. and Peña, J. (2016b) Sorption selectivity of birnessite particle edges: a d-PDF analysis of Cd(ii) and Pb(ii) sorption by δ-MnO2 and ferrihydrite. Environmental Science: Processes & Impacts 18(8), 1030-1041.
Van Genuchten, C.M., Pena, J., Amrose S, E. and Gadgil, A.J. (2014b) Structure of Fe(III) precipitates genberated by the electrolytric dissolution of Fe(0) in the presence of groundwater ions. Geochimica et Cosmochimica Acta 127, 285-304.
Villalobos, M. (2015) Advances in the Environmental Biogeochemistry of Manganese Oxides. Feng, X., Li, W., Zhu, M. and Sparks, D. (eds), American Chemical Society.
Villalobos, M., Bargar, J. and Sposito, G. (2005) Mechanisms of Pb(II) sorption on a biogenic manganese oxide. Environmental Science & Technology 39(2), 569-576.
Voegelin, A., Kaegi, R., Frommer, J., Vantelon, D. and Hug, S.J. (2010) Effect of phosphate, silicate, and Ca on Fe(III)-precipitates formed in aerated Fe(II)- and As(III)-containing water studied by X-ray absorption spectroscopy. Geochimica et Cosmochimica Acta 74(1), 164-186.
Von Gunten, U. (2003) Ozonation of drinking water: Part II. Disinfection and by-product formation in presence of bromide, iodide or chlorine. Water Research 37(7), 1469-1487.
Vries, D., Bertelkamp, C., Schoonenberg Kegel, F., Hofs, B., Dusseldorp, J., Bruins, J.H., de Vet, W. and van den Akker, B. (2017) Iron and manganese removal: Recent advances in modelling treatment efficiency by rapid sand filtration. Water Research 109, 35-45.
Wang, S. and Mulligan, C.N. (2006) Occurrence of arsenic contamination in Canada: Sources, behavior and distribution. Science of the Total Environment 366, 701 - 721.
Waychunas, G.A., Rea, B.A., Fuller, C.C. and Davis, J.A. (1993) Surface chemistry of ferrihydrite: Part 1. EXAFS studies of the geometry of coprecipitated and adsorbed arsenate. Geochimica et Cosmochimica Acta 57(10), 2251-2269.
Webb, S. (2005) SIXPACK: a graphical user interface for XAS analysis using IFEFFIT. Physica Scripta T115, 1011-1014.
Weng, L., Van Riemsdijk, W.H. and Hiemstra, T. (2008) Humic nanoparticles at the oxide-water interface: Interactions with phosphate ion adsorption. Environmental Science and Technology 42(23), 8747-8752.
Weng, L., Van Riemsdijk, W.H. and Hiemstra, T. (2009) Effects of Fulvic and Humic Acids on Arsenate Adsorption to Goethite: Experiments and Modeling. Environmental Science & Technology 43(19), 7198-7204.
WHO (2011) Arsenic in Drinking-water: Background document for development of WHO Guidelines for Drinking-water Quality, p. 16, WHO Press, Geneva, Switzerland.
Wilkie, J.A. and Hering, J.G. (1996) Adsorption of arsenic onto hydrous ferric oxide: effects of adsorbate/adsorbent ratios and co-occurring solutes. Colloids and Surfaces A: Physicochemical and Engineering Aspects 107, 97-110.
Woo, N.C. and Choi, M.C. (2001) Arsenic and metal contamination of water resources from mining wastes in korea. Environmental Geology 40(3), 305-311.
Wyckoff, R.W.G. (1963) Crystal Structures, Wiley.
Youngran, J., Fan, M., Van Leeuwen, J. and Belczyk, J.F. (2007) Effect of competing solutes on arsenic(V) adsorption using iron and aluminum oxides. Journal of Environmental Sciences 19(8), 910-919.

5 Permanganate – Ferric dosing to rapid sand filters: A case study at Katwijk (Dunea)

This chapter is a summary of the following report:

Pieterse, B. 2017. MnO_4 – Fe(III) dosing to rapid sand filters for removing arsenic from drinking water to <1 µg/L: A case study in Katwijk (Dunea). MSc thesis in Sanitary Engineering. Department of Civil Engineering and Geosciences. TU Delft, the Netherlands.

5.1 Introduction

Water treatment plant (WTP) Katwijk is one of the three WTPs of the drinking water company Dunea. It produces drinking water for the region around the city of Leiden. The raw water is obtained from the dammed-up Meuse and recharged into the dunes after pre-treatment by coagulation and rapid sand filtration. The raw water from Meuse contains only traces of As (<1 µg/L), however after the dune infiltration (and retention in dunes for 60 days on average) the As concentration increases up to a concentration of 3.5-4.2 µg/L due to As release during artificial recharge and storage in dunes. The dune-effluent is further treated at WTP Katwijk to achieve drinking water quality (Figure 1). During treatment, As concentration in water somewhat decreases (3.2-3.4 µg/L in produced drinking water), but remains much higher than 1 µg/L. Table 1 presents the water quality data of raw dune-water and treatment plant effluent (drinking water) at WTP Katwijk.

The overall objective of this research was to investigate if MnO_4 – $FeCl_3$ dosing before rapid sand filters (Figure 1) can achieve As removal to <1 µg/L at WTP Katwijk. Particular attention was given to the effect of filtration velocity and filter material on the run times of RSFs, as this is a critical factor for the application of this process at the WTP Katwijk and other WTPs of Dunea where As reduction to <1 µg/L is desired. In addition, the impact of MnO_4 – $FeCl_3$ dosing on backwash water settling was explored in this study.

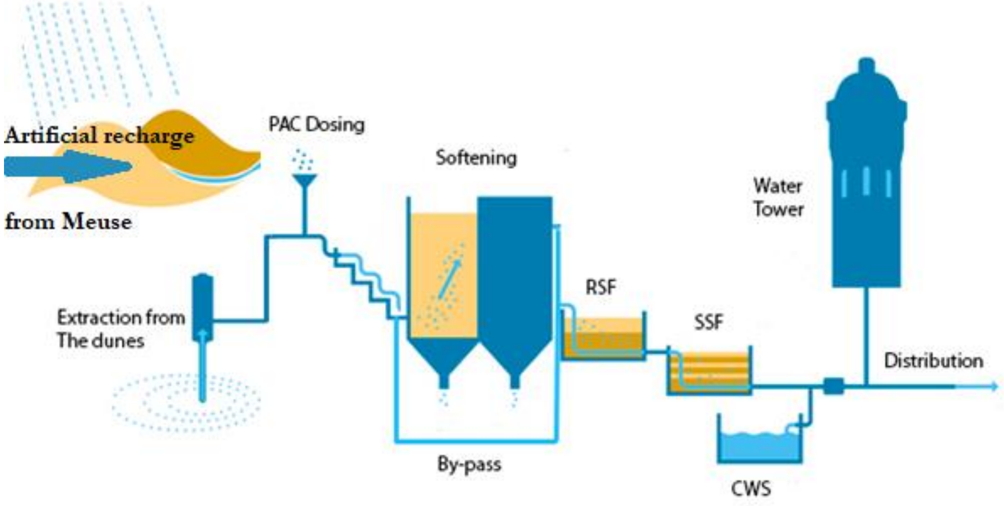

Fig 1. Drinking water production from source to plant effluent at WTP Katwijk.

Table 1. Raw dune-water and treatment plant effluent (drinking water) quality at WTP Katwijk. Data is based on the regular water quality monitoring programs of Dunea in the period 2016–19. For comparison the drinking water quality standards in the Netherlands are also given.

		WTP Katwijk		Drinking water quality standard in the Netherlands*
Parameter	Unit	Raw dune-water	Treatment plant effluent (drinking water)	
Temp	°C	7.7–12.4	13.7–16.8	<25
pH	-	7.62–7.71	$8.17–8.42^+$	7.0–9.5
Dissolved Oxygen	mg/L O_2	1.7–3.5	9.7	>2
Electrical Conductivity	mS/m	47–56	48.5–52.6	<125
Bicarbonate	mg/L HCO_3	200–210	167–184	>60
Turbidity	NTU	0.3–3.5	<0.03	<1
Iron	mg/L Fe	<0.01–1.5	<0.01	<0.2
Manganese	mg/L Mn	0.03–0.2	<0.01	<0.05
Calcium	mg/L Ca	66–72	40–46	-
Magnesium	mg/L Mg	7.4–8.3	7.7–8.3	-
Ammonium	mg/L NH_4	0.03–0.2	<0.02	<0.2
Nitrite	mg/L NO_2	0.05–0.10	<0.007	<0.1
Nitrate	mg/L NO_3	2.0–6.2	1.7–2.2	<50
Arsenic	µg/L As	3.5–4.2	3.2–3.4	<10
Orthophosphate	mg/L P	0.07–0.2	0.02–0.05	-
Silicate	mg/L Si	n.m	n.m	-
Total organic carbon	mg/L C	2.6–2.9	2.1	-
Sulphate	mg/L SO_4	40–46	45–51	<150
Sodium	mg/L Na	30–36	57–60	<150
Chloride	mg/L Cl	45–54	54–56	<150

n.m. not measured
$^+$ pH higher than the raw water because of NaOH dosing during softening
- not regulated
* based on national guideline "Drinkwaterbesluit" available online at
https://wetten.overheid.nl/BWBR0030111/2018-07-01#BijlageA

5.2 Materials and methods

5.2.1 Pilot setup and operation

Pilot experiments were performed at WTP Katwijk using a pilot plant consisted of two stainless steel columns with a total height of 2.5 m and column diameter of 0.25 m (Figure 2). Both filters contained a bottom layer of 1.0 m sand (0.8-1.3mm, with a uniformity coefficient of 1.3), but one of the columns contained 0.5 m anthracite (1.6 – 2.5mm) while the other column contained 0.5 m of pumice (2.5 - 3.5mm) as top layer. These columns are further referred as anthracite and pumice filter respectively. Anthracite filter represents the rapid sand filter design at WTP Katwijk and the pumice filter represents the rapid sand filter design at another WTP of Dunea.

Both columns were fed with the influent of full-scale rapid sand filters of WTP Katwijk (i.e. mixture of cascade effluent and softened water, Figure 1, Table 1). Each column had a separate inflow pump that pumped in water from the buffer tank. Most experiments were carried out with a flow rate of 200 L/h per column which resulted in a filtration rate of 4 m/h. To test higher filtration velocities (6 and 10 m/h), the feed flow was increased.

The filtrate of each column was stored in a buffer tank. This water was used for backwashing of the pilot filter. During backwashing, a flow of 3000 L/h was applied which corresponds to backwash velocities of 60 m/h (similar to what is used at full-scale filters of WTP Katwijk). For the chemicals (solutions of $NaMnO_4$ and $FeCl_3$), tanks of 60 L were used. Peristaltic pumps were used to dose the chemicals into the columns. Each new experiment was started with a clean filter. Filter cleaning was done following a backwash procedure similar to WTP Katwijk (Table 2).

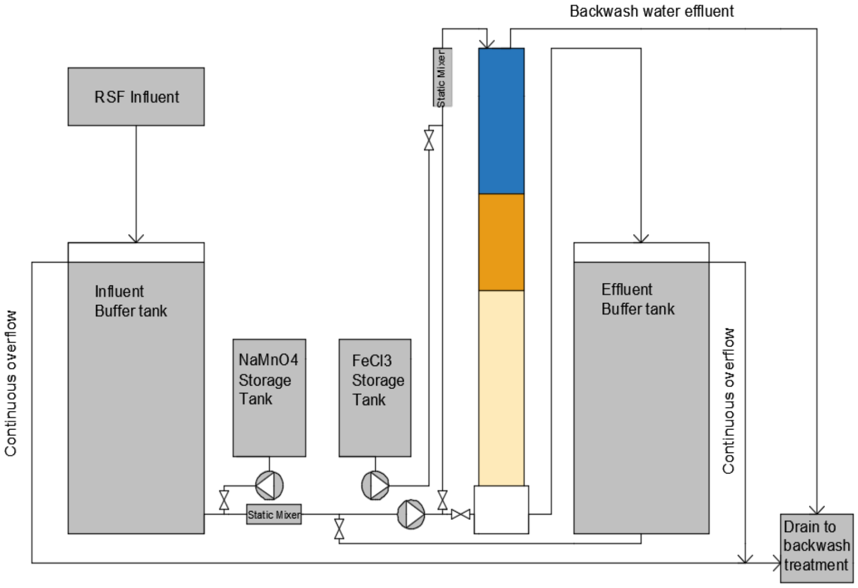

Figure 2: Schematic of pilot installation used in this study. Only one filter column is shown here for simplicity. In experiments, two filter columns were used however.

Table 1: Backwash procedure used in pilot experiments.

Step		Velocity (m/h)	Duration (min)
1	Drain supernatant water until 10cm water is left on top of the filter		
2	Air scour	55	10
3	2 minutes of pause to remove some leftover air bubbles stuck in the filter bed.		
4	Backwash with water	60	10

5.2.2 Pilot experiments

5.2.2.1 Influence of different filter media

The effect of different filter media in As removal with MnO_4-Fe(III) dosing was studied by using two different top layers of filter material in parellel (anthracite in one filter and pumice in the other filter), while the bottom layer comprised of the same type of material (silica sand) in both filters. Both the filters were fed with a same feed water, i.e. influent of rapid sand filters of WTP Katwijk. Also, all other operational parameters were kept constant.

5.2.2.2 Influence of filtration velocity

The effect of filtration velocity was studied by performing experiments with filtration velocities of 4, 6 and 10 m/h. The filtration velocity corresponding to the rapid sand filters of Katwijk is 4 m/h. This was achieved by adjusting the feed flow to each column. Our hypothesis was that when the filtration velocity will increase, the Fe(III)(oxyhydr)oxide flocs will penetrate deeper into the filter bed and will not be removed by cake filtration at the top layer of the filter bed. All experiments to study the effect of filtration velocity were performed with dosages of 0.5 mg $NaMnO_4$ /L and 1.0 mg Fe(III) /L. Every filtration velocity was tested for at least 3 filtration cycles.

5.2.2.3 Backwash water settling experiments

To investigate if any differences in settling properties of backwash water occur with the dosing of MnO_4 and Fe(III), an experiment was performed. Backwash water samples were collected with and without chemical dosing in the feed of the pilot columns. The samples were allowed to settle in 1.5 L measuring cylinders. Every 5 minutes the location of the clear divide between clear water and turbid water (from now on in this thesis referred to as sedimentation front) was noted.

5.2.3 Sampling and analysis

All water samples were analyzed at HWL laboratory. Before collection of each sample the taps were opened for half a minute at constant flow to ensure a representative sample. pH, dissolved oxygen (DO), and temperature were measured on site by a hand-held (Hach HQ40D). Turbidity was measured by hand held device (Hach 2100P ISO Turbidimeter). Turbidity of the effluent of both the columns was also constantly measured and logged by the use of online turbidity meters. In most cases unfiltered and 0.45 µm filtered samples were collected and analyzed for As, Fe and Mn. Filtration of the samples was done by filtration through 0.45 µm disk filters prior to being sent for analysis.

5.3 Results and discussion

5.3.1 Effect of filter media and filtration velocity on arsenic removal

Table 3 shows the average dissolved As concentrations in the influent and effluent of pilot filters, as well as the total As removal efficiency as a function of the filtration velocity. The results show that As removal remained unaffected with an increase in filtration velocity for both filters. Also, there was no apparent difference between the As removal efficiency of the anthracite and pumice filters. These results imply that in all the cases the residence time was sufficient to achieve As(III) oxidation to As(V) and to achieve equilibrium As(V) adsorption onto Fe(III) (oxyhydr)oxides. The Fe(III)(oxyhydr)oxides with adsorbed As were effectively removed in both the filter beds, resulting in an effective overall As reduction to <1 µg/L.

Table 3: Average As removal efficiency at various filtration velocities (n =6).

Filtration velocity	Dissolved As influent (µg/l)	Dissolved As effluent (µg/l)	Removal %
Pumice filter			
4 m/h	2.1 ± 0.17	0.67 ±0.25	68%
6 m/h	2.3 ± 0.05	0.84 ±0.49	64%
10 m/h	2.5 ±0.18	0.71 ±0.27	72%
Anthracite filter			
4 m/h	2.1 ±0.17	0.77 ±0.12	63%
6 m/h	2.4 ±0.13	0.98 ±0.40	59%
10 m/h	2.5 ±0.18	0.54 ±0.16	78%

5.3.2 Filter run time and breakthrough

Due to the dosing of chemicals (MnO_4-Fe(III)), the runtime of the anthracite filter was decreased (Figure 3). These results are similar to the observations in previous studies and can be attributed to increased load of Fe(III)(oxyhydr)oxide flocs to the filter(Ahmad et al. 2018, Ahmad et al. 2015, Ahmad et al. 2014). Nevertheless, the turbidity of the effluent for anthracite filter was decreased significantly (from 0.3 FTU to about 0.03 FTU) with chemical dosing. This reduction in turbidity can be beneficial for the operation of downstream slow sand filters at WTP Katwijk (see Figure 1).

For both the filters, the volume of treated water before breakthrough decreased with increase in the filtration velocity (Figure 3 and Figure 4).

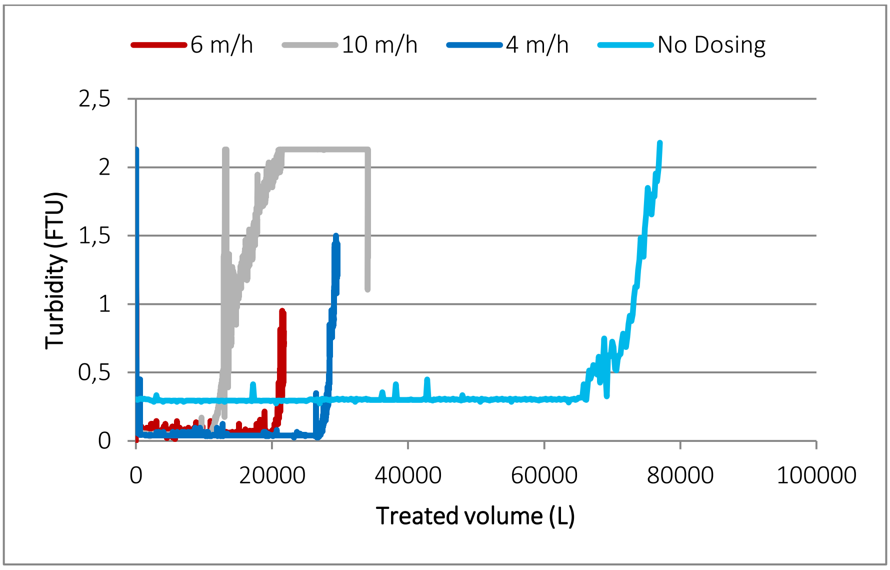

Fig 3. Breakthrough of the anthracite pilot filter with and without MnO_4-Fe(III) dosing. Dosing 0.5 mg NaMnO4/L and 1.0 mg Fe(III)/L. Filtration velocity of 4m/h.

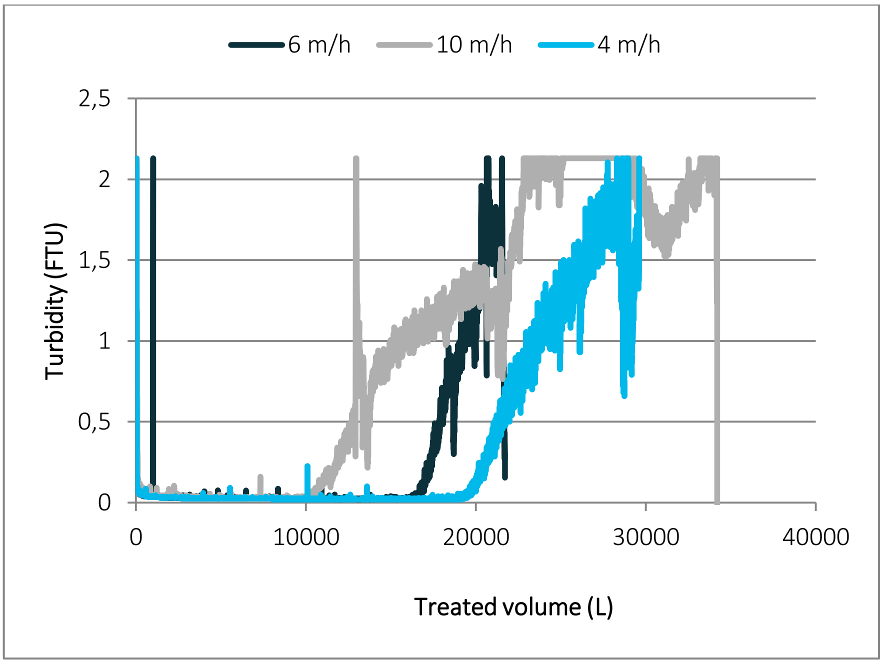

Fig 4. Breakthrough of the pumice pilot filter with and without MnO4-Fe(III) dosing. Dosing 0.5 mg NaMnO4/L and 1.0 mg Fe(III)/L. Filtration velocity of 4m/h.

5.3.3 Backwash water settling tests

Settling characteristics of the backwash water from anthracite filter with and without chemical dosing were studied in batch experiments, using the methodology used by (Ahmad et al. 2018). The results are presented in Figure 5. It was observed that with the dosing of MnO_4 and Fe(III), the backwash water settled much more quickly than without dosing. These results are in agreement with previous study (Ahmad et al. 2018). The quicker settling of backwash water solids in advantageous for backwash water treatment in general because of the fact that the residence time and depth of the settling basins depends strongly on the rate of backwash water settling.

Fig 5. Backwash water settling behaviour. Left jar contains backwash water with filter dosed with MnO4 and Fe(III) dosing. The right jar contains backwash water with filter without any chemical dose. Top picture is taken during settling test at t=8 min and bottom figure is taken at t=26 min during the settling test.

5.4 Conclusions and recommendations

Following conclusions can be drawn from this pilot study.

- At WTP Katwijk a residual As concentration of <1 µg/L can be achieved by dosing a combination of Fe(III) and MnO_4. The dosing that consistently resulted in a residual As concentration of <1 µg/L was 0.5 mg $NaMnO_4$ /L and is 1.0 mg Fe(III)/L.

- Arsenic removal by the use of MnO_4–Fe(III) dosing was not affected by the filtration velocity or filter bed composition in rapid sand filters. This means that at full-scale treatment plant the daily variations in production are not expected to affect As removal in rapid sand filters.

- The runtime of the pilot filters was decreased significantly due to the MnO_4–Fe(III) dosing. This means that an adjustment in the design of rapid sand filters, e.g. by replacing filter media with another size fraction will be required for a sustainable operation of full-scale rapid sand filter .

- Iron, Manganese, Ammonia and nitrite levels in the effluent did not increase during the 9 months of the pilot testing with MnO_4-Fe(IIII) dosing. This contributes to positive feasibility of MnO_4-Fe(III) dosing for WTP Katwijk.

- General filtration performance was enhanced with MnO_4–Fe(III) dosing in pilot column. The turbidity of the effluent was reduced from 0.3 FTU to about 0.03 FTU. This reduction in turbidity can be advantageous for the slow sand filter operation which follow rapid sand filters at WTP Katwijk.

- The settling velocity of the backwash water from pilot filters increased with MnO_4-Fe(III) dosing. This implies that implementation of MnO_4–Fe(III) dosing is expected to have benefits for backwash water treatment, i.e. reduction in settling time in sedimentation basins and more compact (smaller in size)sedimentation basins.

References

Ahmad, A., Cornelissen, E., van de Wetering, S., van Dijk, T., van Genuchten, C., Bundschuh, J., . . . Bhattacharya, P. (2018). Arsenite removal in groundwater treatment plants by sequential Permanganate—Ferric treatment. Journal of Water Process Engineering, 26, 221-229. doi:https://doi.org/10.1016/j.jwpe.2018.10.014

Ahmad, A., Kools, S., Schriks, M., Stuyfzand, P., & Hofs, B. (2015). Arsenic and chromium concentrations and their speciation in groundwater resources and drinking water supply in the Netherlands Retrieved from Nieuwegein, The Netherlands:

Ahmad, A., Van De Wetering, S., Groenendijk, M., & Bhattacharya, P. (2014). Advanced Oxidation-Coagulation-Filtration (AOCF) - An innovative treatment technology for targeting drinking water with <1 µg/L of arsenic. Paper presented at the One Century of the Discovery of Arsenicosis in Latin America (1914-2014): As 2014 - Proceedings of the 5th International Congress on Arsenic in the Environment.

6 Permanganate – Ferric dosing to rapid sand filters: A case study at Ouddorp (Evides)

This chapter is a summary of the following report:

de Ridder, D., Abdoel Gafoer, S., Hogendoorn, A., Ahmad, A. 2019. Arseen onder de één op productielocatie Ouddorp met AOCF. Evides Waterbedrijf (in Dutch).

6.1 Introduction

Water treatment plant (WTP) Ouddorp has a production capacity of 4.8 Mm^3/year. It uses surface water from Haringvliet as its source water. The source water is pre-treated and then infiltrated into the dunes (Figure 1A). The residence time of water in dunes is more than 30 days. The arsenic (As) concentration in the source water from Haringvliet is generally <1 µg/L. However, during the infiltration of water As gets mobilized to water, resulting in As concentration of 6.9–12.1 µg/L in the dune effluent (Table 1). After the treatment of dune effluent at WTP Ouddorp (Figure 1 B), the As concentration in the produced drinking water is 2.4–3.6 µg/L. The As reduction during treatment mainly occurs in rapid sand filters and is attributed to coprecipitation with Fe(III)(oxyhydr)oxides (that form due to aeration of dune-water and Fe(III) dosing=0.5 mg/L) (Ahmad 2017).

This overall goal of this pilot study was to investigate As removal to <1 µg/L by dosing $FeSO_4$, $FeCl_3$ and/or $NaMnO_4$ in the influent of rapid sand filter. The specific objectives were:

- Determination of the individual and combined doses of chemicals ($NaMnO_4$, $FeCl_3$, $FeSO_4$) for As reduction to <1 µg/L
- Study the impact of chemical dosing on nitrification in the rapid sand filters
- Study the impact of chemical dosing on the biological stability of the produced drinking water

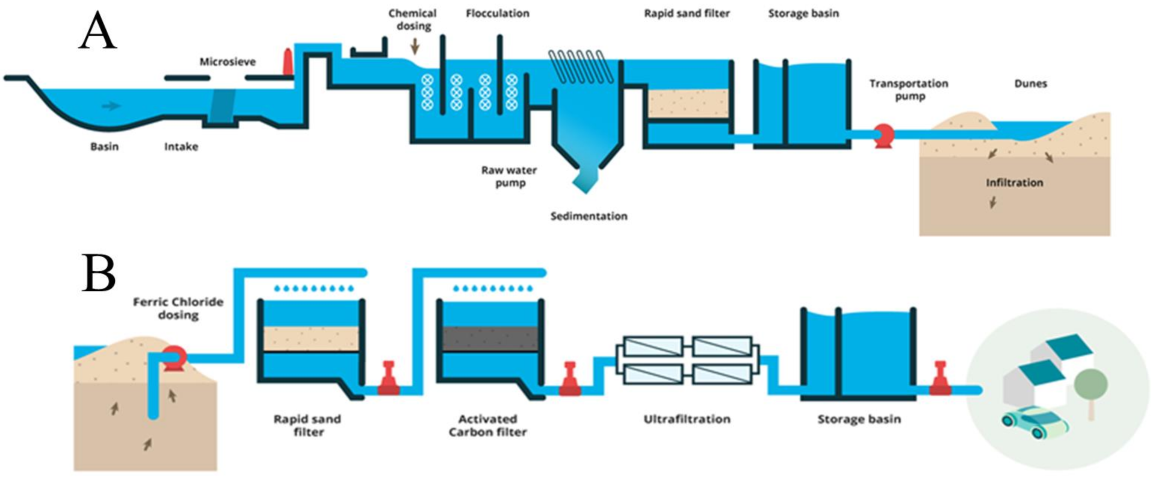

Fig 1. Process schemes of (A) pre-treatment of surface water before dune infiltration. (B) Dune-water treatment at WTP Ouddorp.

Table 1. Raw dune-water and treatment plant effluent (drinking water) quality at WTP Ouddorp. Data is based on the regular water quality monitoring programs of Evides in the period 2016–19. For comparison the drinking water quality standards in the Netherlands are also given.

		WTP Ouddorp		Drinking water quality standard in the Netherlands*
Parameter	Unit	Raw dune-water	Treatment plant effluent (drinking water)	
Temp	°C	11.5–12.2	11.7–15.0	<25
pH	-	7.45–7.85	7.74–7.91	7.0–9.5
Dissolved Oxygen	mg/L O_2	<0.1–2.0	9.2–10.1	>2
Electrical Conductivity	mS/m	64.5–67.5	n.m	<125
Bicarbonate	mg/L HCO_3	230–250	n.m	>60
Turbidity	NTU	n.m	<0.03	<1
Iron	mg/L Fe	0.7–1.9	<0.01	<0.2
Manganese	mg/L Mn	0.08–0.11	<0.01	<0.05
Calcium	mg/L Ca	83–88	82–87	-
Magnesium	mg/L Mg	10	10	-
Ammonium	mg/L NH_4	0.25–0.33	<0.02	<0.2
Nitrite	mg/L NO_2	0.013–0.02	<0.007	<0.1
Nitrate	mg/L NO_3	<0.2–0.3	2.6–3.7	<50
Arsenic	µg/L As	6.9–12.1	2.4–3.6	<10
Orthophosphate	mg/L P	0.03–0.25	0.007–0.03	-
Silicate	mg/L Si	3.0–4.6	3.1–4.5	-
Total organic carbon	mg/L C	3.3–3.9	1.6–3.0	-
Sulphate	mg/L SO_4	27–50	30–52	<150
Sodium	mg/L Na	34–55	34–55	<150
Chloride	mg/L Cl	67–110	66–108	<150

n.m. not measured

$^+$ pH higher than the raw water because of NaOH dosing during softening

- not regulated

* based on national guideline "Drinkwaterbesluit" available online at https://wetten.overheid.nl/BWBR0030111/2018-07-01#BijlageA

6.2 Materials and methods

A pilot installation, comprising of two columns was installed at WTP Ouddorp for the experiments. For simplicity, here we provide the process scheme of one of the pilot columns (Figure 2). Design and process details are further summed-up in Table 2. During all the experiments, one of the columns was used as a reference and the other column was used to study the effect of chemical dosing, i.e. dosing of $NaMnO_4$, $FeCl_3$ and $FeSO_4$. The columns were fed with the dune effluent, i.e. influent of rapid sand filters of WTP Ouddorp.

An overview of the experiments performed during the pilot study is provided in Table 3. All experiments were performed in at least duplicates. It is noted that achieving and maintaining the desired dosing of chemicals could not take place at several instances during the experiments because of the problems with the chemical dosing pumps. Therefore, we rely on the measurements of Fe and Mn in the supernatant water of the pilot columns to ascertain the amount of chemicals dosed, i.e. doses of Fe(II) and Fe(III) were calculated from the measured amount of total Fe in the supernatant water and the dose of MnO4 was calculated from the measured amount of Mn in the supernatant water. Supernatant storage on sand filters is typically not a completely mixed system. Therefore, it is noted here that the chemical doses indicated in Table 3 and further used for discussion in this chapter may be in accurate. Therefore, we kept the discussion of results rather qualitative.

All chemicals were obtained from Brenntag company. All analysis were carried out at Aqualab Zuid, except BPP analysis which was carried out at KWR. Detailed methodology of analysis of water samples for different parameters is provided in chapter 4.

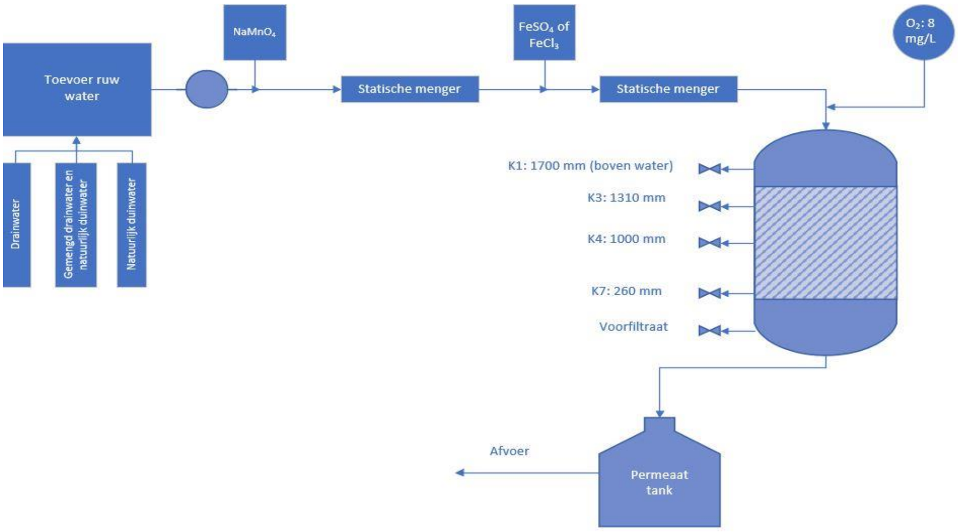

Fig 2. Schematic overview of a pilot column. For the experiments, two pilot columns with similar process details were used.

Table 2. Details of the pilot columns

Dimensions	
Column height (m)	2.50
Column diameter (m)	0.23
Filter bed height (m)	1.40 (filter material obtained from a full scale filter of WTP Ouddorp)
Grain size (mm)	2.0 – 4.0
Process details during filter run	
Filtration velocity (m/h)	2
Backwash frequency	1x per week
Aeration	In-line aeration
Backwashing	Water - air – water (until filter becomes clean)

Table 3. An overview of the experiments performed (conditions tested) during the pilot study at WTP Ouddorp. Fe(II) was dosed as $FeSO_4$, Fe(III) was dosed as $FeCl_3$ and MnO_4 was dosed as $NaMnO_4$. The doses were calculated from the Fe and Mn concentration in the supernatant water.

Experiment/conditions	Reference column		Experimental column		Duration (h)
	Dosing MnO_4 (mg/L)	Dosing Fe (mg/L)	Dosing MnO_4 (mg/L)	Dosing Fe (mg/L)	
Start-up	-	-	-	-	336
Fe (II)	-	-	-	3.2	67
Fe (II)	-	-	-	0.6	23
Fe (III)	-	-	-	6.3	5
Fe (III)	-	-	-	6.8	7
Fe (III)	-	-	-	4.0	5
MnO_4	-	-	0.65	-	115
MnO_4	-	-	0.35	-	117
MnO_4 + Fe(III)	-	1.7	0.28	3.1	96
MnO_4 + Fe(III)	-	0.8	6.5	1.5	90
MnO_4 + Fe(III)	-	2.2	0.21	2.4	91
MnO_4 + Fe(III)	-	3.5	0.43	3.0	40

6.3 Results and discussion

6.3.1 Start-up of pilot filters

Before performing the experiments, both the pilot filters were operated for some time (336 h) without any dosing of chemicals and samples of the raw water, supernatant water, pore water of the filter bed and filter effluent were collected to study the removal of As and Fe. The As and Fe concentrations during this start-up phase are presented in Figure 3 and Figure 4 respectively. In general, both the columns showed similar As and Fe removal profiles, which matched with the removal profiles of these elements in the full-scale rapid sand filters of WTP Ouddorp (Ahmad 2017). The oxidation and precipitation of natural Fe(II) in the raw water was complete in the supernatant storage of the both the columns. The removal of the precipitated Fe however occurred throughout the filter beds, in such a way that most removal occurring in the upper part of the filter beds and a relatively small amount of Fe particles were removed further deep in the filter bed (Figure 3 and Figure 4) . Arsenic removal followed Fe removal profile in both columns, thus it can be concluded that As removal was due to coprecipitation with Fe(III)(oxyhydr)oxides.

Figure 3 and Figure 4 further show that approximately 30% of the total amount of As in the raw water was present in the oxidized form As(V) and 70% was As(III). During the passage of water through the filter beds As(III) was completely oxidized to As(V), mainly in the upper part of the filter beds. A similar As(III) oxidation behaviour during rapid sand filtration has been observed at WTP Dorst (Chapter 4) and Katwijk (Chapter 5). The oxidation of As(III) to As(V) in rapid sand filters has been attributed to the activity of As(III) oxidizing bacteria (Gude et al. 2018a, Gude et al. 2018c).

These results indicate that both the pilot filters removed As and Fe effectively and in a similar manner. Moreover, they also reflected As and Fe removal behaviour in full-scale rapid sand filters of WTP Ouddorp.

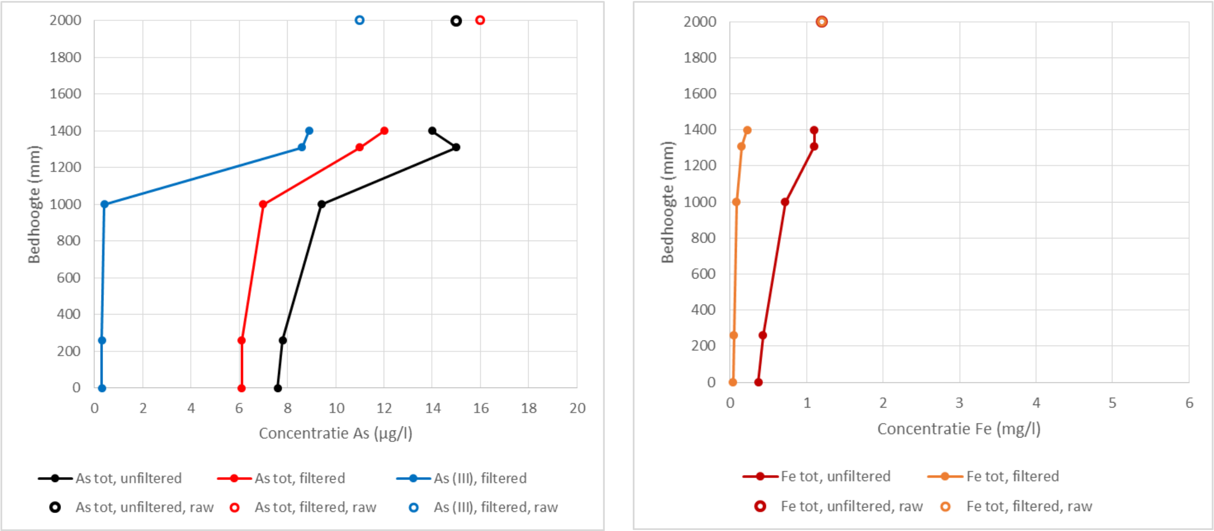

Fig 3. Concentrations of As (left) and Fe (right) over the filter bed height in the reference pilot column. No dosing of chemicals.

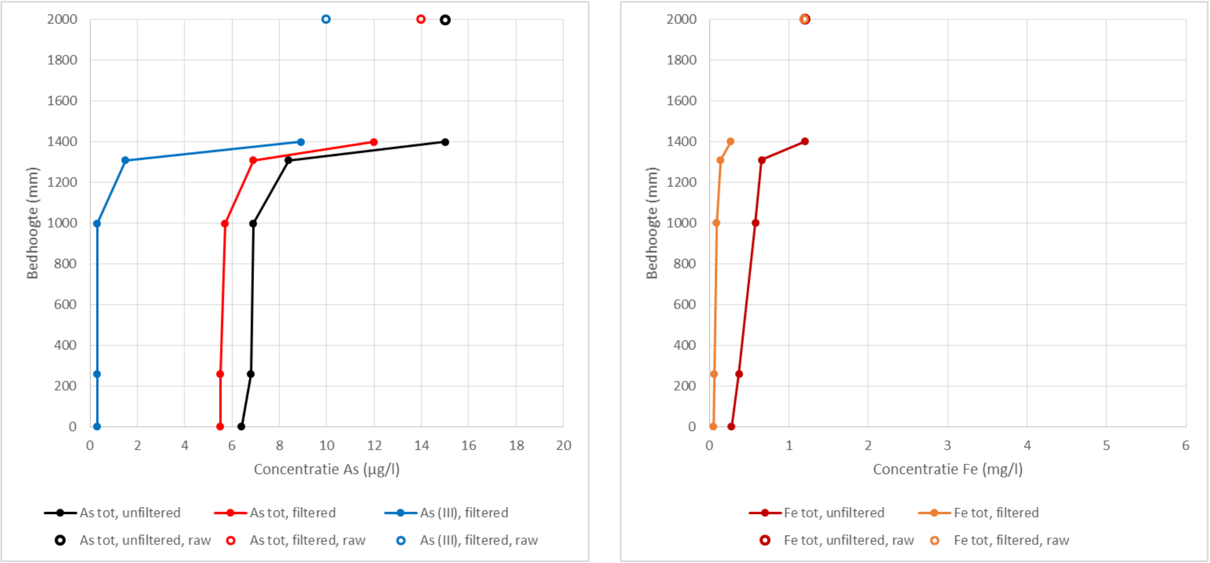

Fig 4. Concentrations of As (left) and Fe (right) over the filter bed height in the experimental pilot column. No dosing of chemicals.

6.3.2 Individual dosing of FeSO$_4$ and FeCl$_3$

To increase As removal in rapid sand filters a common approach is to dose an Fe based coagulant. FeSO$_4$ and FeCl$_3$ are two common Fe based coagulants, but FeSO$_4$ provides Fe(II) and FeCl$_3$ provides Fe(III) in water. In aerobic waters Fe(II) oxidizes to for Fe(III)(oxyhydr)oxide precipitates, similar to the hydrolysis of Fe(III) in water. However, some studies have reported a difference in As removal performance between FeSO$_4$ and FeCl$_3$ (Gude et al. 2018b). Thus, we studied As removal in pilot filter as a function of Fe based coagulant.

To study the effect of Fe(II) dosing on As removal, the experimental column was dosed with 3.2 mg/L of Fe(II) (FeSO$_4$ dosing). Results of As and Fe removal with FeSO$_4$ are presented in Figure 5. The oxidation of dosed Fe(II) and precipitation of Fe was not complete in the supernatant (approximately 1 mg/L Fe could not be filtered through 0.45 µm disc filter which is typically used to separate dissolved and precipitated compounds). This was in contrast to the reference column (Figure 3, absence of any chemical dosing) where all the Fe in raw water was completely precipitated in the supernatant storage of the pilot filter. Nevertheless, in the top of the filter bed (approximately 400 mm from the filter surface), Fe was completely precipitated. Most (77%) of the precipitated Fe was also removed in the upper part of the filter bed, however some (23%) of the precipitated Fe penetrated deeper into the filter bed and was removed completely deep in the filter bed (Figure 5).

The dosing of 3.2 mg/L Fe(II) lowered the As concentration to 4 µg/L in the filter effluent. In the absence of chemical dosing As concentration in the filter effluent was approximately 6 µg/L. Thus, Fe(II) dosing improved As removal in the pilot filter, however the <1 µg/L As was not achieved . Arsenic removal mainly occurred in the upper part of the filter bed, as Fe removal. However, As and Fe removal profiles did not match in the lower part of the pilot filter bed. We suspect release of As from the filter media, however exact reason is not known.

To study the effect of Fe(III) dosing on As removal, the experimental column was dosed with Fe(III) ($FeCl_3$ dosing). We aimed at a similar dosing of Fe as $FeSO_4$ experiment (i.e. 3.2 mg/L), however Fe(III) dosing of 4 mg/L was realized. Therefore, a direct quantitative comparison between the effects of Fe(II) and Fe(III) dosing is difficult. Moreover, during Fe(III) dosing experiments the natural concentration of Fe in raw dune-water was unusually high due to some maintenance activity on raw water supply pipes at WTP Ouddorp. Nevertheless, we discuss here the results of Fe(III) dosing experiment to draw qualitative conclusions (Figure 6). The results show that all the Fe in water (natural + dosed) was completely precipitated in the supernatant storage and the removal of most of the precipitated Fe mainly occurred in the upper part of the filter bed.

Even with 4 mg/L Fe(III) dosing, the column effluent contains 2 µg/L As. Therefore, dosing Fe(III) alone is not suitable to achieve As removal to <1 µg/L in the rapid sand filters of Ouddorp. The biological oxidation of As(III) to As(V) was not hindered by Fe(III) dosing. Arsenic removal was strongly correlated with Fe removal, as previously observed in case of $FeSO_4$ dosing.

All in all, the individual dosing of Fe(II) (3.2 mg/L) and Fe(III) (4 mg/L) was not effective to reduce As concentration to <1 µg/L. The dosing of Fe based coagulants did not hinder the biological As(III) oxidation in the pilot filters.

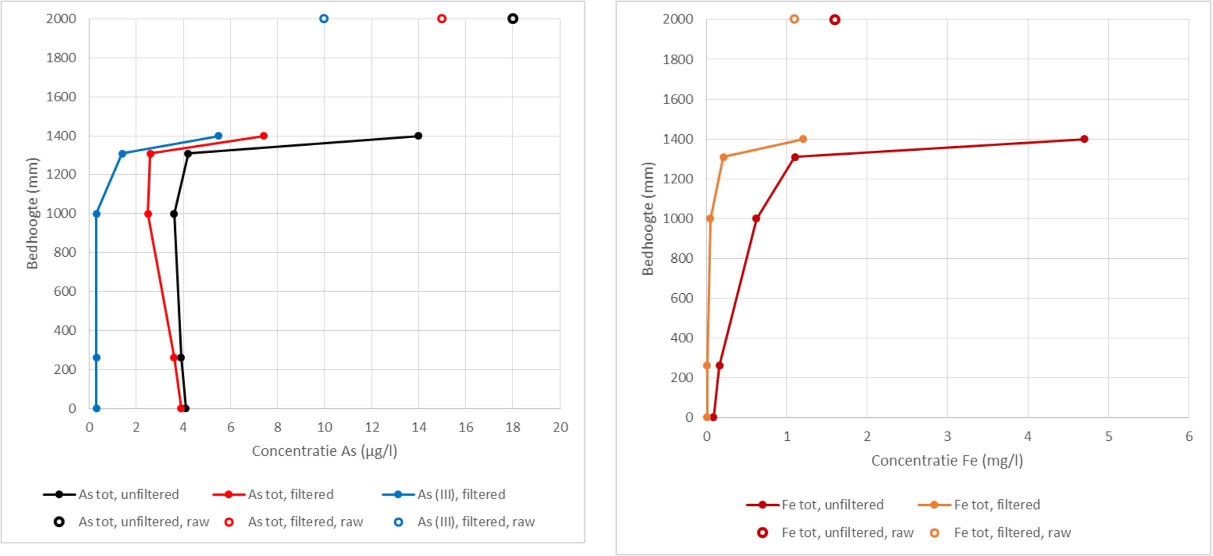

Fig 5. Concentrations of As (left) and Fe (right) over the filter bed height in the experimental pilot column. No MnO_4 dosing. Fe(II) dose 3.2 mg/L

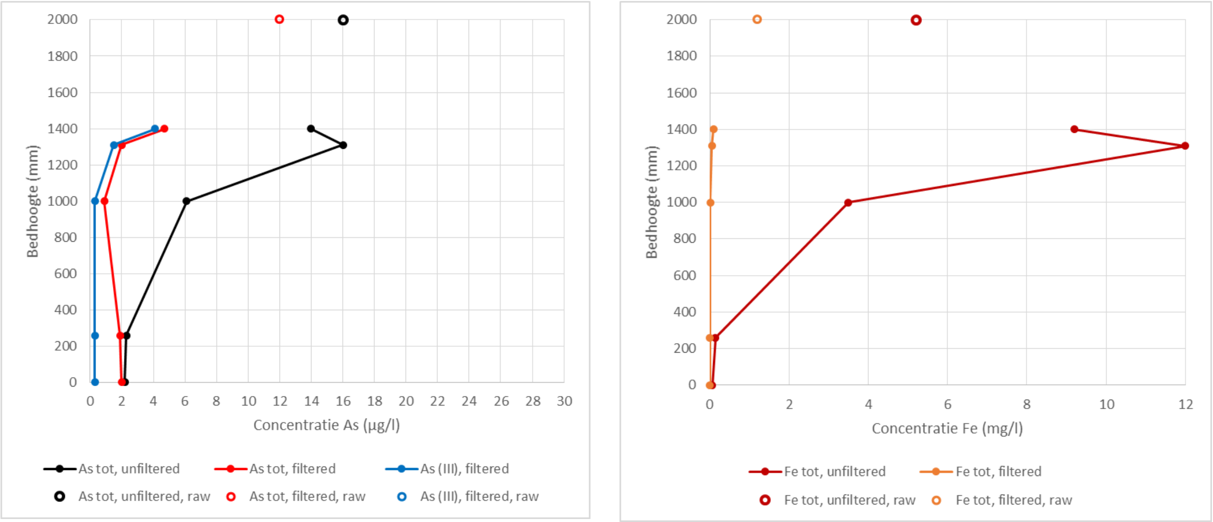

Fig 6. Concentrations of As (left) and Fe (right) over the filter bed height in the experimental pilot column. No MnO_4 dosing. Fe(III) dose 4 mg/L

6.3.3 Individual dosing of $NaMnO_4$ and $NaMnO_4$-$FeCl_3$ dosing

The dune effluent at WTP Ouddorp contains about 70% As(III) and 30% As(V). As(III) is not adsorbed effectively by Fe(III)(oxyhydr)oxides. Oxidizing As(III) to As(V) by a strong oxidant such as MnO_4 has been shown previously to increase As removal efficiency (Chapter 4). Therefore, we investigated the effect of dosing MnO4 in the influent of a pilot filter. To study the effect of MnO_4 dosing on As removal, the experimental column was dosed with 0.4 mg/L of MnO_4 ($NaMnO_4$ dosing). Results of As and Fe removal are presented in Figure 7. Effluent As concentration did not reach <1 µg/L, however the effluent As concentration was much lower (3 µg/L) compared to the reference (6 µg/L). Arsenic was present almost entirely in the form of As(V) in the supernatant and in the filter bed which indicates that MnO_4 dosing was sufficient to oxidize As(III) to As(V). This result confirms that oxidation of As(III) to As(V) increases As uptake by Fe(III)(oxyhydr)oxides. However, removal to <1 µg/L As was not achieved due to the Fe deficiency in water. Therefore, we studied the effect of dosing MnO_4 and Fe(III) on As removal.

To study the effect of MnO_4 and Fe(III) dosing on As removal, the experimental column was dosed with 0.4 mg/L of MnO_4 and 3.1 mg/L Fe(III). Results of As and Fe removal are presented in Figure 8. As(III) was completely oxidized to As(V) due to MnO_4 dosing and the dissolved As concentration (0.45 µm filtered) in the supernatant was <1 µg/L. This shows that MnO4-Fe(III) dosing was effective in adsorbing As to Fe(III)(oxyhydr)oxides resulting in a residual solution phase As concentration of <1 µg/L. However, as soon as the water entered the filter bed, a severe Fe and As release from the filter media was observed. The released Fe and As was removed deeper in the filter bed, but As concentration was not reduced to <1 µg/L.

From these results it can be concluded that with MnO_4-Fe(III) dosing, As(III) oxidation and coprecipitation with Fe(III)(oxyhydr)oxides was efficient to achieve residual As concentration of <1 µg/L, but the release of As from the filter media hindered achievability of <1 µg/L in the filter effluent. We propose further investigation of the MnO_4-Fe(III) process for As removal at WTP Ouddorp with a virgin filter media.

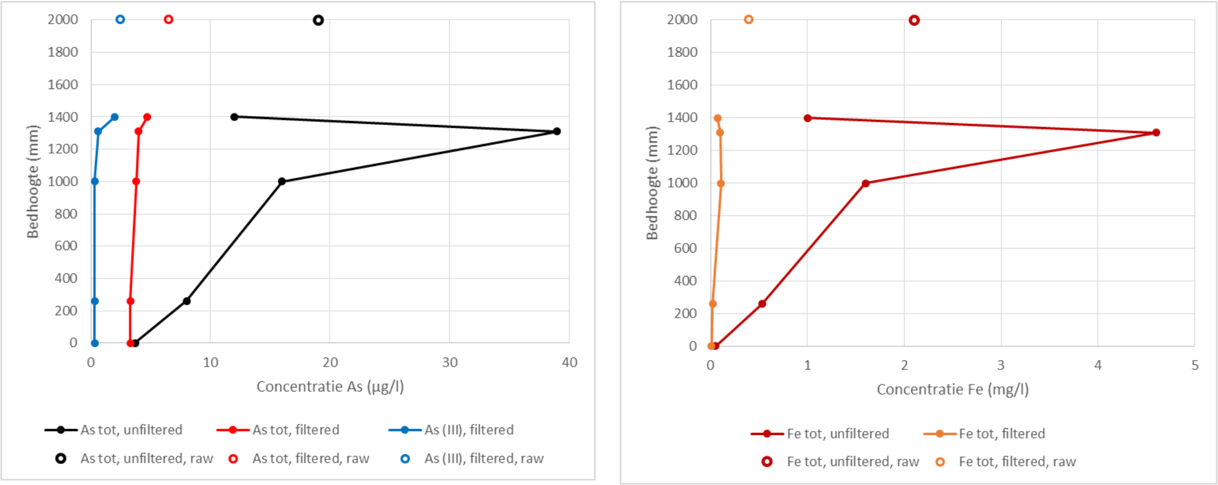

Fig 7. Concentrations of As (left) and Fe (right) over the filter bed height in the experimental pilot column. MnO_4 dose 0.4 mg/L. No Fe dose.

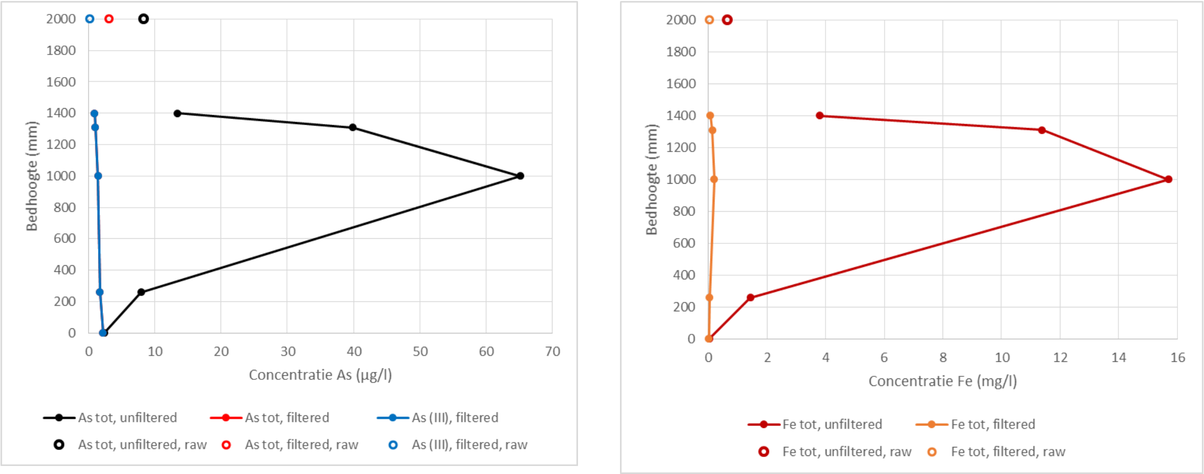

Fig 8. Concentrations of As (left) and Fe (right) over the filter bed height in the experimental pilot column. MnO_4 dose 0.4 mg/L. Fe(III) dose 3.1 mg/L

6.3.4 Nitrification

Figure 9 presents the ammonium concentrations in the raw water, supernatant and the column effluent during different pilot experiments. It can be concluded from the results that the biological oxidation of ammonium in pilot filters remained active when chemicals were dosed, i.e. ammonium removal efficiency was not disturbed due to the dosing of MnO_4 or Fe based coagulants. These results are in agreement with the pilot investigations at WTP Katwijk (chapter 5) and WTP Dorst (chapter 4), and in general agreement with (Ahmad et al. 2018).

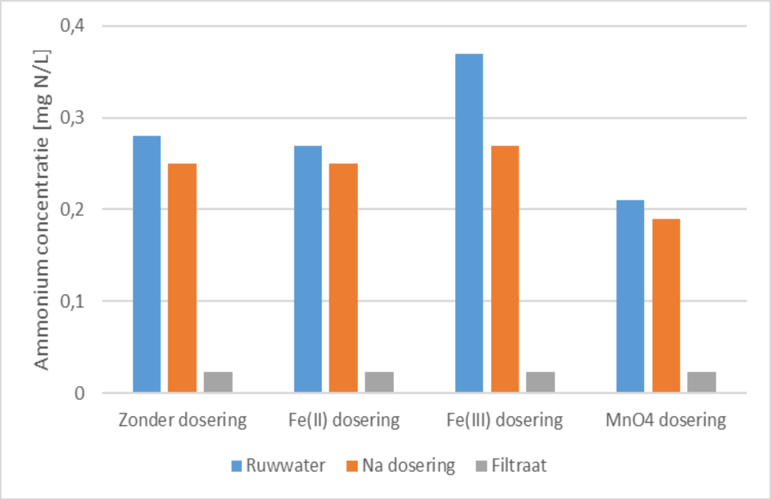

Fig 9. Effect of chemical dosing on ammonium removal in filters.

6.3.5 Results biostability

To investigate the impact of chemical dosing on the biological stability, several BPC-14 measurements were performed (Figure 10). The column effluent contained approximately 100 ng ATP/L, except for the experiment where MnO_4 and $FeCl_3$ were dosed. Possibly, this observation can be put in perspective together with the strange results described earlier (dissolution of Fe and release of As deeper into the filter bed). All in all, no significant differences in BPC-14 value was observed for columns fed with- and without chemicals-added feed water. Thus, it can be concluded that no changes in bio stability can be expected by application of MnO_4 and Fe based coagulant dosing.

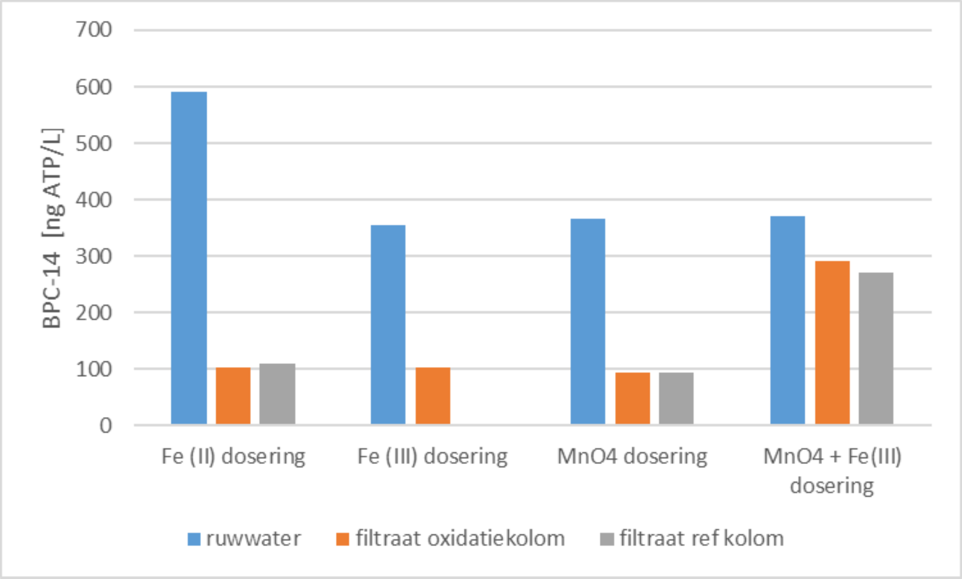

Fig 10. BPC-14 in raw water and column effluent during different experiments.

6.4 Conclusions and recommendations

Although achieving and maintaining accurate dosing of chemicals (MnO_4, Fe(II), Fe(III)) during pilot experiments remained an issue in this pilot study, it was concluded that As reduction to <1 µg/L with individual dosing of MnO_4, Fe(II) or Fe(III) is not feasible for WTP Ouddorp. Dosing a combination of MnO_4 and Fe(III) in the influent of rapid sand filters can be an effective method to reduce As concentration to <1 µg/L, however further research is proposed using virgin filter media. In this study, we observed As reduction to <1 µg/L in the supernatant of the pilot filter. However, release of As in the filter bed from the filter media (obtained from a full scale filter of WTP Ouddorp) hindered consistent As reduction to <1 µg/L in the filter effluent. Thus, further research is recommended with virgin filter media to investigate the feasibility of MnO_4-Fe(III) dosing for WTP Ouddorp.

We also conclude that dosing of Fe(II), Fe(III) and MnO_4 does not threaten ammonium removal in rapid sand filters. Moreover, the biological stability of produced water did not seem to be affected by chemical dosing in any of our pilot experiments.

7 Modelling arsenic removal by coprecipitation with Fe(III)(oxyhydr)oxides

This chapter is authored by Martin Korevaar (KWR). An excel based tool is delivered to the project partners along with this chapter.

7.1 Introduction

The aim of this study is to develop a model that describes co-precipitation of As(III) and As(V) with Fe(III)(oxyhydr)oxides in different water quality conditions. The redox environments are controlled by oxygen (O2) or permanganate (MnO_4). The model's accuracy is assessed by comparing it to the experiments described in chapter 2.

7.2 Model description

The model consists of two parts, (i) oxidation of Fe(II) to Fe(III) and precipitation of Fe(III)(oxyhydr)oxides and (ii) adsorption of arsenic to Fe(III)(oxyhydr)oxides. The oxidation kinetics of Fe(II) is modelled with the classic relation proposed by (Stumm & Lee, 1961) that accounts for its dependence on pH:

$$\frac{d}{dt}[Fe^{2+}] = -k\frac{[Fe^{2+}][O_2]}{[H^+]^2} \tag{1}$$

with $k = 2.2 \cdot 10^{-15}\left[\frac{\mathrm{mol}}{\mathrm{s}}\right]$ the oxidation constant. It is assumed that the hydrolysis and precipitation is much faster than the oxidation. Therefore, it is modelled as an instantaneous process, i.e. all formed Fe(III)(oxyhydr)oxides exist as ferrihydrite. To further simplify the model, the formed ferrihydrite is assumed to be pure in the sense that no foreign ions are present in its structure. Foreign ions are only allowed to adsorb to the outer surface of the precipitate that is available to the bulk fluid.

Adsorption can be modelled in different ways. A classic approach is to use the adsorption isotherms that describe the relation between the loading of a certain ion on a solid as a function of the concentration of the ion in the solution, while all other parameters remain constant (*ceteris paribus*). Well-known examples are the Freundlich and Langmuir isotherm models. The major drawback of this approach is that in practice, not all parameters remain constant during adsorption. As soon as a parameter changes, a new isotherm needs to be derived which becomes a time-consuming exercise. Moreover, it is not possible to use the same isotherm to model a system that changes pH as happens e.g. during iron oxidation. Therefore, we chose to use a more robust model that is applicable for a wide range of water quality parameters like pH, but also for a range of ionic concentrations. This is possible with the so-called surface complexation models. Another strength of these models is their ability to describe competition between different species that try to adsorb on the limited number of adsorption sites. E.g. the competition between the adsorption of PO_4^-, As(III) and As(V) on ferrihydrite (Antelo, Arce, & Fiol, 2015).

There exist different surface complexation models but they all share the same basic principles. When looking at the surface of an iron oxide from a chemical point of view, it consist of Fe-OH groups with different levels of protonation.

For each level of protonation one can derive an equilibrium equation, equivalent to the law of mass action of aqueous species:

$$Fh - OH_2^+ \overset{K_1}{\Leftrightarrow} Fh - OH + H^+ \tag{2}$$

$$Fh - OH \overset{K_2}{\Leftrightarrow} Fh - O^- + H^+ \tag{3}$$

where Fh is a ferrihydrite sorption site; and equilibrium constants K_1 and K_2 determine the ratio between the concentrations on the left and right hand side of the equations. Consequently, the combination of the H^+ concentration, the Fh concentration and the values of K_1 and K_2 determines how much of the sites have two, one or no proton chemically bound to it. This means that these type of models inherently describe pH dependence of the sorption capacity. To model the adsorption of arsenic one needs to determine its surface species and their accompanying K-values. For example for As(III) this looks like:

$$Fh - H_2AsO_4 + H_2O \overset{K_{As,1}}{\Longleftrightarrow} Fh - OH + AsO_4^{3-} + 3H^+ \tag{4}$$

$$Fh - HAsO_4^- + H_2O \overset{K_{As,2}}{\Longleftrightarrow} Fh - OH + AsO_4^{3-} + 2H^+ \tag{5}$$

$$Fh - AsO_4^{2-} + H_2O \overset{K_{As,3}}{\Longleftrightarrow} Fh - OH + AsO_4^{3-} + H^+ \tag{6}$$

Here the surface species refer to the ions sorbed to the Fh sorption site, that is, the AsO_4^- ion with different levels of protonation. Equations (2) and Equation (3) determine how the different species are distributed over the different sorption sites; that depends on the values of $K_{As,1}$, $K_{As,2}$ and $K_{As,3}$ in combination with the concentration of H^+, As, and Fh. However, also the equilibria of the protonation of Fh should hold (Equations (2)-(3)). So to determine which surface species will occur at which concentration, one need to take into those Equations as well. This effectively models the competition between H^+ and $HAsO_4$ for sorption sites. By adding such equilibrium equations for all other relevant species as well (e,g, PO_4^- and H_3AsO_3) one can model their competitive adsorption as well. Note that on top of this, one need to *simultaneously* determine the speciation of aqueous species as well.

Another important feature of surface complexation models is their ability to determine the surface charge of the precipitates. This is clearly seen from the above equations (Equation (2) and (3)) as the different order of protonation yield negative, neutral and positive charged surface sites respectively; this determines the surface charge. Furthermore, the surface charge itself influences the affinity of adsorbed ions; ions which charge has opposite polarity compared to the surface, bind stronger to the surface sites than ions with neutral or opposite sign (given that their K-values are the same). By knowing the surface charge, it is also possible to model a different type of adsorption, that is, pure electrostatic adsorption. E.g. when a surface is positively charged due to its positively charged surface species (as explained above) negatively charged ions in the solution are attracted to the surface. They do not form a chemical bond, but should be considered intimately related to the surface. This is often referred to as a type of physical sorption and is illustrated in Figure 1 where the surface is positively charged due to positively charged surface species.

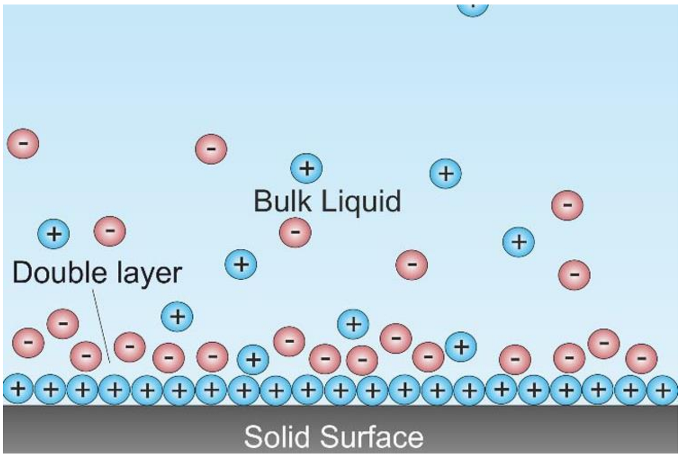

Figure 2- illustration of physical adsorption. The blue ions adsorb chemically to the surface with covalent bonds. Due to the electrostatic interactions, negatively charged ions are attracted to this surface and their abundance near the surface is higher than the positively charged ions. As a matter of fact, they cannot easily be removed from the surface and can therefore considered being adsorbed. Because the layer near the surface consists of a layer of positive charged ions and a layer of negatively charged ions this is often referred to as electric double layer.

Above description of surface complexation models applies to several models. The diffuse double layer (Dzombak, David A. and Morel, 1990) also known as the Dzombak and Morel model has been developed first and has been widely applied. Major advantage of this model is the availability of the surface species and association constants of many ions for different iron(hydrox)oxides, mainly ferrihydrite and goethite. Furthermore, it is implemented in popular programs like Minteq and PHREEQC which make them readily available. Later more refined models have been developed, like CD-MUSIC (Antelo et al., 2010; Hiemstra & Van Riemsdijk, 2009) and the triple layer model (Hayes, 1987). In this study we chose to use the diffuse double layer (DDL) model because of the availability of the surface speciation parameters of a wide range of species and because it is already implemented in PHREEQC software. PHREEQC is used for all the calculations.

The DDL model assumes there are two types of binding sites on the surface, strong and weak binding sites. While developing the model, however, there was not a theoretical basis for it. But using the different sites allowed for better fits. Later, support for different types of binding sites have been found; ions can bind to one surface (mono-dentate complexes) or two or even three binding sites (bi- or tridentate complexes). Despite the weak basis for the use of two type of binding sites, the model has been applied successfully widely in literature. As explained above, the input variable for this model are the equilibrium equations for all surface species and their equilibrium constants; for the DDL-model this is required for both type of sites. Furthermore, the model requires the amount of sorption sites per surface area together with the total surface area per gram of the precipitated iron. Their values are in principle, a property of the iron(hydroxy)oxide but literature is not unambiguous about them; this is shown in Table 2 for ferrihydrite. In this work, we chose to model ferrihyrite with the widely applied value of 600 m^2/g for the specific surface and 2.37 and 0.06 sites/nm^2 for weak and strong sites respectively (Dzombak & Morel., 1990; Wallis, Prommer, Simmons, Post, & Stuyfzand, 2010).

Table 2- Overview of different values found for the specific surface area and site density of ferrihydrite.

Mineral	Specific surface [m^2/g]	Site Density [$sites/nm^2$]	Site type	Bron
Ferrihydrite	600	2.3721	weak site	(Appelo, Van Der Weiden, Tournassat, & Charlet, 2002)
Ferrihydrite	600	0.0610	strong site	(Appelo et al., 2002)
Ferrihydrite	244	2.2700	weak site	(Liger, Charlet, & Van Cappellen, 1999)
Ferrihydrite	0	0	strong site	(Liger et al., 1999)

PHREEQC comes with an extensive database with parameters that describe aqueous and surface speciation of many ions (Fe, Mn, As, P and many more) on ferrihydrite. However, new research continuously suggests improved values. Therefore, we have used the wateq4f.dat database from PHREEQC, improved with following literature insights. Arsenic adsorption constants and reactions are modified according to the average values presented in (Gustafsson & Bhattacharya, 2007). The equilibrium equations and constants of aqueous As-species are also set equal to those used by Gustafsson & Bhattacharya, 2007 to maintain consistency of the database. The adsorption of H_4SiO_4 and CO_3 is modelled with the surface species and equilibrium constants proposed in (Stollenwerk et al., 2007) and (Appelo et al. , 2002) respectively.

7.3 Experimental and simulation set-up

The simulation results are compared with experiments to assess its accuracy. The experiments are described in detail in chapter 2. Here only a brief description of these batch experiments is given. The solutions as indicated in Table 3 are prepared in the reaction vessel under anaerobic conditions. The reactor is stirred with a rotor stirrer and will be stirred during the whole experiment. Then the oxidant is added (either O_2 or MnO_4). After 30 minutes oxidation, precipitation (growth) and adsorption is assumed to be completed. Filtered samples (0.45 µm) are taken to determine concentrations of As, Fe, Mn, and P remaining in the solution. The pH is kept constant at pH=7.5 during the whole experiment.

To compare simulation results to these experiments, the following approach is taken. Fe(II) is allowed to oxidize by oxygen according to Equation (1), Mn(II) and As(III) oxidation by oxygen is assumed negligible in the residence time of one hour. Oxidation of As(III), Fe(II) and Mn(II) by MnO_4 is assumed to be instantaneously. The pH is kept constant and the system is modelled as a batch reactor.

The experimental values are only measured at the beginning of the experiment and after 30 minutes. It is assumed that the system is in equilibrium for those cases, but it is necessary to check with the model whether this is true. Because if this is true, the values at the end of simulation and experiments can safely be compared and differences between model and experiments cannot be attributed by not reaching equilibrium. This only needs to be checked for the cases where O_2 is used as oxidant, because oxidation by MnO_4 is assumed to be instantaneous.

Simulations of iron oxidation by oxygen will reach an equilibrium where all Fe(II) is oxidized to Fe(III) because of the surplus of oxygen. It should be noted that this result will be exactly the same as simulation where Fe(III) is dosed instead of dosing Fe(II). This is caused by the modelling assumptions that the precipitate is homogeneous during precipitate growth and its type constant. Furthermore, during the precipitate growth, adsorption is only allowed at the surface of the crystal available to the bulk solution.

Table 3 - Overview of concentrations of all simulated water matrices. The headers correspond to the labels in the figures.

	unit	Ref	90 Fe + 0.7 As	90 Fe + 0.7 As + 9.0 Mn (Ref)	90 Fe + 0.7 As + 18 Mn	180 Si	350 Si	700 Si	4 P	10 P	16 P	350 Si + 500 Ca	700 Si + 1000 Ca	700 Si + 2500 Ca	16 P + 1000 Ca
HCO3	mg/L	150	150	150	150	150	150	150	150	150	150	150	150	150	150
NaCl	mg/L	30	30	30	30	30	30	30	30	30	30	30	30	30	30
Fe(II)	mg/L	5	5	5	5	5	5	5	5	5	5	5	5	5	5
As(III)	ug/L	0	50	50	50	50	50	50	50	50	50	50	50	50	50
pH		7.5	7.5	7.5	7.5	7.5	7.5	7.5	7.5	7.5	7.5	7.5	7.5	7.5	7.5
Mn(II)	mg/L	0	0	0.5	1	0.5	0.5	0.5	0.5	0.5	0.5	0.5	0.5	0.5	0.5
Si	mg/L	0	0	0	0	5	10	20	0	0	0	10	20	20	0
P	mg/L	0	0	0	0	0	0	0	0.1	0.3	0.5	0	0	0	0.5
Ca	mg/L	0	0	0	0	0	0	0	0	0	0	20	40	100	40
DOC	mg/L	0	0	0	0	0	0	0	0	0	0	0	0	0	0

7.4 Results and discussion

In Figure 2 the oxidation of iron and adsorption of arsenate is shown as function of time. It shows that they are both completed within 20 minutes. So hereafter, only the results are shown where all oxidation is finished and the system is in equilibrium. First the results for the system of oxidation by oxygen are presented, then those by $KMnO_4$.

7.4.1 Oxidation with oxygen

The iron removal is shown for different water matrices in Figure 3 for both the experiments and simulations. They both show nearly complete removal for all cases, except for the cases containing only Si. In those cases, the experiments show a sharp decline in iron removal, while the simulation show no difference compared to other cases. This discrepancy can partly be attributed to the fact that simulations and experiments are not referring to exactly the same 'iron removal'. For experiments, iron removal refers to all iron that remains on a 0.45 µm filter after filtration. While for the simulations, iron removal refers to all iron that has precipitated. Not all iron that has precipitated, necessarily grows to particles larger than 0.45 µm. This amount of growth is, amongst others, related to the charge on the surface of the particles. Particles with equal polarity repel each other and are less likely to form larger aggregates. The charge on the surface is determined by the amount and charge of the sorbed species. It is possible to determine this surface charge with the model which is shown in Figure 4 for all water matrices. Indeed, it demonstrates increasingly negative surface charge with increasing Si-concentration (with and without Ca). Also, with increasing P concentration the surface charge becomes more negative with similar order of magnitude. However, the removal of iron is hardly reduced by even the highest P-concentration; the modelled surface charge does not relate to iron removal. It is possible that the surface charge of ferrihydrite in the P-containing water matrices is overestimated by the model. One explanation may be that phosphate is incorporated in the precipitates itself instead of on its surface, as described in literature. In that case, phosphate in the precipitate does not contribute to the surface charge and consequently leads to a less negative surface charge compared to the case where it bind to the surface. This is indeed reported in literature. There is also no relation found between surface charge and iron removal in waters that contain both Ca and Si. This may partly be explained by the lack of incorporation of so-called ternary Ca-complexes in the model. These are complexes of ferrihydrite-group that binds to some anion like P or As on which Ca-ions can bind; this obviously reduces the surface charge. Furthermore, Ca-ions will reside in the diffuse double layer instead of Na which has influence on the behaviour of the colloid as a whole and thus its filterability. All in all, the modelled surface charge has only limited applicability to predict iron removal.

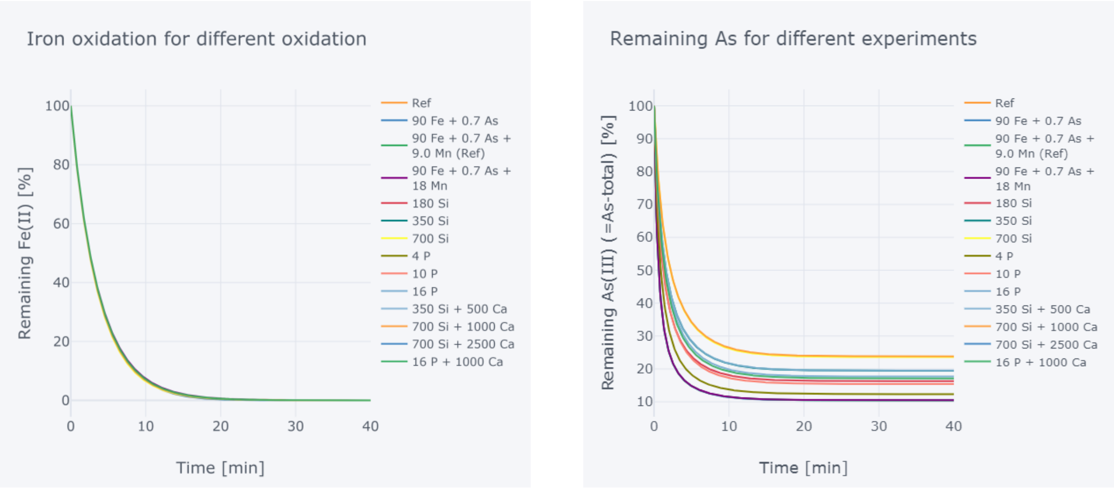

Figure 3 – the remaining relative iron and arsenic concentration as function of time for iron oxidation with oxygen. The different lines indicate the results for the water qualities depicted in Table 3. Note that lines in the left and right figure are obscured by the lines on top of them because simulation have the same results.

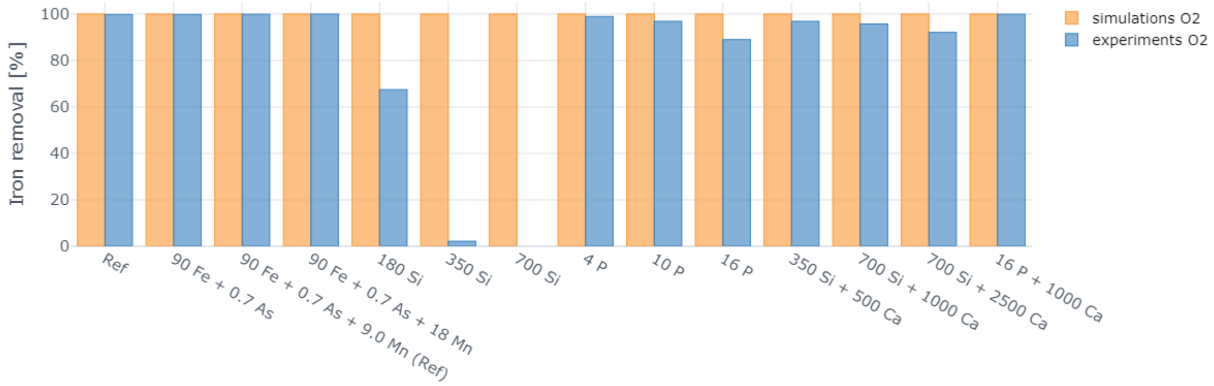

Figure 4 – Iron removal for different water matrices according to simulations and experiments; O₂ is used as oxidant.

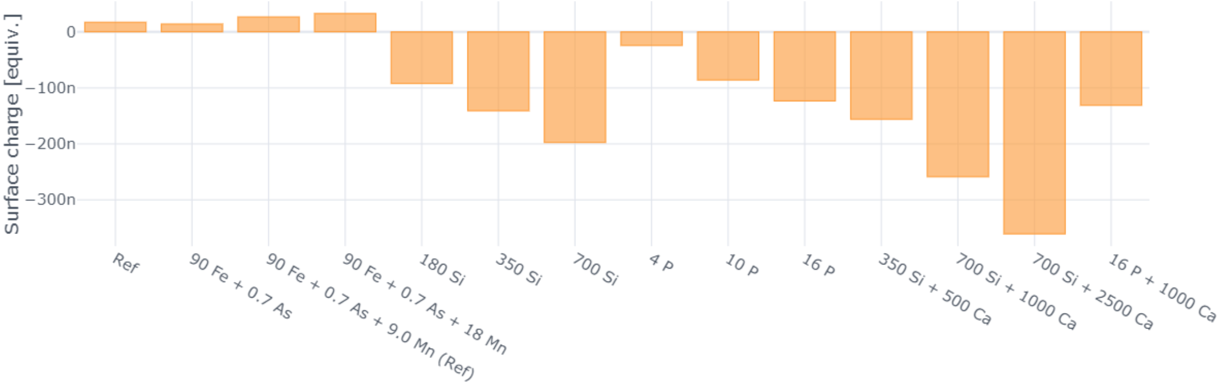

Figure 5 – Surface charge on the ferrihydrite surface in different water matrices. The surface charge is given in equivalent charge.

An important performance indicator is the amount of arsenic (or phosphate) removed per unit of removed iron. These are shown respectively in Figure 6 and Figure 7. For arsenic, most trends are predicted correctly: the loading is insensitive to low Mn-concentration, decreases with phosphate concentration and calcium concentration. It misses a decrease in loading with the highest Mn-concentration. Furthermore, it predicts a decrease in loading with Si, while the experiments show an increase. The latter can be explained by the fact that iron removal for that case was also modelled inaccurately. The magnitude shows an over-prediction of 40% to 80%, which is reasonable given the fact that no parameters are fitted to the experiments. As shown in Table 3, literature shows a wide range of specific surface and site density of ferrihydrite. Decreasing the loading can be achieved by decreasing the specific surface this is indeed allowed given the values in Table 3.

The trends of phosphate loading with different water qualities is predicted correctly: with increasing phosphate concentrations, the loading increases and is insensitive to addition of calcium. However, the loading is under-predicted by 60% for the higher phosphate concentrations, while for the lowest concentration it under-predicts only 30%. Hence, it deviates more with higher phosphate concentrations. An explanation for this might be that incorporation of phosphate in ferrihydrite during crystal growth is significant, while this mechanism is neglected in this model. Another reason may be incorrect values for the specific surface and sites density; higher site density and/or specific surface yields higher loading. However, based on the results of arsenic loading discussed above, site density and/or specific surface may be too high. Consequently, it is more likely that neglecting phosphate incorporation in the ferrihydrite crystal is the cause of the discrepancy between model and experiments. Also, this is in line with the discussion of the surface charge above.

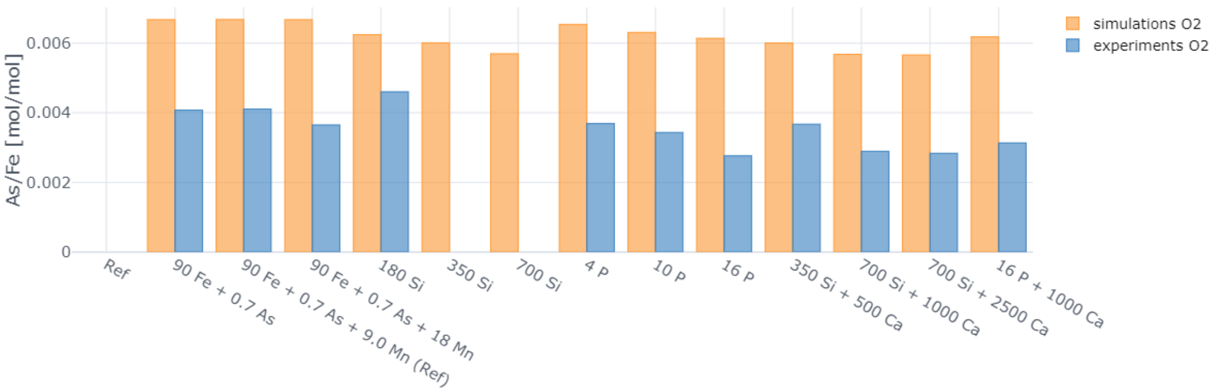

Figure 6 - Arsenic loading on iron precipitates according to model and experiments, for different water matrices.O_2 is used as oxidant

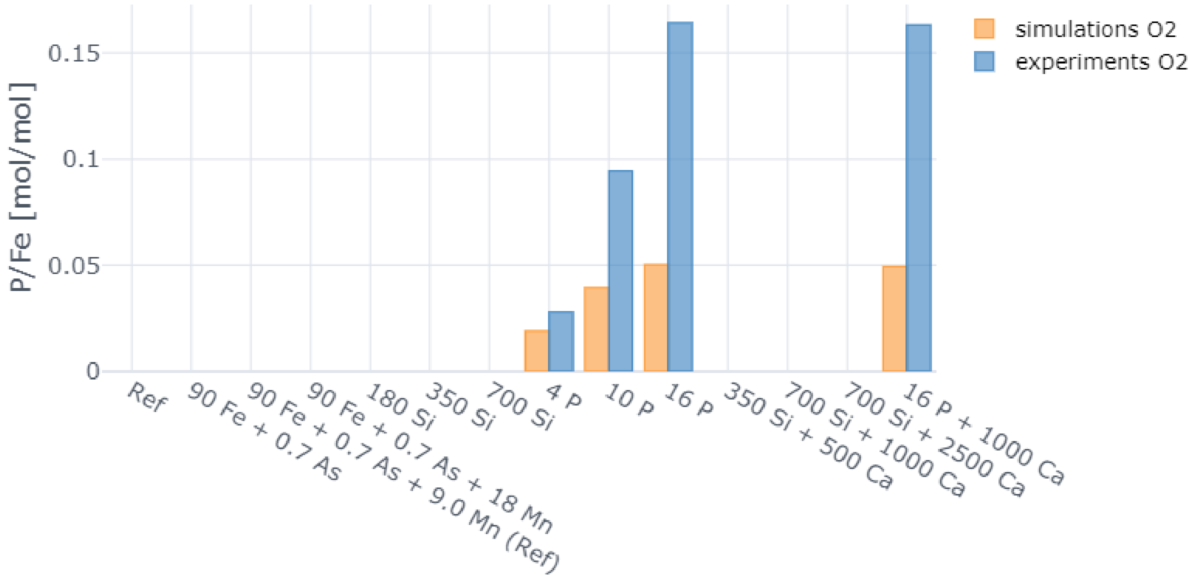

Figure 7- Phosphorous loading on iron precipitates according to model and experiments, for different water matrices.O_2 is used as oxidant

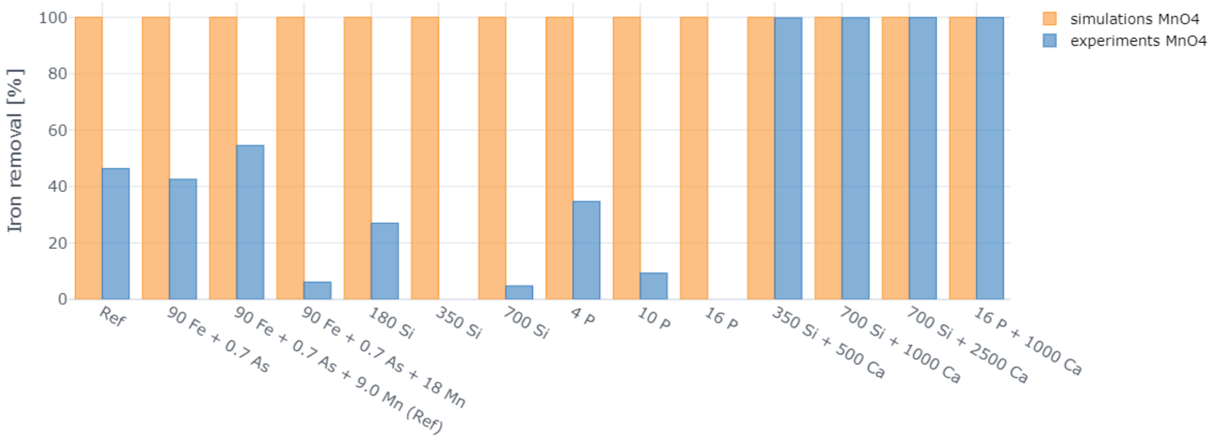

Figure 7- Iron removal according to model and experiments, for different water matrices.KMnO$_4$ is used as oxidant.

7.4.2 **Permanganate as oxidant**

In the preceding section oxygen was used as oxidant and therefore Mn(II) and As(III) remained in their redox state while Fe(II) was oxidized to Fe(III). In this section, permanganate is used as oxidant. This is a strong oxidant, so Mn(II), As(III) and Fe(II) are allowed to oxidize. As expected, simulation predicts 100% iron removal because all iron is oxidized and precipitated and it is assumed all precipitated iron is removed (Figure Figure 2). On the other hand, it has major implications for the experiments. Iron removal becomes much worse compared to oxidation by oxygen; only calcium containing solutions show 100% iron removal. This cannot be predicted from the surface charge on ferrihydrite, because it virtually stays the same (not shown). Most likely, it is caused by the manganese oxide precipitates that are formed from the reduction of KMnO$_4$. These are highly negatively charged, stable colloids that will hardly agglomerate. Possibly, they stabilize ferrihydrite-like particles which makes them less filterable as well (Ahmad et al., 2019). This mechanism is not accounted for in the model and the modelling framework of PHREEQC does not allow for modelling of agglomeration of different precipitates.

On the other hand, the prediction accuracy of arsenic and phosphate loading is similar compared to the oxygen case. Accuracy of absolute values for arsenic are 20% and lower; this is more accurate compared to the oxygen system. This may indicate that the specific surface and site density are more suited for the ferrihydrite formed by oxidation with MnO$_4$ compared to oxidation by O$_2$. This is in line with the observation that MnO$_4$ yields more disordered crystals (Ahmad et al., 2019) as this is associated with higher specific surface. However, please note that here As(V) is sorbed to the surface, while in the O$_2$ case, As(III) is sorbed. However, trends of arsenic loading are most of the time not correct with changing water quality; an increase or decrease of loading in the experiments does not translate to the same increase/decrease in the simulations. This again, is most likely caused by the different type of precipitates that are formed by permanganate oxidation. There are not sufficient experiments for phosphate to draw any conclusions in this respect.

Phosphate loading is underestimated up to 75%, which is slightly worse than for O$_2$ system. Just as with the oxygen case, this may be caused by neglecting incorporation of phosphate during crystal growth in the model. Another possibility is that the site density and specific surface are too high, but this is not likely considering predictions of the arsenic loading.

It is interestingly that the predictions for arsenic loading in both MnO_4 and O_2 system are in absolute sense quite accurate without fitting any parameters. This is not the case for PO_4. If above reasoning is correct, this indicates that the removal of phosphate is much more dominated by incorporation in the crystal structure compared to arsenic, which can be modelled by sorption on the surface of the final formed ferrihydrite. This indicates that first P is removed and that arsenic is only removed when precipitate growth has finished. This can either be caused by a kinetically favourable adsorption of P compared to As, or because P is much more abundant than As and therefore initially displaces As.

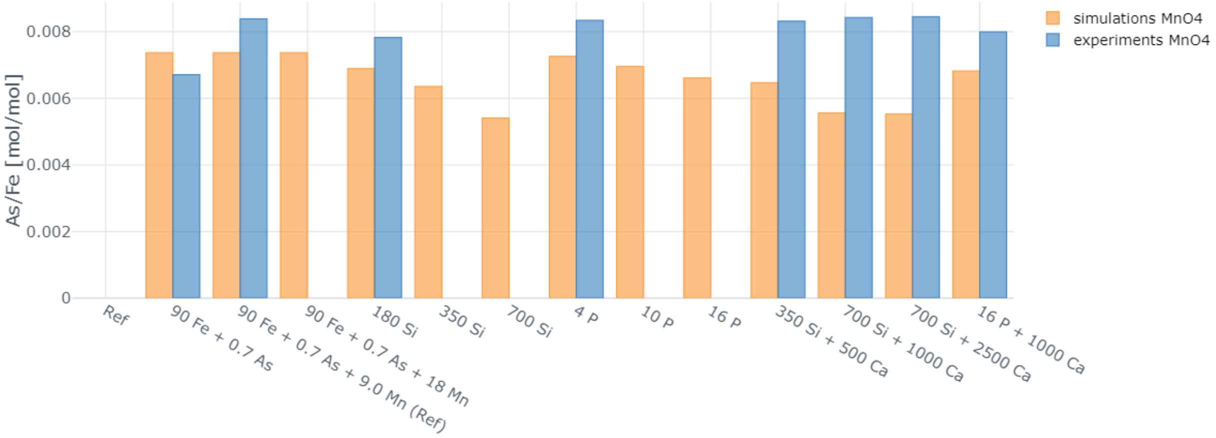

Figure 8 – arsenic loading on iron precipitates according to model and experiments, for different water matrices.$KMnO_4$ is used as oxidant.

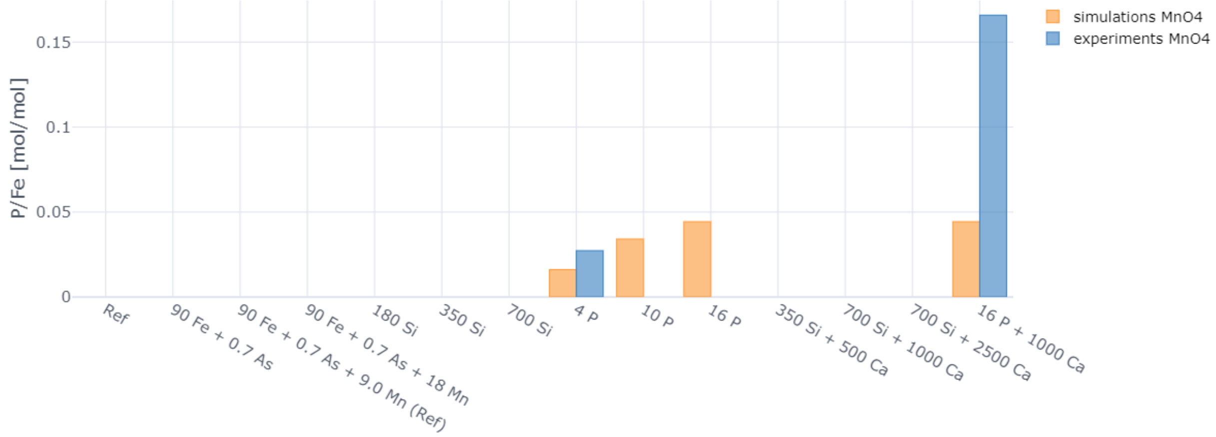

Figure 9 – Phosphorous loading on iron precipitates according to model and experiments, for different water matrices.$KMnO_4$ is used as oxidant.

7.5 Conclusion

In this work it is demonstrated that it is possible to model arsenic removal with a system in which iron precipitates after oxidation by either oxygen or permanganate. The trend of arsenic and phosphate loading with different water matrices is correctly predicted for O_2 as oxidant, but not so much for MnO_4^-. The order of magnitude of the modelled arsenic loading is 40% to 80% too high for the oxygen system while it was 10% to 30% accurate for the permanganate system. The loading of phosphate was underpredicted for the oxygen system (30% to 60%) and permanganate system

(50% to 75%).It is likely that neglecting the incorporation of phosphate in the precipitate by the model is the reason for the deviation for the phosphate loading, while the arsenic loading is caused by incorrect settings of the site density and/or specific surface of ferrihydrite.

To be able to translate the loading of arsenic and phosphate to their removal, the removal of iron needs to be determined as well. It is shown that for the oxygen system it is possible to determine iron removal based on the amount of precipitated iron, except for the silica containing solutions (without calcium). Apparently, for those solutions, precipitates are smaller than the filter pores of 0.45 µm. When precipitates maintain this small and apparently do not aggregate they are often referred as stable colloids; stable colloids are associated with high surface charge. But it is shown here that the surface charge as calculated by the model has little relation to the filterability. This holds even more for the permanganate system.

References

Ahmad, A., Rutten, S., Eikelboom, M., de Waal, L., Bruning, H., Bhattacharya, P., & van der Wal, A. (2020). Impact of phosphate, silicate and natural organic matter on the size of Fe(III) precipitates and arsenate co-precipitation efficiency in calcium containing water. *Separation and Purification Technology*, *235*, 116117. https://doi.org/10.1016/j.seppur.2019.116117

Ahmad, A., van der Wal, A., Bhattacharya, P., & van Genuchten, C. M. (2019). Characteristics of Fe and Mn bearing precipitates generated by Fe(II) and Mn(II) co-oxidation with O2, MnO4 and HOCl in the presence of groundwater ions. *Water Research*, *161*, 505–516. https://doi.org/10.1016/j.watres.2019.06.036

Antelo, J., Arce, F., & Fiol, S. (2015). Arsenate and phosphate adsorption on ferrihydrite nanoparticles. Synergetic interaction with calcium ions. *Chemical Geology*, *410*, 53–62. https://doi.org/10.1016/j.chemgeo.2015.06.011

Antelo, J., Fiol, S., Pérez, C., Mariño, S., Arce, F., Gondar, D., & López, R. (2010). Analysis of phosphate adsorption onto ferrihydrite using the CD-MUSIC model. *Journal of Colloid and Interface Science*, *347*(1), 112–119. https://doi.org/10.1016/j.jcis.2010.03.020

Appelo, C. A. J., Van Der Weiden, M. J. J., Tournassat, C., & Charlet, L. (2002). Surface complexation of ferrous iron and carbonate on ferrihydrite and the mobilization of arsenic. *Environmental Science and Technology*, *36*(14), 3096–3103. https://doi.org/10.1021/es010130n

Dzombak, David A. and Morel, F. M. (1990). *Surface complexation modeling: hydrous ferric oxide*. John Wiley & Sons.

Dzombak, D. A., & Morel., F. M. (1990). *Surface complexation modeling: hydrous ferric oxide*. https://doi.org/10.1016/B978-0-12-409548-9.05311-2

Hayes, K. F. (1987). Equilibrium, spectroscopic, and kinetic studies of ion adsorption at the oxide-aqueous interface. *Ph. D., Stanford University*.

Hiemstra, T., & Van Riemsdijk, W. H. (2009). A surface structural model for ferrihydrite I: Sites related to primary charge, molar mass, and mass density. *Geochimica et Cosmochimica Acta*, *73*(15), 4423–4436. https://doi.org/10.1016/j.gca.2009.04.032

Jobin, R., & Ghosh, M. M. (1972). Effect of Buffer Intensity and Organic-Matter on Oxygenation of Ferrous Iron (Vol. 64).

Liger, E., Charlet, L., & Van Cappellen, P. (1999). Surface catalysis of uranium(VI) reduction by iron(II). *Geochimica et Cosmochimica Acta*, *63*(19–20), 2939–2955. https://doi.org/10.1016/S0016-7037(99)00265-3

Senn, A. C., Kaegi, R., Hug, S. J., Hering, J. G., Mangold, S., & Voegelin, A. (2015). Composition and structure of Fe(III)-precipitates formed by Fe(II) oxidation in water at near-neutral pH: Interdependent effects of phosphate, silicate and Ca. *Geochimica et Cosmochimica Acta*, *162*, 220–246. https://doi.org/10.1016/j.gca.2015.04.032

Stumm, W., & Lee, G. F. (1961). Oxygenation of Ferrous Iron. *Industrial & Engineering Chemistry*, *53*(2), 143–146. https://doi.org/10.1021/ie50614a030

Wallis, I., Prommer, H., Simmons, C. T., Post, V., & Stuyfzand, P. J. (2010). Evaluation of conceptual and numerical models for arsenic mobilization and attenuation during managed aquifer recharge (Vol. 44). https://doi.org/10.1021/es100463q

8 Conclusions and future work

Arsenic (As) is highly toxic element and its chronic ingestion is associated with several types of cancer and other detrimental effects on human health. Recent studies show that As can be toxic to human health even at concentrations lower than the WHO guideline (10 µg/L). Therefore, water companies in the Netherlands aim to reduce As to <1 µg/L in drinking water. Advanced Oxidation – Coprecipitation – Filtration (AOCF) is a promising method to remove As from water, however systematic studies providing detailed understanding of the arsenic-iron interactions in complex multi-solute solutions has been lacking. Moreover, the implications of dosing MnO_4 and Fe based coagulant at existing water treatment plants (WTPs) has not been addressed in previous studies. Consequently, the overarching objective of this study was to investigate As reduction to <1 µg/L by AOCF under different ionic compositions of water and filtration conditions, as well as to gain mechanistic understanding of the process details to guide full scale implementation. In the following sections we summarize the main conclusions of this study and highlight direction for future work.

8.1 Impact of oxidant type on Fe and Mn precipitate characteristics

Oxygen (O_2) is capable of oxidizing Fe(II) on the time scale of typical groundwater treatment (e.g. 30 min), however O_2 alone is ineffective at oxidizing As(III) to As(V) and Mn(II) to Mn(III,IV) (Diem and Stumm 1984, Gude et al. 2016, Van Beek et al. 2012). Chemical oxidants such as $KMnO_4$ and NaOCl can improve co-oxidative removal of Fe(II), Mn(II) and As(III) at WTPs, however little was known about how different oxidants impact key properties of the precipitates, including the structure, composition and crystallinity. In an extensive laboratory study, we combined macroscopic measurements of precipitate aggregation and chemical composition with X-ray absorption spectroscopy to investigate the solids formed by co-oxidation of Fe(II) and Mn(II) with O_2, $KMnO_4$, and NaOCl in the presence of groundwater ions at near-neutral pH. We found that in the absence of phosphate (P), silicate (Si) and calcium (Ca), O_2 and HOCl produced suspensions that aggregated rapidly, whereas co-oxidation of Fe(II) and Mn(II) by MnO_4 generated colloidally stable suspensions. The aggregation tendency of all the suspensions decreased in P and Si bearing solutions, but the presence of Ca counteracted these oxyanion effects, i.e. improved aggregation of the precipitates. The speciation of oxidized Fe and Mn in the absence of P and Si also depended on the type of oxidant, with O_2 producing Mn(III)-incorporated lepidocrocite, HOCl producing Mn(III)-incorporated hydrous ferric oxide (HFO) and MnO_4 producing poorly-ordered MnO_2 and HFO as separate phases. In general, the presence of P and Si in solution decreased the crystallinity of the Fe(III) phase and increased the Mn/Fe solids ratio, which was found by Mn K-edge XAS analysis to be due to an increase in surface-bound Mn(II). In contrast, Ca decreased the Mn/Fe solids ratio and decreased the fraction of Mn(II) associated with the solids, suggesting that Ca and Mn(II) compete for adsorption sites.

Based on these results, we conclude that the composition of water and the identity of the oxidant strongly determines the macroscopic and molecular-scale characteristics of Fe and Mn bearing precipitates generated by Fe(II) and Mn(II) co-oxidation. Future work on molecular scale structural analysis of Fe and Mn precipitates should also include other strong oxidants such as H_2O_2 and O_3, as well aa the influence of a broad spectrum of ions in water including bicarbonate, sulphate, nitrate etc.

8.2 Impact of water composition on the size of Fe(III) precipitates and arsenic uptake efficiency

A laboratory study was performed to gain more understanding of the independent and combined effects of Si, P, natural organic matter (NOM) and Ca on As(V) co-precipitation efficiency and the size of Fe(III) precipitates formed by the hydrolysis of $FeCl_3$ at near-neutral pH. We found that, in complex solutions, containing multiple solutes and high levels of Ca, Si and P presence in typical groundwater concentrations reduce As(V) removal slightly, mainly due to a decreased adsorption of As(V) onto Fe(III) precipitates. On the other hand, NOM concentrations reduced As(V) removal to a much greater extent, due to possible formation of mobile Fe(III)–NOM complexes that were difficult to remove by 0.45 µm disc filtration.

These findings indicate that at WTPs the effectiveness of As removal not only depends on As adsorption to Fe(III)(oxyhydr)oxide precipitates, but also on the separation of As bearing Fe(III) precipitates from water. Calcium effectively counteracts the negative effect of oxyanions and promotes the growth of Fe(III) precipitates, which can be easily separated from water by gravitation settling and rapid sand filtration. Thus, hardness of water should be carefully considered in designing As removal processes that rely on the co-precipitation of As and Fe.

Obviously, effective separation of the colloidal particles can also be achieved by employing low-pressure membrane filtration (MF/UF) instead of the conventional rapid sand filtration for effective separation of the colloidal particles. Nevertheless, also in this case, the charge and size distribution of Fe(III) precipitates will remain crucial in determining the membrane fouling mechanisms.

8.3 Arsenic removal pilot investigations

Pilot investigations to assess the feasibility of AOCF concept were carried out at WTPs Dorst (Brabant Water), Katwijk (Dunea) and Ouddorp (Evides). During the investigations, experiments were carried out to study the impact of individual and combined dosing of treatment chemicals ($NaMnO_4$, $FeCl_3$, $FeSO_4$) on As removal, as well the removal of Fe, Mn and NH_4^+ in rapid sand filters. Moreover, process parameters such as filter run time and settling characteristics of backwash water were also studied. Following major conclusions can be drawn based on the pilot investigations.

- MnO_4–Fe(III) dosing in the influent of rapid sand filters is an effective technique to improve As removal in rapid sand filters. The optimum dosages of MnO_4 and Fe(III) were found to be dependent on the concentration of As(III) in water and ionic composition of the water matrix. In general, raw water with a higher concentration of reduced Fe(II), Mn(II) and As(III) required a higher dose of MnO_4. The raw water with a higher concentration of oxyanions and NOM required a higher dose of Fe(III).

- MnO_4–Fe(III) dosing in rapid sand filters did not show any negative effect on NH_4^+ and Mn removal in rapid sand filters

- The dosing of MnO_4—Fe(III) improved the settling rate of backwash solids. Thus, the implementation of MnO_4–Fe(III) dosing at WTPs is expected to have benefits for backwash water treatment, i.e. reduction in settling time in sedimentation basins.

- General filtration performance can be enhanced with MnO_4–Fe(III) dosing in pilot column. At WTP Katwijk we observed that the turbidity of the filter effluent was reduced from 0.3 FTU to about 0.03 FTU.

- The runtime of the pilot filters was decreased significantly due to the MnO_4–Fe(III) dosing. This means that an adjustment in the design of rapid sand filters, e.g. by replacing filter media with another size fraction will be required for a sustainable operation of full-scale rapid sand filter

- Although achieving and maintaining accurate dosing of chemicals (MnO_4, Fe(II), Fe(III)) during pilot experiments remained an issue in this pilot study at WTP Ouddorp, it can be concluded that dosing a combination of MnO_4 and Fe(III) in the influent of rapid sand filters can be an effective method to reduce As concentration to <1 µg/L, however further research is proposed using virgin filter media because we observed a release of As in the filter bed from the filter media (obtained from a full scale filter of WTP Ouddorp) which hindered consistent As reduction to <1 µg/L in the filter effluent. Thus, further research at WTP Ouddorp is recommended with virgin filter media to investigate the feasibility of MnO_4-Fe(III) dosing for WTP Ouddorp.

8.4 Modelling arsenic removal

We have demonstrated that it is possible to model As removal with a system in which Fe precipitates after oxidation by either O_2 or MnO_4. The trend of As loading on Fe(III) precipitates with different water matrices is correctly predicted for both oxidants. However, the order of magnitudes are too far off to use it as accurate predictions of real life cases. Moreover, Fe filterability could not be predicted by this model.

References

Ahmad, A. (2017) Towards achieving <1 ug/L arsenic at Katwijk, Ouddorp and Leiduin: Baseline study and batch experiments with $KMnO_4$ and $FeCl_3$ to remove arsenic, p. 44.

Ahmad, A. and Bhattacharya, P. (2019) Arsenic in Drinking Water: Is 10 µg/L a Safe Limit? Current Pollution Reports.

Ahmad, A., Cornelissen, E., van de Wetering, S., van Dijk, T., van Genuchten, C., Bundschuh, J., van der Wal, A. and Bhattacharya, P. (2018) Arsenite removal in groundwater treatment plants by sequential Permanganate—Ferric treatment. Journal of Water Process Engineering 26, 221-229.

Ahmad, A., Kools, S., Schriks, M., Stuyfzand, P. and Hofs, B. (2015) Arsenic and chromium concentrations and their speciation in groundwater resources and drinking water supply in the Netherlands p. 78, KWR Water Cycle Research Institute, Nieuwegein, The Netherlands.

Ahmad, A., Van De Wetering, S., Groenendijk, M. and Bhattacharya, P. (2014) Advanced Oxidation-Coagulation-Filtration (AOCF) - An innovative treatment technology for targeting drinking water with <1 µg/L of arsenic, pp. 817-819.

Ahmad, A., van der Wal, B., Bhattacharya, P. and van Genuchten, C.M. (2019a) Characteristics of Fe and Mn bearing precipitates generated by Fe(II) and Mn(II) co-oxidation with O2, MnO4 and HOCl in the presence of groundwater ions. Water Research.

Ahmad, A., Van der Wens, P., Baken, K., De Waal, L., Bhattacharya, P. and Stuyfzand, P. (2019b) Arsenic reduction to <1 ug/L in Dutch drinking water. Environ Int.

Allard, S., Fouché, L., Dick, J., Heitz, A. and von Gunten, U. (2013) Oxidation of Manganese(II) during Chlorination: Role of Bromide.

Bhattacharya, P., Frisbie, S.H., Smith, E., Naidu, R., Jacks, G. and Sarkar, B. (2002) Handbook of Heavy Metals in the Environment. Sarkar, B. (ed), pp. 145-215, Taylor & Francis Inc., New York.

Bhattacharya, P., Welch, A.H., Stollenwerk, K.G., McLaughlin, M.J., Bundschuh, J. and Panaullah, G. (2007) Arsenic in the environment: Biology and Chemistry. Science of the Total Environment 379(2), 109-120.

Bissen, M. and Frimmel, F.H. (2003) Arsenic - A review. Part II: Oxidation of arsenic and its removal in water treatment. Acta hydrochimica et hydrobiologica 31(2), 97-107.

Borba, R.P., Figueiredo, B.R. and Matschullat, J. (2003) Geochemical distribution of arsenic in waters, sediments and weathered gold mineralized rocks from Iron Quadrangle, Brazil. Environmental Geology 44(1), 39-52.

Bordoloi, S., Nath, S.K., Gogoi, S. and Dutta, R.K. (2013) Arsenic and iron removal from groundwater by oxidation–coagulation at optimized pH: Laboratory and field studies. Journal of Hazardous Materials 260, 618-626.

Borho, M. and Wilderer, P. (1996) Optimized removal of arsenate(III) by adaptation of oxidation and precipitation processes to the filtration step. Water Science and Technology 34(9), 25-31.

Borsboom, M., Bras, W., Cerjak, I., Detollenaere, D., van Loon, D., Goedtkindt, P., Konijnenburg, M., Lassing, P., Levine, Y., Munneke, B., Oversluizen, M., van Tol, R. and Vlieg, E. (1998) The Dutch-Belgian beamline at the ESRF. Journal of Synchrotron Radiation 5, 518-520.

Bruins, J.H., Petrusevski, B., Slokar, Y.M., Kruithof, J.C. and Kennedy, M.D. (2015) Manganese removal from groundwater: Characterization of filter media coating. Desalination and Water Treatment 55(7), 1851-1863.
Bundschuh, J., Maity, J.P., Mushtaq, S., Vithanage, M., Seneweera, S., Schneider, J., Bhattacharya, P., Khan, N.I., Hamawand, I., Guilherme, L.R.G., Reardon-Smith, K., Parvez, F., Morales-Simfors, N., Ghaze, S., Pudmenzky, C., Kouadio, L. and Chen, C.Y. (2017) Medical geology in the framework of the sustainable development goals. Science of the Total Environment 581-582, 87-104.
Chen, C., Dynes, J.J., Wang, J., Karunakaran, C. and Sparks, D.L. (2014) Soft X-ray Spectromicroscopy Study of Mineral-Organic Matter Associations in Pasture Soil Clay Fractions. Environmental Science & Technology 48(12), 6678-6686.
Choi, K.Y.-j. and Dempsey, B.A. (2004) In-line coagulation with low-pressure membrane filtration. Water Research 38(19), 4271-4281.
Clifford, D.A., Ceber, L. and Chow, S. (1983) Separation of Arsenic III and AsV by Ion Exchange, AWWA, Denver, Colo.
Cornell, R.M. and Schwertmann, U. (2003) The Iron Oxides: Structure, Properties, Reactions, Occurances and Uses, WILEY-VCH Verlag GmbH & Co. .
Davis, C.C. and Edwards, M. (2017) Role of Calcium in the Coagulation of NOM with Ferric Chloride. Environmental Science & Technology 51(20), 11652-11659.
de Moel, P.J., Verberk, J.Q.J.C. and van Dijk, J.C. (2006) Drinking Water: Principles and Practices, Delft, The Netherlands.
de Ridder, D.J., van de Wetering, S., van Dijk, T. and van Halem, D. (2018) Influence of HPO 4 2- , H 4 SiO 4 , Ca 2+ , Mg 2+ on Fe floc growth and As(III) removal in aerated, natural groundwater.
De Vet, W. (2011) Biological drinking water treatment of anaerobic groundwater in trickling filters, Technical University of Delft, Delft.
Delaire, C., van Genuchten, C., Amrose, S. and Gadgil, A. (2016) Bacteria attenuation by iron electrocoagulation governed by interactions between bacterial phosphate groups and Fe(III) precipitates. Water Research 103, 74-82.
Diem, D. and Stumm, W. (1984) Is dissolved Mn^{+2} being oxidized by O_2 in absence of Mn-bacteria and surface catalysts? Geochimica et Cosmochimica Acta 48, 1571-1573.
Dixit, S. and Hering, J.G. (2003) Comparison of arsenic(V) and arsenic(III) sorption onto iron oxide minerals: Implications for arsenic mobility. Environmental Science and Technology 37(18), 4182-4189.
Doelsch, E., Rose, J., Masion, A., Bottero, J.Y., Nahon, D. and Bertsch, P.M. (2000) Speciation and Crystal Chemistry of Iron(III) Chloride Hydrolyzed in the Presence of SiO4 Ligands. 1. An Fe K-Edge EXAFS Study. Langmuir 16(10), 4726-4731.
Dong, H.R., Guan, X.H., Wang, D.S. and Ma, J. (2011) Individual and combined influence of calcium and anions on simultaneous removal of chromate and arsenate by Fe(II) under suboxic conditions

Separation and Purification Technology 80, 284-292.
Driehaus, W., Seith, R. and Jekel, M. (1995) Oxidation of arsenate(III) with manganese oxides in water treatment. Water Research 29(1), 297-305.
Dzombak, D.A. and Morel, F.M.M. (1990) Surface Complexation Modeling: Hydrous Ferric Oxide, John Wiley & Sons, New York, New York.
Ebinger, M.H. and Schulze, D.G. (1989) Mn-Substituted Goethite and Fe-Substituted Groutite Synthesized at Acid pH. Clays and clay minerals 37(2), 151-156.
Edwards, M. (1994) Chemistry of arsenic removal during coagulation and Fe-Mn oxidation. American Water Works Association, 64-78.
Ferguson, J.F. and Gavis, J. (1972) A review of the arsenic cycle in natural waters. Water Research 6(11), 1259-1274.
Floris, R., Nijmeijer, K. and Cornelissen, E.R. (2016) Removal of Aqueous nC_{60} Fullerene from Water by Low Pressure Membrane Filtration. Water Research 91, 115-125.
Frank, P. and Clifford, D. (1986) Arsenic(III) oxidation and removal from drinking water, p. 69, US Environmental Protection Agency, Cincinnati, OH.
Fuller, C.C., Davis, J.A. and Waychunas, G.A. (1993) Surface chemistry of ferrihydrite: Part 2. Kinetics of arsenate adsorption and coprecipitation. Geochimica et Cosmochimica Acta 57(10), 2271-2282.
Ghurye, G. and Clifford, D.A. (2001) Laboratory Study on the Oxidation of Arsenic III to As V, p. 87, Unites States Environmental Protection Agency, Washington DC.
Guan, X., Dong, H., Ma, J. and Jiang, L. (2009a) Removal of arsenic from water: Effects of competing anions on As(III) removal in KMnO4–Fe(II) process. Water Research 43(15), 3891-3899.
Guan, X., Ma, J., Dong, H. and Jiang, L. (2009b) Removal of arsenic from water: Effect of calcium ions on As(III) removal in the KMnO4–Fe(II) process. Water Research 43(20), 5119-5128.
Gude, J.C.J., Joris, K., Huysman, K., Rietveld, L.C. and van Halem, D. (2018a) Effect of supernatant water level on As removal in biological rapid sand filters. Water Research X 1, 100013.
Gude, J.C.J., Rietveld, L.C. and van Halem, D. (2016) Fate of low arsenic concentrations during full-scale aeration and rapid filtration. Water Research 88, 566-574.

Gude, J.C.J., Rietveld, L.C. and van Halem, D. (2017) As(III) oxidation by MnO2 during groundwater treatment. Water Research 111, 41-51.
Gude, J.C.J., Rietveld, L.C. and van Halem, D. (2018b) As(III) removal in rapid filters: Effect of pH, Fe(II)/Fe(III), filtration velocity and media size. Water Research 147, 342-349.
Gude, J.C.J., Rietveld, L.C. and van Halem, D. (2018c) Biological As(III) oxidation in rapid sand filters. Journal of Water Process Engineering 21, 107-115.
Gunduz, O., Simsek, C. and Hasozbek, A. (2010) Arsenic pollution in the groundwater of Simav Plain, Turkey: Its impact on water quality and human health. Water, Air, and Soil Pollution 205(1-4), 43-62.
Hao, O., P. Davis, A. and H. Chang, P. (1991) Kinetics of Manganese(II) Oxidation with Chlorine.
Herath, I., Vithanage, M., Bundschuh, J., Maity, J.P. and Bhattacharya, P. (2016) Natural Arsenic in Global Groundwaters: Distribution and Geochemical Triggers for Mobilization. Current Pollution Reports 2(1), 68-89.
Hering, J.G., Chen, P.-Y., Wilkie, J.A., Elimelech, M. and Liang, S. (1996) Arsenic removal by ferric chloride. American Water Works Association 88(4), 155-167.
Hiemstra, T. and Van Riemsdijk, W.H. (1999) Surface structural ion adsorption modeling of competitive binding of oxyanions by metal (Hydr)oxides. Journal of Colloid and Interface Science 210(1), 182-193.
Hsu, J.C., Lin, C.J., Liao, C.H. and Chen, S.T. (2008) Removal of As(V) and As(III) by reclaimed iron-oxide coated sands. Journal of Hazardous Materials 153(1-2), 817-826.
Jain, A., Raven, K. and R.H., L. (1999) Arsenite and Arsenate Adsorption on Ferrihydrite: Surface Charge Reduction and Net OH- Release Stoichiometry.
Jain, C.K. and Ali, I. (2000) Arsenic: Occurrence, toxicity and speciation techniques. Water Research 34(17), 4304-4312.
Jessen, S., Larsen, F., Koch, C.B. and Arvin, E. (2005) Sorption and Desorption of Arsenic to Ferrihydrite in a Sand Filter. Environmental Science & Technology 39(20), 8045-8051.
Kaegi, R., Voegelin, A., Folini, D. and Hug, S.J. (2010) Effect of phosphate, silicate, and Ca on the morphology, structure and elemental composition of Fe(III)-precipitates formed in aerated Fe(II) and As(III) containing water. Geochimica et Cosmochimica Acta 74(20), 5798-5816.
Kanematsu, M., Young, T., Fukushi, K., Green, P. and Darby, J. (2013a) Arsenic(III, V) adsorption on a goethite-based adsorbent in the presence of major co-existing ions: Modeling competitive adsorption consistent with spectroscopic and molecular evidence. Geochimica Et Cosmochimica Acta 106, 404-428.
Kanematsu, M., Young, T.M., Fukushi, K., Green, P.G. and Darby, J.L. (2010) Extended Triple Layer Modeling of Arsenate and Phosphate Adsorption on a Goethite-based Granular Porous Adsorbent. Environmental Science & Technology 44(9), 3388-3394.
Kanematsu, M., Young, T.M., Fukushi, K., Green, P.G. and Darby, J.L. (2013b) Arsenic(III, V) adsorption on a goethite-based adsorbent in the presence of major co-existing ions: Modeling competitive adsorption consistent with spectroscopic and molecular evidence. Geochimica et Cosmochimica Acta 106, 404-428.
Katsoyiannis, I.A., Zikoudi, A. and Hug, S.J. (2008) Arsenic removal from groundwaters containing iron, ammonium, manganese and phosphate: A case study from a treatment unit in northern Greece. Desalination 224(1-3), 330-339.
Kelly, S.D., Hesterberg, D. and Ravel, B. (2008) Analysis of soils and minerals using X-ray absorption spectroscopy. In *Methods of Soil Analysis. Part 5. Mineralogical Methods. SSA Book Series No.5.*
Kim, E.J., Hwang, B.-R. and Baek, K. (2015) Effects of natural organic matter on the coprecipitation of arsenic with iron. Environmental Geochemistry and Health 37(6), 1029-1039.
Kim, M.-J. and Nriagu, J. (2000) Oxidation of arsenite in groundwater using ozone and oxygen. Science of the Total Environment 247(1), 71-79.
Knocke, W.R., Van Benschoten, J.E., Kearney, M.J., Soborski, A.W. and Reckhow, D.A. (1991) Kinetics of Manganese and Iron Oxidation by Potassium Permanganate and Chlorine Dioxide. AWWA 83(6), 80-87.
Kozisek, F. (2017) Best Practice Guide on the Control of Arsenic in Drinking Water. . Bhattacharya, P., Polya, D.A. and Jovanovic, D. (eds), IWA Publishing, London, UK.
Lakshmanan, D., Clifford, D. and Samanta, G. (2008) Arsenic Removal by Coagulation with Aluminum, Iron, Titanium, and Zirconium. American Water Works Association 100(2), 76-88.
Laky, D. and Licskó, I. (2011) Arsenic removal by ferric-chloride coagulation – effect of phosphate, bicarbonate and silicate. Water Science and Technology 64(5), 1046-1055.
Lan, S., Wang, X., Xiang, Q., Yin, H., Tan, W., Qiu, G., Liu, F., Zhang, J. and Feng, X. (2017) Mechanisms of Mn(II) catalytic oxidation on ferrihydrite surfaces and the formation of manganese (oxyhydr)oxides.
Lanson, B., Drits, V., Feng, Q. and Manceau, A. (2002) Structure of synthetic Na-birnessite: Evidence for a triclinic one-layer unit cell. American Mineralogist 87(11-12), 1662-1671.
Lee, G., Song, K. and Bae, J. (2011) Permanganate oxidation of arsenic (III): Reaction stoichiometry and the characterization of solid product

Lihua, S., Ruiping, L., Shengji, X., Yanling, Y. and Guibai, L. (2009) Enhanced As(III) removal with permanganate oxidation, ferric chloride precipitation and sand filtration as pretreatment of ultrafiltration. Desalination 243(1), 122-131.

Lytle, D.A., Chen, A.S., Sorg, T.J., Phillips, S. and French, K. (2007) Microbial As(III) oxidation in water treatment plant filters. American Water Works Association 99(12), 72-86.

Lytle, D.A., Sorg, T.J. and Snoeyink, V.L. (2005) Optimizing arsenic removal during iron removal: Theoretical and practical considerations. Journal of Water Supply: Research and Technology - AQUA 54(8), 545-560.

MacDonald, A.M., Bonsor, H.C., Ahmed, K.M., Burgess, W.G., Basharat, M., Calow, R.C., Dixit, A., Foster, S.S.D., Gopal, K., Lapworth, D.J., Lark, R.M., Moench, M., Mukherjee, A., Rao, M.S., Shamsudduha, M., Smith, L., Taylor, R.G., Tucker, J., Van Steenbergen, F. and Yadav, S.K. (2016) Groundwater quality and depletion in the Indo-Gangetic Basin mapped from in situ observations. Nature Geoscience 9(10), 762-766.

Manceau, A. and Combes, J.M. (1988) Structure of Mn and Fe oxides and oxyhydroxides: A topological approach by EXAFS. Physics and Chemistry of Minerals 15(3), 283-295.

Manceau, A., Marcus, M. and Grangeon, S. (2012) Determination of Mn valence states in mixed-valent manganates by XANES spectroscopy.

Marszałek, H. and Wąsik, M. (2000) Influence of arsenic-bearing gold deposits on water quality in Zloty Stok mining area (SW Poland). Environmental Geology 39(8), 888-892.

Masue, Y., Loeppert, R.H. and Kramer, T.A. (2007) Arsenate and Arsenite Adsorption and Desorption Behavior on Coprecipitated Aluminum:Iron Hydroxides. Environmental Science & Technology 41(3), 837-842.

Mayer, T.D. and Jarrell, W.M. (1996) Formation and stability of iron(II) oxidation products under natural concentrations of dissolved silica. Water Research 30(5), 1208-1214.

McCarty, K.M., Hanh, H.T. and Kim, K.W. (2011) Arsenic geochemistry and human health in South East Asia. Rev Environ Health 26(1), 71-78.

McNeill, L.S. and Edwards, M. (1995) Soluble arsenic removal at water treatment plants. American Water Works Association 87(4), 105-113.

Meng, X., Bang, S. and Korfiatis, G.P. (2000) Effects of silicate, sulfate, and carbonate on arsenic removal by ferric chloride. Water Research 34(4), 1255-1261.

Mukherjee, A., Sengupta, M.K., Hossain, M.A., Ahamed, S., Das, B., Nayak, B., Lodh, D., Rahman, M.M. and Chakraborti, D. (2006) Arsenic contamination in groundwater: A global perspective with emphasis on the Asian scenario. Journal of Health, Population and Nutrition 24(2), 142-163.

Murcott, S. (2012) Arsenic Contamination in the World, IWA Publishing, London, UK.

Naujokas, M.F., Anderson, B., Ahsan, H., Aposhian, H.V., Graziano, J.H., Thompson, C. and Suk, W.A. (2013) The broad scope of health effects from chronic arsenic exposure: update on a worldwide public health problem. Environ Health Perspect 121(3), 295-302.

Newville, M. (2001) IFEFFIT: interactive XAFS analysis and FEFF fitting. Journal of Synchrotron Radiation, 322-324.

Nikitenko, S., Beale, A., van der Eerden, A., Jacques, S., Leynaud, O., O'Brien, M., Detollenaere, D., Kaptein, R., Weckhuysen, B. and Bras, W. (2008) Implementation of a combined SAXS/WAXS/QEXAFS set-up for time-resolved in situ experiments. Journal of Synchrotron Radiation 15, 632-640.

Nriagu, J.O., Bhattacharya, P., Mukherjee, A.B., Bundschuh, J., Zevenhoven, R. and Loeppert, R.H. (2007) Trace Metals and other Contaminants in the Environment, pp. 3-60.

Pedersen, H.D., Postma, D., Jakobsen, R. and Larsen, O. (2005) Fast transformation of iron oxyhydroxides by the catalytic action of aqueous Fe(II). Geochimica et Cosmochimica Acta 69(16), 3967-3977.

Peña, J., Bargar, J.R. and Sposito, G. (2015) Copper sorption by the edge surface of synthetic birnessite nanoparticles. Chemical Geology.

Pena, J., Kwon, K., Refson, K., Bargar, J. and Sposito, G. (2010) Mechanisms of nickel sorption by a bacteriogenic birnessite. Geochimica Et Cosmochimica Acta 74(11), 3076-3089.

Perera, P.A.C.T., Sundarabarathy, T.V., Sivananthawerl, T., Kodithuwakku, S.P. and Edirisinghe, U. (2016) Arsenic and Cadmium Contamination in Water, Sediments and Fish is a Consequence of Paddy Cultivation: Evidence of River Pollution in Sri Lanka. Achievements in the Life Sciences 10(2), 144-160.

Pierce, M.L. and Moore, C.B. (1982) Adsorption of arsenite and arsenate on amorphous iron hydroxide. Water Research 16(7), 1247-1253.

Pontius, F.W., Brown, K.G. and Chen, C.-J. (1994) Health Implications of Arsenic in Drinking Water. American Water Works Association 86(9), 52-63.

Qiao, J., Jiang, Z., Sun, B., Sun, Y., Wang, Q. and Guan, X. (2012) Arsenate and arsenite removal by FeCl3: Effects of pH, As/Fe ratio, initial As concentration and co-existing solutes. Separation and Purification Technology 92, 106-114.

Raven, K.P., Jain, A. and Loeppert, R.H. (1998) Arsenite and arsenate adsorption on ferrihydrite: Kinetics, equilibrium, and adsorption envelopes. Environmental Science and Technology 32(3), 344-349.

Rehr, J., Albers, R. and Zabinsky, S. (1992) High-order multiple-scattering calculations of X-ray absorption fine structure. Physical Review Letters, 3397-3400.

Roberts, L.C., Hug, S.J., Ruettimann, T., Billah, M.M., Khan, A.W. and Rahman, M.T. (2004) Arsenic Removal with Iron(II) and Iron(III) in Waters with High Silicate and Phosphate Concentrations. Environmental Science & Technology 38(1), 307-315.

Rose, J., Manceau, A., Bottero, J.-Y., Masion, A. and Garcia, F. (1996) Nucleation and Growth Mechanisms of Fe Oxyhydroxide in the Presence of PO 4 Ions. 1. Fe KEdge EXAFS Study.

Rossberg, A., Reich, T. and Bernhard, G. (2003) Complexation of uranium(VI) with protocatechuic acid - application of iterative transformation factor analysis to EXAFS spectroscopy. Analytical and Bioanalytical Chemistry 376(5), 631-638.

Saint-Jacques, N., Brown, P., Nauta, L., Boxall, J., Parker, L. and Dummer, T.J.B. (2018) Estimating the risk of bladder and kidney cancer from exposure to low-levels of arsenic in drinking water, Nova Scotia, Canada. Environ Int 110, 95-104.

Scheinost, A., Rossberg, A., Vantelon, D., Xifra, I., Kretzschmar, R., Leuz, A., Funke, H. and Johnson, C. (2006) Quantitative antimony speciation in shooting-range soils by EXAFS spectroscopy. Geochimica Et Cosmochimica Acta 70(13), 3299-3312.

Schmidt, C.W. (2014) Low-Dose Arsenic: In Search of a Risk Threshold. Environ Health Perspect 122(5), A131-134.

Schuhmacher-Wolz, U., Dieter, H.H., Klein, D. and Schneider, K. (2009) Oral exposure to inorganic arsenic: evaluation of its carcinogenic and non-carcinogenic effects. Critical reviews in toxicology 39(4), 271-298.

Senn, A.-C., Hug, S.J., Kaegi, R., Hering, J.G. and Voegelin, A. (2017) Arsenate co-precipitation with Fe(II) oxidation products and retention or release during precipitate aging. Water Research.

Senn, A.-C., Kaegi, R., Hug, S.J., Hering, J.G., Mangold, S. and Voegelin, A. (2015) Composition and structure of Fe(III)-precipitates formed by Fe(II) oxidation in water at near-neutral pH: Interdependent effects of phosphate, silicate and Ca. Geochimica et Cosmochimica Acta 162, 220-246.

Sharma, P., Ofner, J. and Kappler, A. (2010) Formation of Binary and Ternary Colloids and Dissolved Complexes of Organic Matter, Fe and As. Environmental Science & Technology 44(12), 4479-4485.

Smedley, P.L. and Kinniburgh, D.G. (2002) A review of the source, behaviour and distribution of arsenic in natural waters. Applied Geochemistry 17(5), 517-568.

Smeets, P., Medema, G. and Dijk, J. (2009) The Dutch secret: How to provide safe drinking water without chlorine in the Netherlands.

Smith, A.H., Hopenhayn-Rich, C., Bates, M.N., Goeden, H.M., Hertz-Picciotto, I., Duggan, H.M., Wood, R., Kosnett, M.J. and Smith, M.T. (1992) Cancer risks from arsenic in drinking water. Environ Health Perspect 97, 259-267.

Sorlini, S. and Gialdini, F. (2010) Conventional oxidation treatments for the removal of arsenic with chlorine dioxide, hypochlorite, potassium permanganate and monochloramine. Water Research 44(19), 5653-5659.

Sorlini, S., Gialdini, F. and Collivignarelli, M.C. (2014) Survey on full-scale drinking water treatment plants for arsenic removal in Italy. Water Practice and Technology 9(1), 42-51.

Sposito, G. (2008) The Chemistry of Soils, Oxford University Press, New York.

Stachowicz, M., Hiemstra, T. and van Riemsdijk, W.H. (2008) Multi-competitive interaction of As(III) and As(V) oxyanions with Ca(2+), Mg(2+), PO(3-)(4), and CO(2-)(3) ions on goethite. J Colloid Interface Sci 320(2), 400-414.

Stumm, W. and Morgan, J.J. (1996) Aquatic Chemistry, Chemical Equilibria and Rates in Natural Waters, John Wiley & Sons, Inc., New York.

Stuyfzand, P., van Rossum, P. and Mendizabal, I. (2008) Arsenic in groundwater - A world problem. Appelo, T. (ed), pp. 102-125, Netherlands National Committee of the IAH, Utrecht, The Netherlands.

Su, C. and Puls, R.W. (2001) Arsenate and Arsenite Removal by Zerovalent Iron: Effects of Phosphate, Silicate, Carbonate, Borate, Sulfate, Chromate, Molybdate, and Nitrate, Relative to Chloride. Environ. Sci. Technol. 35(22), 4562-4568.

Tebo, B.M., Johnson, H.A., McCarthy, J.K. and Templeton, A.S. (2005) Geomicrobiology of manganese(II) oxidation. Trends in Microbiology 13(9), 421-428.

Vahter, M. (2008) Health effects of early life exposure to arsenic. Basic and Clinical Pharmacology and Toxicology 102(2), 204-211.

Vahter, M., Gardner, R., Ahmed, S., Kippler, M., Hamadani, J.D., Tofail, F. and Raqib, R. (2012) Effects of early-life arsenic exposure on child health and development, pp. 173-174.

van Beek, C.G.E.M., Dusseldorp, J., Joris, K., Huysman, K., Leijssen, H., Schoonenberg Kegel, F., de Vet, W.W.J.M., van de Wetering, S. and Hofs, B. (2016) Contributions of homogeneous, heterogeneous and biological iron(II) oxidation in aeration and rapid sand filtration (RSF) in field sites. Journal of Water Supply: Research and Technology—AQUA 65(3), 195-207.

Van Beek, C.G.E.M., Hiemstra, T., Hofs, B., Bederlof, M.M., van Paassen, J.A.M. and Reijnen, G.K. (2012) Homogeneous, heterogeneous and biological oxidation of iron(II) in rapid sand filtration. Journal of Water Supply: Research and Technology—AQUA 61(1), 1-2012.

Van der Wens, P., Baken, K. and Schriks, M. (2016) Arsenic at low concentrations in Dutch drinking water: assessment of removal costs and health benefits. . Bhattacharya, P., Vahter, M., Jarsjö, J., Kumpiene, J., Ahmad, A., Sparrenbom, C., Jacks, G., Donselaar, M.E., Bundschuh, J. and Naidu, R. (eds), pp. 563-564, CRC Press, Stockholm, Sweden.

van Genuchten, C., Addy, S., Pena, J. and Gadgil, A. (2012a) Removing arsenic from synthetic groundwater with iron electrocoagulation: An Fe and As K-edge EXAFS study. Environmental Science & Technology 46(2), 986-994.

van Genuchten, C., Behrends, T., Kraal, P., Stipp, S. and Dideriksen, K. (2018) Controls on the formation of Fe(II,III) (hydr)oxides by Fe(0) electrolysis. Electrochimica Acta 286, 324-338.

van Genuchten, C. and Pena, J. (2017a) Mn(II) Oxidation in Fenton and Fenton Type Systems: Identification of Reaction Efficiency and Reaction Products. Environmental Science & Technology 51(5), 2982-2991.

van Genuchten, C.M., Addy, S.E.A., Peña, J. and Gadgil, A.J. (2012b) Removing Arsenic from Synthetic Groundwater with Iron Electrocoagulation: An Fe and As K-Edge EXAFS Study. Environmental Science & Technology 46(2), 986-994.

van Genuchten, C.M., Gadgil, A.J. and Peña, J. (2014a) Fe(III) Nucleation in the Presence of Bivalent Cations and Oxyanions Leads to Subnanoscale 7 Å Polymers. Environmental Science & Technology 48(20), 11828-11836.

van Genuchten, C.M. and Pena, J. (2017b) Mn(II) Oxidation in Fenton and Fenton Type Systems: Identification of Reaction Efficiency and Reaction Products. Environ. Sci. Technol. 51(5), 2982-2991.

van Genuchten, C.M. and Peña, J. (2016a) Antimonate and arsenate speciation on reactive soil minerals studied by differential pair distribution function analysis. Chemical Geology 429, 1-9.

van Genuchten, C.M. and Peña, J. (2016b) Sorption selectivity of birnessite particle edges: a d-PDF analysis of Cd(ii) and Pb(ii) sorption by δ-MnO2 and ferrihydrite. Environmental Science: Processes & Impacts 18(8), 1030-1041.

Van Genuchten, C.M., Pena, J., Amrose S, E. and Gadgil, A.J. (2014b) Structure of Fe(III) precipitates genberated by the electrolytric dissolution of Fe(0) in the presence of groundwater ions. Geochimica et Cosmochimica Acta 127, 285-304.

Villalobos, M. (2015) Advances in the Environmental Biogeochemistry of Manganese Oxides. Feng, X., Li, W., Zhu, M. and Sparks, D. (eds), American Chemical Society.

Villalobos, M., Bargar, J. and Sposito, G. (2005) Mechanisms of Pb(II) sorption on a biogenic manganese oxide. Environmental Science & Technology 39(2), 569-576.

Voegelin, A., Kaegi, R., Frommer, J., Vantelon, D. and Hug, S.J. (2010) Effect of phosphate, silicate, and Ca on Fe(III)-precipitates formed in aerated Fe(II)- and As(III)-containing water studied by X-ray absorption spectroscopy. Geochimica et Cosmochimica Acta 74(1), 164-186.

Von Gunten, U. (2003) Ozonation of drinking water: Part II. Disinfection and by-product formation in presence of bromide, iodide or chlorine. Water Research 37(7), 1469-1487.

Vries, D., Bertelkamp, C., Schoonenberg Kegel, F., Hofs, B., Dusseldorp, J., Bruins, J.H., de Vet, W. and van den Akker, B. (2017) Iron and manganese removal: Recent advances in modelling treatment efficiency by rapid sand filtration. Water Research 109, 35-45.

Wang, S. and Mulligan, C.N. (2006) Occurrence of arsenic contamination in Canada: Sources, behavior and distribution. Science of the Total Environment 366, 701 - 721.

Waychunas, G.A., Rea, B.A., Fuller, C.C. and Davis, J.A. (1993) Surface chemistry of ferrihydrite: Part 1. EXAFS studies of the geometry of coprecipitated and adsorbed arsenate. Geochimica et Cosmochimica Acta 57(10), 2251-2269.

Webb, S. (2005) SIXPACK: a graphical user interface for XAS analysis using IFEFFIT. Physica Scripta T115, 1011-1014.

Weng, L., Van Riemsdijk, W.H. and Hiemstra, T. (2008) Humic nanoparticles at the oxide-water interface: Interactions with phosphate ion adsorption. Environmental Science and Technology 42(23), 8747-8752.

Weng, L., Van Riemsdijk, W.H. and Hiemstra, T. (2009) Effects of Fulvic and Humic Acids on Arsenate Adsorption to Goethite: Experiments and Modeling. Environmental Science & Technology 43(19), 7198-7204.

WHO (2011) Arsenic in Drinking-water: Background document for development of WHO Guidelines for Drinking-water Quality, p. 16, WHO Press, Geneva, Switzerland.

Wilkie, J.A. and Hering, J.G. (1996) Adsorption of arsenic onto hydrous ferric oxide: effects of adsorbate/adsorbent ratios and co-occurring solutes. Colloids and Surfaces A: Physicochemical and Engineering Aspects 107, 97-110.

Woo, N.C. and Choi, M.C. (2001) Arsenic and metal contamination of water resources from mining wastes in korea. Environmental Geology 40(3), 305-311.

Wyckoff, R.W.G. (1963) Crystal Structures, Wiley.

Youngran, J., Fan, M., Van Leeuwen, J. and Belczyk, J.F. (2007) Effect of competing solutes on arsenic(V) adsorption using iron and aluminum oxides. Journal of Environmental Sciences 19(8), 910-919.